Strategies and methods for the evaluation of T cell receptor cross-reactivity in cancer immunotherapeutic approaches

Dissertation

der Mathematisch-Naturwissenschaftlichen Fakultät

der Eberhard Karls Universität Tübingen

zur Erlangung des Grades eines

Doktors der Naturwissenschaften

(Dr. rer. nat.)

vorgelegt von

Dipl. Biochem. Andreas Moritz

aus Tübingen

Tübingen

2020

Gedruckt mit Genehmigung der Mathematisch-Naturwissenschaftlichen Fakultät der Eberhard Karls Universität Tübingen.

Tag der mündlichen Qualifikation:	05.03.2021
Stellvertretender Dekan:	Prof. Dr. József Fortágh
1. Berichterstatter:	Prof. Dr. Hans-Georg Rammensee
2. Berichterstatter:	Prof. Dr. Stefan Stevanović

Eidesstattliche Erklärung

Ich erkläre hiermit an Eides statt, dass die vorliegende Arbeit selbstständig und ohne erlaubte Hilfsmittel angefertigt wurde. Es wurden keine anderen als die angegebenen Quellen oder Hilfsmittel genutzt. Wörtliche und sinngemäße Zitate sind als solche gekennzeichnet.

Die Arbeit wurde bisher in gleicher oder ähnlicher Form keinem anderen Prüfungsamt vorgelegt und auch nicht veröffentlicht.

Ort, Datum Unterschrift

Table of Contents

1. Summary

Cancer immunotherapy has presented itself as a promising approach in the treatment of cancers. Actively incorporating the immune system in cancer treatment has proven to be successful in many different therapeutic approaches, ranging from CAR-T therapy or adoptive cellular transfer to peptide or RNA-based vaccines or biologics.

One particularly attractive target for modifications in adoptive cellular transfer or adoptive cell therapy is the T cell receptor. This molecule expressed by T cells can bind to major histocompatibility complex molecules on target cells where they present peptide ligands derived from extra- or intracellular proteins by degradation. Successful recognition can lead to activation of the T cell and an immune response. Thus, introducing TCRs with optimal binding affinity for activation that are specific for a particular peptide-MHC known to be expressed on cancer cells has emerged as an attractive strategy.

In anti-cancer biologics, TCR variable domains have also been used in place of antibodies in bispecific constructs that combine a tumor targeting moiety with a T cell engager like an anti-CD3 antibody. Here, the goal is to specifically bind to tumor cells and broadly activate T cells within the tumor microenvironment. In both approaches, reaching the optimal affinity may require increasing candidate TCRs affinity through maturation. Since the TCR repertoire seems to have evolutionally evolved to cover the very large number of possible peptide-MHC complexes by cross-reactivity of individual TCRs, these maturations may entail unwanted affinity changes towards peptide-MHCs that are not the intended target and express on healthy tissues as well for example, severely compromising the clinical safety of these approaches.

To counteract these tendencies during development of these approaches, strategies were evaluated to determine the binding motif and potential cross-reactivity of either cellularly expressed or soluble TCRs with affinities which can be encountered in the natural TCR repertoire, as well as highly affinity maturated TCRs in soluble bispecific constructs. The different screening strategies were evaluated both with well-established cell biological approaches to determine T cell activation and more recent biochemical methods like bio-layer interferometry to directly measure binding kinetics between TCRs and peptide-HLA molecules. To facilitate screenings with the latter platform, a newly developed empty HLA-A*02:01 mutant stabilized by a disulfide bridge is introduced that greatly facilitates the generation of large peptide-HLA libraries for screenings. The different combinations of screening strategies and measurement method were compared within each TCR group with respect to sensitivity and usefulness. In addition, an approach is demonstrated to convert a determined binding motif into a search motif and used to identify off-target binders for high-affinity bispecific TCR constructs.

2. Zusammenfassung

Krebsimmuntherapien haben sich als vielversprechender Ansatz in der Behandlung von Krebserkrankungen herausgestellt. Das Immunsystem gezielt in die Krebsbehandlung miteinzubeziehen ist mittlerweile in vielen unterschiedlichen therapeutischen Ansätzen, von CAR-T Therapie über adoptiven Zelltransfer hinzu Peptid- und RNA-Vakzinen oder Biologika von Erfolg gekrönt.

Ein besonders attraktives Ziel für Modifikationen im Rahmen von adoptiver Zellthreapie ist der T-Zell-Rezeptor. Dieses Molekül, das von T-Zellen exprimiert wird, kann an major histocompatibility complex (MHC) Moleküle auf Zielzellen binden, wo dieser Peptidliganden, die vom Abbau intra- oder extrazellulärer Proteine stammen, präsentieren kann. Erfolgreiche Erkennung durch den TCR kann zur Aktivierung der T-Zelle und der Initiation einer Immunantwort führen. Daher hat sich die Einführung von TCRs mit optimaler Bindeaffinität zur Auslösung einer Immunantwort, die zugleich spezifisch für einen Peptid-MHC Komplex mit bekannter Expression auf Krebszellen sind, als attraktive Strategie herauskristallisiert.

In krebsbekämpfenden Biologika werden die variablen Domänen des TCRs anstelle von Antikörperdomänen in bispezifischen Molekülen verwendet, die eine Tumor-bindende Domäne mit einer T-Zell-aktivierenden Domäne wie einem anti-CD3 Antikörper verbinden. Hierbei ist es das Ziel spezifisch an Tumorzellen zu binden und T-Zellen in der Tumormikroumgebung zu aktivieren. In beiden Fällen kann es notwendig sein die Affinität des TCRs durch Maturierung zu erhöhen, um optimale Funktionalität zu erreichen. Da das T-Zell-Rezeptor Repertoire in seiner evolutionären Entwicklung jedoch ein hohes Maß an Kreuzreaktivitätspotenzial individueller TCRs gegenüber vielen unterschiedlichen Peptid-MHC Komplexen ausgebildet hat, kann dies nicht erwünschte Änderungen gegenüber Peptid-MHC Komplexen bedeuten, die auf gesunden Zellen exprimiert werden und damit die klinische Sicherheit stark einschränken.

Um derartigen Tendenzen während der Entwicklung dieser Therapien gegen zu wirken wurden Strategien zur Bestimmung von Bindemotifen und Kreuzreaktivitäten für zelluläre exprimierte oder lösliche TCRs mit Wildtyp Affinitäten sowie maturierten hoch-affinen TCRs in bispezifischen Konstrukten untersucht. Die unterschiedlichen Strategien wurden sowohl mit zellbiologischen Ansätzen zur Bestimmung der T-Zell Aktivierung als auch mit biochemischen Methoden wie bio-layer interferometry zur direkten Messung der kinetischen Bindung zwischen TCR und Peptid-MHC geprüft. Um letztere Untersuchungen zu vereinfach wird eine neue entwickelte leere Disulfid-stabilisierte Mutante von HLA-A*02:01 vorgestellt, die die Erstellung großer Peptid-MHC Bibliotheken stark vereinfacht. Die unterschiedlichen Strategien werden hinsichtlich ihrer Sensitivität für die jeweilige TCR Kategorie verglichen und bewertet. Zusätzlich wird ein Ansatz demonstriert, mit dem aus einem gewonnen Bindemotif für einen hoch-affinen TCR ein Suchmotif zur Identifikation von potenziellen Nebenreaktionen erstellt und verwendet werden kann.

3. Introduction

3.1. Cancer immunotherapy is an effective cancer treatment approach

At least since the bestowal of the Nobel prize in medicine to James P. Allison and Tasuku Honjo in 2018 for their discovery of cancer therapy through modulation of immune regulation, cancer immunotherapy can be regarded as an established approach in the treatment of cancers. It's roots go back more than 60 years, to the immune surveillance hypothesis first prominently advocated for by Frank McFarlane Burnet, and it is by now widely accepted that the immune system plays an integral part in each individuals cancer prevention machinery (*1*–*3*). Actively incorporating the immune system in cancer treatment has proven to be successful in many different therapeutic approaches, ranging from CAR-T therapy or adoptive cellular transfer to peptide or RNA-based vaccines or biologics(*4*–*12*). While these approaches can have significant differences with respect to their individual structure, they nevertheless share the same key principles: identification of suitable molecular targets that offer at least a therapeutic window for targeting specific tumors and combination of them with an effector function, either through activation of existing potential in the immune system or introduction of new components.

3.2. Target classes for cancer immunotherapy

Selection of a suitable target is critical for every therapeutic approach, as it not only influences efficacy but has also huge implications for safety. Since tumors are derived from self, those that escape the elimination and equilibrium phase as described by the immune surveillance hypothesis often lack obvious differentiators compared to healthy tissue, else they would not have developed in the first place(*13*, *14*).

Current clinically successful approaches like CAR-T therapy, e.g. tisagenlecleucel for ALL targeting the B lymphocyte antigen CD19, or monoclonal antibody treatment, e.g. trastuzumab targeting the HER2/neu growth receptor in HER2/neu positive breast cancer, have mostly been developed using membrane proteins as target(*15*, *16*). Unfortunately, these targets are seldomly tumor-specific: while they may be overexpressed on tumor tissue, they can still be found on various healthy tissues as well. This has significant consequences: CAR-T cell therapy for example also eradicates healthy B cells, resulting in potentially cancer free but immunodeficient patients and toxicity can be difficult to manage.

Antigenic peptides presented on cell surface through the MHC pathway represent another potential target class: while they are ultimately part of a membrane protein as well, the peptide ligands presented as part of MHC class I or class II complexes are derived from all potentially available proteins after proteasomal degradation. Therefore, they also showcase the intracellular part of the proteome that would otherwise be largely invisible to the immune system(*17*, *18*).

Peptide-MHC complexes and their cognate receptor, the T cell receptor expressed on multiple T lymphocyte subsets, play a fundamental role for the immune response against viral infection or cancer(*19*). T cells can recognize specific peptide-MHC complexes, for example presenting peptide derived from a virus protein within an infected cell, if expressing a matching TCR and initiate an immune response(*20*). This system is not restricted to infectious diseases but has also been observed in early and partially successful clinical approaches focusing on isolation, *in vitro* expansion, stimulation and retransfer of TILs in melanoma patients, including the identification of the non-mutated peptides that mediated T cell activity(*21–24*). Presence of TILs has also recently emerged as a potentially important factor in predicting the effectiveness of checkpoint inhibitor therapy besides PD-L1 expression on the tumor(*25*).

Consequently, peptides identified as tumor associated antigens represent an attractive target class. Based on the wealth of data collected through various technologies in the last decades about the immunopeptidome, the entirety of peptides presented on healthy or malignant tissues, antigens over-expressed on tumor tissue have been identified as well shared tumor-specific antigens(*26–29*). These are either derived from tumor-expressed germline genes, otherwise only active in germ cells, or the consequence of mutations that have accumulated in the tumor genome and ultimately resulted in non-self peptides called neoantigens(*28*, *30*). While merely overexpressed tumor associated antigens may face similar challenges compared to targeting of overexpressed membrane proteins, tumor-specific antigens might allow more focused applications in cancer immunotherapy.

3.3. Adoptive cell therapy or transfer for peptide-MHC based tumor targeting

After recognition of the importance of the immune system and particularly the role of lymphocytes in the response against tumors, adoptive cell therapy emerged as one of the first approaches utilizing this knowledge, supported by the then recent discovery of IL-2 as major stimulant(*8*, *24*, *31*). These approaches involved expansion and reinfusion of genetically unaltered, patient-derived cells, e.g. tumor-infiltrating lymphocytes, but success was limited to melanoma.

Based on the hypothesis that enrichment and activation of lymphocytes was only of limited use when none of the T cells were capable of recognizing tumor-presented antigens, efforts to genetically alter lymphocytes to express receptors with known reactivity led to further advances in the field.

TCR sequences can be retrieved from selected clones or even single cells, for example after stimulation with tumor associated peptides like the cancer testis antigen NY-ESO-1, and expressed in different lymphocytes through various means, e.g. electroporation of mRNA(*32*, *33*).

Translation of this approach from the bench to bedside has already been successful: in one of the first trials using genetically modified autologous T cells, which express a MART-1 specific TCR in melanoma, two out of 15 patients demonstrated lasting engraftment and objective regression(*34*). The number of trials investigating these approaches has risen significantly since then, with many targeting NY-ESO-1 or MART-1 in various cancer indications(*35*).

Among the different factors influencing the activity upon antigen recognition, the binding affinity and avidity of TCRs for their cognate pMHC certainly has a substantial impact on the functionality of the T cell(*36*–*39*). T cell receptors that recognize viral peptides often display significantly higher binding affinity or avidity compared to those recognizing tumor associated or specific antigens (*40*). This is probably due to the relatively high similarity of these peptides compared to those presented on healthy tissues and thus the removal of high affinity binders during thymic selection. Instead of only relying on identifying efficient TCRs with adequate affinity in TIL samples or those from healthy donors, affinity enhancement of TCR receptors through maturation has emerged as an alternative approach to reach optimal efficacy(*41*–*43*). This can be achieved either by rational design, smaller scale single or double amino acid substitution in the CDR regions or through large, directed evolution approaches, enabled by display technologies like phage or yeast cell display.

In one example of this approach, the NY-ESO-1 specific TCR 1G4 isolated from a melanoma patient, which already demonstrates a relatively strong affinity for a tumor associated antigen recognizing TCR with a single digit µM K_D, could be modified by a dual amino acid substitution in the CDR3 region of the TCR alpha chain to achieve a significantly increased K_D of 730 nM(*44*, *45*). Efficacy of this enhanced TCR could be demonstrated in clinical trials, achieving objective responses in multiple patients with synovial cell sarcomas or melanomas(*46*, *47*). Several other TCRs, for example against the cancer testis antigen MAGE-A10, are currently undergoing phase I clinical trials(*48*).

Aside from TCR identification, isolation and – potentially – modification, another focus currently lies on enabling allogeneic therapeutic approaches. The current autologous adoptive transfer requires isolation of T cells and – if desired – specific T cell subsets from patients for transduction, for example using lentiviral vectors, of the desired TCR. This process is quite costly due to cGMP requirements, has a relatively long delay between the identification of enrollable patients and completed manufacturing of the product and can be error prone with respect to the quality of the final cell product.

Tisagenlecleucel for example did fail to produce product for 9% of enrolled patients in the ELIANA study ((*41*), clinical trial register CT02228096).

Allogeneic cell products, for example derived from iPSCs, could serve as off-the-shelf product, significantly increasing treatment speed while potentially decreasing the cost. They also might enable the inclusion of additional modifications, for example suicide genes for better clinical management of cytotoxicity or additional stimulatory changes to increase their efficacy, e.g. deactivation or functional reversal of PD-L1(*49*–*51*). While these approaches are currently investigated mainly with respect to CAR-T therapies as those are already approved for clinical use, T cell receptor-based therapies could also benefit from such modifications and are an active target of research (*52*, *53*). This also includes direct TCR modifications that serve to enhance its function and safety, e.g. by preventing mispairing with endogenous TCRs(*54*, *55*).

3.4. Bispecific T cell engager as biopharmaceutical approach in cancer immunotherapy

B cells and the antibodies they secrete are also an integral part of the immune response. While adoptive cellular transfer of B cells has thus far been lagging behind the research conducted on T cells, the use of antibodies is much more widespread in cancer immunotherapy(*56*). Augmented by the development of the hybridoma technology and humanization of mouse antibodies, many different monoclonals have been developed since the late 2000s and are currently available on the market(*57*–*60*). Interestingly, the exact methodology behind the respective therapeutic approaches can differ significantly: while some antibodies like trastuzumab seemingly inhibit signalling by their target molecules, e.g. through inhibiting of receptor dimerization, besides promotion of ADCC through NK cells, others like checkpoint inhibitors work by blocking or masking unfavourable interactions between tumor tissue and immune cells in the tumor microenvironment.

To also induce other parts of the immune response with antibodies, a large variety of bispecific antibodies have been developed based on the work by Morrison et al., with two currently having received approval by the FDA(*61*–*64*). In bispecific approaches, instead of using two Fab binding domains to increase the avidity in the interaction with the target molecule, two different specificities are combined to enable specific targeting and homing of two cell types, target and effector cell. In the case of blinatumomab, one of the approved therapies, CD19 is targeted in haematological malignancies to bind to B cells whereas an anti-CD3 engaging domain is used to stimulate T lymphocytes in close vicinity to target cell, ultimately forming an immune synapse(*65*). A broad structural variety is currently tested in the field, ranging from very small diabodies and BiTEs to IgG-like or even larger constructs.

Due to the use of regular of single chain Fab domains, these bispecifics typically target membrane proteins similar to the way CAR-T cells are currently employed. In recognition of the potential of MHC pathway as target class, some efforts have been made to produce antibodies specifically targeting peptide-MHC molecules (*66*–*68*). While the structure of the Fab fragment and the TCR are quite similar as each compromise two Immunoglobulin domains, the affinities and thus interaction half-lives they exhibit bear striking differences. Antibody interactions often last for hours, whereas TCR binding is characterized by a relatively fast on but quick off rate, potentially to allow serial triggering(*66*).

Instead of identifying antibodies that are capable of binding to peptide-MHCs, others have focused on using the aforementioned affinity maturation processes to transform target specific TCRs in high affinity variants capable of functioning similar to antibody Fab fragments(*6*, *43*, *69*, *70*). One of the first molecules of that kind, targeting another melanoma-related antigenic peptide from the protein gp100, the ImmTAC IMCgp100 is currently investigated in clinical trials in uveal melanoma.

3.5. Cross-reactivity and off-target toxicity are significant risk factors in cancer immunotherapy

On-target off-tumor cytotoxicity is to be expected in therapeutic approaches targeting molecules that are shared between tumor and healthy tissue. While overexpression on tumor tissue can enable a therapeutic window, which can be exploited by dosing regiments, efficacy will most likely be compromised if the on-target off-tumor toxicity can't be tolerated.

But on-target toxicity is not the only risk that has to be assessed. Off-target toxicities have been observed for antibodies as well as T cell receptor-based therapeutics. For the latter, this is a side effect of the broad repertoire of antigens each TCR must cover: in current the literature, it is estimated that any given T cell receptor can potentially recognize thousands of different peptides with adequate affinity to lead to T cell activation(*71*, *72*). While this number is somewhat speculative, the concept cross-reactivity is widely recognized. Even in the fully autologous TIL therapy approach, autoimmunity like side reactions have been observed, for example vitiligo or uveitis(*73*, *74*). This is remarkable, as these results indicate that even in presence of thymic selection, some T cells with the capability to recognize self-peptides may prevail that are capable of autoimmune reactions under the right circumstances.

These risks are even more pronounced when T cell receptors are transferred between individuals, especially when affinity maturation has occurred. Off-target cytotoxicity related deaths have occurred in at least two different trials using affinity enhanced TCRs. In one of the cases, transfer of autologous T cells transduced with the MAGE-A3 restricted TCR a3a, which recognizes the antigenic peptide EVDPIGHLY with a K_D of 2.3 µM, led to death of two enrolled patients by cardiac arrest(*75*–*77*).

A peptide from the muscle protein titin with relatively high sequence similarity compared to MAGE-A3, ESDPIAVQY, could be isolated that was recognized by the same TCR with a K_D of 100 µM and expressed on heart tissue *in vivo* and IPSC-derived cardiomyocytes but on cardiac-derived primary cell lines.

Following these casualties, much more time and work has been invested to study the science behind TCR cross-reactivity and develop techniques and strategies to improve the detection of relevant interactions before entry into the clinic(*78*, *79*).

One method also used in identifying titin as the source of the a3a induced off-target toxicity is alanine scanning. This method was previously used to identify important peptide positions in other protein-protein interaction system, for example for identifying important positions on the TCR side(*80*). In cross-reactivity screening for TCRs, alanine scanning involves separate substitution of the target peptide amino by alanine, making it a comparatively small assay. The peptides are then tested for T cell activation decreases in activation compared to the target peptide identifies important amino acids at these positions whereas increases or unchanged behavior means less importance of this position for TCR recognition.

While using the same general strategy as the alanine scanning, a positional scanning library aims at providing a more nuanced image by not only substituting an alanine at each position but every proteinogenic amino acid. This approach was first demonstrated by Wucherpfenning et al. to identify cross-reactive MHC class II presented peptides for a MBP peptide(*81*). The strategy of this more complex assay in comparison is not to define the importance of the position in the wild type peptide but to identify which amino acids are or are not compatible with binding by a given TCR. From this data, a search matrix can then be applied to identify potentially cross-reactive peptides that exist in the proteome.

A third approach also based on the concept of the positional scanning library is the positional scanning synthetic combinatorial peptide library (PS-SCL)(*82–88*). While the resulting matrix itself is similar, peptide pools are used instead of defined substituted peptides. To create each pool, one proteinogenic amino acid is fixed at one position of the peptide whereas the other positions can feature all 19 amino acids at random, with cysteine excluded to prevent dimerization. For a nonameric peptide, each of the 180 peptide pools theoretically contains 1.6×10^{10} different peptides. The proposed advantage of this approach over a conventional PSL is a more thorough binding motif, as some substitutions that will not be recognized in conjunction with the fixed wild type amino acids in a PSL might still be well recognized when combined with other amino acids.

Sets of peptides which have large discrepancies in their primary amino acids sequence but can still activate the same TCR are often called mimotopes and often rely on molecular mimicry, resulting in similar structures in the peptide binding groove despite the different amino acid sequence(*77*, *89–91*). But cross-reactivity can be even more complex than that, as TCRs can also react similarly with peptides that do not exhibit molecular mimicry and structural similarity(*92*). Given this large number of potential variables, so far there has been no clear consensus on which strategy can provide the most safety and still be applicable in practice with respect to clinical development of TCR based therapeutics. Thus, current approaches combine many different strategies, ranging from binding motif determination and off-target prediction to allo-reactivity assessments and testing of cultured healthy tissue cells(*48*, *93*). In addition, a vast number of different readouts are currently available, especially for bispecific approaches as they intersect between the T cell and antibody field.

3.6. Production of soluble peptide-MHC complexes is crucial for many experimental approaches involving TCRs

Soluble pMHCs were first generated using protein expression and refolding techniques in 1992 and have since found use for many immunological research applications, e.g. identification of antigen-specific T cells through flow cytometry or affinity measurements of pMHC-TCR interactions(*94–97*). The production itself is not trivial since MHC molecules are unstable and decay without a peptide. Therefore, different pMHCs had to produced separately, making the production of large libraries time consuming. To improve upon this, several strategies have been developed to separate refolding and loading of desired peptides and thus increase throughput and library sizes. These strategies mostly rely on exchange of an initial ligand peptide against the desired peptide, either by refolding with weak peptide binders that can be replaced by strong binders, UV light mediated exchange with UV-cleavable peptide ligands or temperature-mediated exchanges(*98–102*).

While these have expanded the scope for some applications, e.g. allow large library flow cytometry analysis with hundreds of different, exchange approaches are not without drawbacks. For the UV exchange, exchange efficiency is dependent on rapid complex stabilization by the new peptide during the UV exposure. Especially lower-affinity peptides can fail to do so, resulting in a decreased functional pMHC concentration after the exchange which can be detected using an anti-b2m ELISA. This makes it a less reliable tool to produce pMHCs for some approaches, for example binding kinetic screenings with peptide-MHCs as soluble analytes, since precise knowledge of the concentration is necessary to obtain accurate curve fitting results and kinetic constants.

On alternative approach is structural modification: molecular dynamics simulations of empty and peptide loaded MHC class I molecules have indicated an increased mobility in the F-pocket, the region that typically accommodates the C terminus of peptide ligands, in absence of bound peptide(*103*). In studies with the mouse MHC class I molecule H-2K^b, introduction of a disulfide bond between opposing residues in the F-pocket, by mutating a tyrosine at position 84 and an alanine at position 139 to cysteines, has resulted in the stabilization of the complex. The mutant could be refolded as empty MHC molecule and was capable of binding peptide ligands(*104*, *105*). Translation of this approach to other alleles could enable quick peptide loading reactions that do not require specialized hardware or conditions.

3.7. Aim of the thesis

The objective of this thesis was to individually test and compare the previously outlined strategies typically used to assess the cross-reactivity of T cell receptors and determine their usefulness for both adoptive cell therapy and bispecific T cell engager approaches. For this purpose, it was first necessary to identify and evaluate the appropriate readout system that could allow efficient and routine application of the respective strategy, including selection of fitting experimental parameters, setting up and establishing new technology platforms or evaluate new and existing strategies to generate the required reagents among others. The final setups were then used to analyze published examples for both therapeutic approaches to demonstrate and deepen the understanding of these approaches. In addition, proof-of-concept for non-motif-based screening approaches based on peptide libraries with known makeup should be established.

4. Materials and Methods

4.1. Materials

4.1.1. Chemicals and reagents

Table 4.1 Chemicals and reagents obtained from the respective manufacturers.

Reagent name	Manufacturer
DMSO	Sigma, Cat. Nr. 41640
TFA	Sigma, Cat. Nr. T6508
Triton X-100	Roth, Cat. Nr. 3051.2
Tris base	Roth. Cat. Nr. 4855.2
L-Arginine base	Sigma, Cat. Nr. A5006-1KG
EDTA	Roth, Cat. Nr. 8040.3
Glutathione reduced	Sigma, Cat. Nr. G4251-50G
Glutathione oxidized	Sigma, Cat Nr. G4376-10G
Sodium chloride	Roth, Cat. Nr. 3957.1
PMSF	Sigma, Cat. Nr. P7625
Guanindine-HCl	Roth, Cat. Nr. 0035.2
Sodium acetate, 3*H_2O	Fluka, Cat. Nr. 71188
Sodium acetate, water-free	Fisher Scientific, Cat. Nr. 10122350
Sodium azide 10%	Merck, Cat. Nr. 1.06688.0100
Formaldehyde, 37%	Sigma, Cat. Nr. F8775-500,l
DEPC	Roth, Cat. Nr. K028.3
Ethanol, 96%	VWR, Cat. Nr. 20824.365
Lithium Chloride	Ambion, Cat. Nr. AM1344
Agarose	Invitrogen, Cat. Nr. 16500-500
Sodium hydroxide	Roth, Cat. Nr. 6771.1

Reagent name	Manufacturer
MOPS	Roth, Cat. Nr. 6979.2
Glycerol	Calbiochem, Cat. Nr. 356352
Acetic acid 100%	Merck, Cat. Nr. 1.00063.1000
H_2SO_4 98%	Roth, Cat. Nr. X944.1
Coomassie Brilliant Blue R250	Sigma, Cat. Nr. B0149
Urea	Sigma, Cat. Nr. U2150
Cystamine	Fluka, Cat. Nr. 30050
Cysteamine	Sigma, Cat. Nr. 30070
Agar-Agar	Roth, Cat. Nr. 2266.1
Bacto Trypton	BD, Cat. Nr. 211705
Bacto Yeast	BD, Cat. Nr. 212750
IPTG	Peqlab, Cat. Nr. 37-2030

4.1.2. Buffers and solutions

4.1.2.1. Commercial buffers and solutions

Table 4.2 Commerically available buffer systems or solutions and their respective manufacturers.

Buffer name	Manufacturer
DPBS	Lonza, Cat. Nr. BE17-512F/122
RPMI 1640 GlutaMAX	Invitrogen, Cat. Nr. 72400-021
Fetal calf serum (FCS)	Life Technologies, Cat. Nr. 10270106
Human serum albumin 20%	Octapharma, Cat. Nr. PZN-020031
Human serum	PAN, Cat. Nr. P30-2901
X-Vivo	Biozym, Cat. Nr. 881204
CTL-Wash	C.T.L., Cat. Nr. CTLW-010

Buffer name	Manufacturer
L-Glutamine 200mM	ThermoFisher Scientific, Cat. Nr. 25030-024
Buffer name	**Manufacturer**
Sodium Pyruvate	C. C. Pro, Cat Nr. Z-20M
Penicillum-Streptomycin	Biozym, Cat. Nr. 882082
Ampicillin	Roth, Cat. Nr. K029.1
Chloramphenicol	Sigma, Cat. Nr. C0378
Hygromicin B	Merck Millipore, Cat. Nr. 400052
IL-2	Pharmacy, Cat. Nr. PZN02238131
BSA	Sigma, Cat. Nr A7030
Trypan blue	Merck, Cat. Nr. 1.11732.0025
Tuerk solution	Fluka, Cat. Nr. 93770
Biocoll	Biochrom, L6115
Auto-MACs buffer kit	Miltenyi Biotec, Cat. Nr. 130-091-222/376
Bio-Glo Luciferase Assay System	Promega, Cat. Nr. G7940
Streptavidin	Sigma, Cat. Nr. S4762-5mg

4.1.2.2. Cell biology methods buffers

Table 4.3 Names and composition of buffers used in cell biology methods.

Buffer name	Components
Jurkat Assay Medium (JAM)	RPMI Medium 1640 GlutaMAX 10% heat inactivated FCS Penicillin and streptomycin 100 µg ml^{-1} each 1% Sodium pyruvate
Jurkat Culture Medium (JCM)	RPMI Medium 1640 GlutaMAX 10% heat inactivated FCS penicillin and streptomycin 100 µg ml^{-1} each Hygromicine B, 200 µg ml^{-1} 1% Sodium pyruvate

Buffer name	Components
T cell medium (TCM)	RPMI Medium 1640 GlutaMAX 10% heat inactivated human serum Penicillin and streptomycin 100 µg ml^{-1} each Gentamicin 20 µg ml^{-1} 1% Sodium pyruvate
Flow cytometry buffer (PFEA)	DPBS 2% FCS EDTA 2 mM 0.01% Sodium azide

4.1.2.3. Molecular biology & protein biochemistry buffers

Table 4.4 Names and composition of buffers used in molecular biology or protein biochemistry methods.

Buffer name	Components
LB-Medium high salt	MilliQ-H_2O 10 g l^{-1} Bacto Trypton 5 g l^{-1} Bacto Yeast 10 g l^{-1} NaCl
LB-Medium low salt	MilliQ-H_2O 10 g l^{-1} Bacto Trypton 5 g l^{-1} Bacto Yeast 5 g l^{-1} NaCl
LB-Agar plates	MilliQ-H_2O 10 g l^{-1} Baco Trypton 10 g l^{-1} NaCl 5 g l^{-1} Baco Yeast 15 g l^{-1} Agar-Agar
Kinetics Buffer	DPBS 0.5% BSA 0.05% Triton X-100

Buffer name	**Components**
Injection Buffer MHC refolding	MilliQ-H_2O Guanidine-HCl 3 M Sodium acetate 10 mM EDTA 10 mM
Injection Buffer TCR refolding	MilliQ-H_2O Guanidine-HCl 6 M Sodium acetate 10 mM EDTA 10 mM
MHC refolding buffer	MilliQ-H_2O 100 mM Tris base pH8 500 mM arginine 2 mM EDTA 0.5 mM oxidized glutathione 5 mM reduced glutathione Sterile filtrated, degassed and adjusted to pH 8 with HCl prior to use.
SEC running buffer (TBSA)	MilliQ-H_2O 20 mM Tris base pH8 150 mM sodium chloride 0.02 % sodium azide Sterile filtrated and degassed prior to use.
TCR refolding buffer	MilliQ-H_2O 5 M Urea 400 mM L-Arginine 3.7 mM Cystamine 6.6 mM Cysteamine 100 mM Tris base pH8 Sterile filtrated prior to use.
TAE buffer (1x)	MilliQ-H_2O 40 mM Tris Base 20 mM Acetic Acid 1 mM EDTA

Buffer name	Components
MOPS buffer (1x)	DEPC-H_2O 20 mM MOPS 5 mM sodium acetate 1 mM EDTA Adjust to pH 7.0 using NaOH 10M and pH indicator paper

4.1.3. ELISA kits and reagents

Table 4.5 Commercially available kits and reagents used for ELISA assays.

Reagent name	Manufacturer
ELISA MAX Deluxe Set Human IFN-gamma kit	Biolegend, Cat. Nr. 430104
ELISA Wash Buffer	Biolegend, Cat. Nr. 421601
Nunc MaxiSorp ELISA plates	Biolegend, Cat. Nr. 423501
Recombinant human IFN-gamma protein	Abcam, Cat. Nr. ab119140

4.1.4. Gel electrophoresis kits and reagents

Table 4.6 Commercially available kits and reagents used for SDS-PAGE.

Reagent name	Manufacturer
NuPAGE LDS sample buffer 4x	ThermoFisher Scientific, Cat. Nr. NP0007
NuPAGE MES SDS Running buffer 20x	ThermoFisher Scientific, Cat. Nr. NP0002
NuPAGE Sample reducing agent 10x	ThermoFisher Scientific, Cat. Nr. NP0004
Reagent name	**Manufacturer**
NuPAGE 10% Bis-Tris Gel	ThermoFisher Scientific, Cat. Nr. NP0302Box
NuPAGE Antioxidant	ThermoFisher Scientific, Cat. Nr. NP0005
SeeBlue Plus2 Prestained Standard 1x	ThermoFisher Scientific, Cat. Nr. LC5925

Table 4.7 Commercially available kits and reagents used for Native PAGE.

Reagent name	Manufacturer
Novex WedgeWell 10-20% Tris-Glycine Mini Gel	ThermoFisher Scientific, Cat. Nr. XP10202BOX
Novex Tris-Glycine Native Running Buffer 10x	ThermoFisher Scientific, Cat. Nr. LC2672
Novex Tris-Glycine Native Sample Buffer 2x	ThermoFisher Scientific, Cat. Nr. LC2673
SeeBlue Plus2 Prestained Standard 1x	ThermoFisher Scientific, Cat. Nr. LC5925

Table 4.8 Commercially available kits and reagents used for aragarose gel electrophoresis

Reagent name	Manufacturer
PeqGREEN DNA/RNA Dye	Peqlab, Cat. Nr. 37-5010
Orange G	Sigma, Cat. Nr. 03756-25G
1 kb DNA ladder	NEB, Cat. Nr. N3272

Table 4.9 Commercially available kits and reagents used for denaturing agarose gel electrophoresis.

Reagent name	Manufacturer
PeqGREEN DNA/RNA Dye	Peqlab, Cat. Nr. 37-5010
Gel Loading Buffer II	Ambion, AM1344
peqGOLD High Range RNA ladder	Peqlab, Cat. Nr. 37-5010

4.1.5. DNA template amplification and *in vitro* transcription kits and reagents

Table 4.10 PrimeSTAR HS DNA Polymerase kit for DNA template amplification.

Reagent name	Manufacturer
5X PrimeSTAR Buffer (Mg^{2+} plus (5mM))	Takara, Cat. Nr. R010B
dNTPs (2.5 mM each)	
PrimeSTAR HS DNA Polymerase (2.5 U μl^{-1})	

Table 4.11 mMESSAGE mMACHINE T7 transcription and LiCl precipitation kit for *in vitro* transcription.

Reagent name	Manufacturer
Nuclease free water	Ambion, Cat. Nr. AM1344
2x NTP/CAP	
10x Reaction Buffer	
T7 Enzyme Mix	
Turbo DNASE 2U μl^{-1}	
LiCl	

4.1.6. Chromatography

Table 4.12 Columns used for MHC monomer purification.

Column type	Manufacturer
HiLoad 26/600 Superdex 75 pg	GE Healthcare

Table 4.13 Columns used for soluble TCR purification.

Column type	Manufacturer
POROS HQ 50 µm column, 10 x 100 mm	ThermoFisher Scientific
HiLoad 26/600 Superdex 75 pg	GE Healthcare

Table 4.14 Columns used for bispecific T cell engager purification.

Column type	Manufacturer
HiTrap protein L, 1 ml	GE Healthcare
HiLoad 16/600 Superdex 200 pg	GE Healthcare

4.1.7. Octet RED384 biosensors

Table 4.15 Biosensors used for kinetic measurements on the Octet RED384 system.

Biosensor type	Manufacturer
Streptavidin biosensors	Molecular Devices (Fortébio), Cat. Nr. 18-5021
Anti-Fab-CH1 2. generation biosensors	Molecular Devices (Fortébio), Cat. Nr. 18-5127
Anti-Penta-HIS1K biosensors	Molecular Devices (Fortébio), Cat. Nr.

4.1.8. Antibodies and MACS beads

Table 4.16 Antibodies and MACS beads used for CD8+ T cell isolation, stimulation and flow cytometry experiments.

Antibody	Clone	Manufacturer
Anti-HLA-A2-PE	BB7.2	Biolegend, Cat. Nr. 343305
CD8 MicroBeads, human	-	Miltenyi Biotec, Cat. Nr. 130-045-201
Anti-CD3	OKT3	Biolegend, Cat. Nr. 317302
Anti-CD28	9.3	University of Tuebingen

4.1.9. Enzymes

Table 4.17 Enzymes used and their respective manufacturer.

Enzyme name	Manufacturer
Benzonase	VWR, Cat. Nr. 1.01695.0001
DNase I	Roche, Cat. Nr. 11284932001
BirA ligase	Avidity, Cat. Nr. Bulk BirA
Leupeptin	Roche, Cat. Nr. 11017101001
Pepstatin	Roche, Cat. Nr. 11359053001
DpnI	NEB, Cat. Nr. R0176L

4.1.10. Cell lines and bacteria strains

Table 4.18 Cell lines used and their respective provider.

Cell line name	Provider
E. coli BL21(DE3)pLysS	Merck Millipore, Cat. Nr. 70236
T2	ATCC, Cat. Nr. CRL-1992, ExPASy accession CVCL_2211
GloResponse NFAT-RE-luc2 Jurkat	Promega, Cat. Nr. CS1764 (discontinued), ExPASy accession CVCL_LB63
ExpiCHO	ThermoFisher Scientific, Cat. Nr. A29133, ExPASy accession CVCL_5J31

4.1.11. Expression plasmids

4.1.11.1. pET-3a

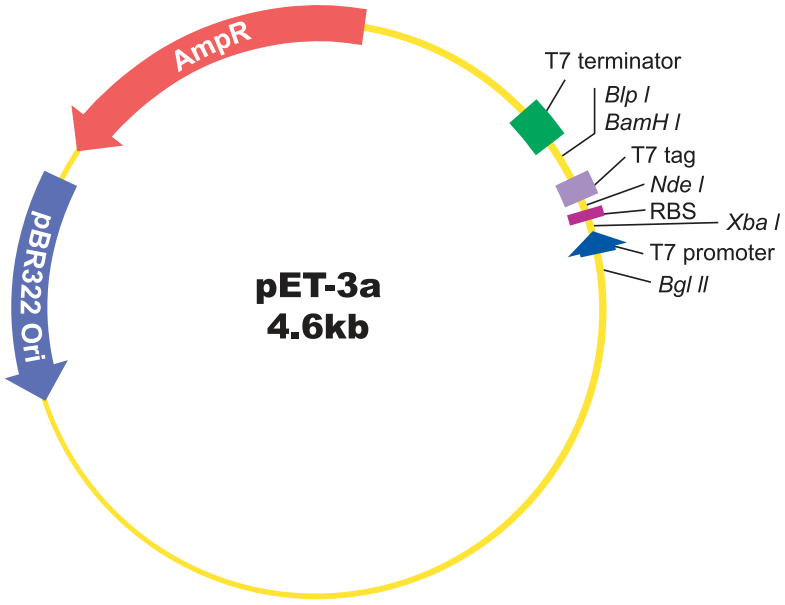

Fig. 4.1 Vector map of the pET-3A plasmid (Source: Genscript).

The pET-3a expression plasmid was used as vector for inclusion body synthesis in the *E. coli* strain Bl21(DE3)pLysS (Fig. 4.1). This strain possesses and IPTG-inducable T7 polymerase, matching the T7 promoter of pET-3a vector. Desired codon optimized DNA sequences were introduced using the BamH I and Nde I restriction sites, synthesis and ligation was performed by Genscript.

4.1.11.2. pGEM-3Z

The pGEM-3Z plasmid was obtained from Promega (Cat. Nr. P2151) and used as vector for amplification of template DNA for *in vitro* transcription of TCR alpha and beta chain encoding sequences inserted into the multiple cloning site (Fig. 4.2).

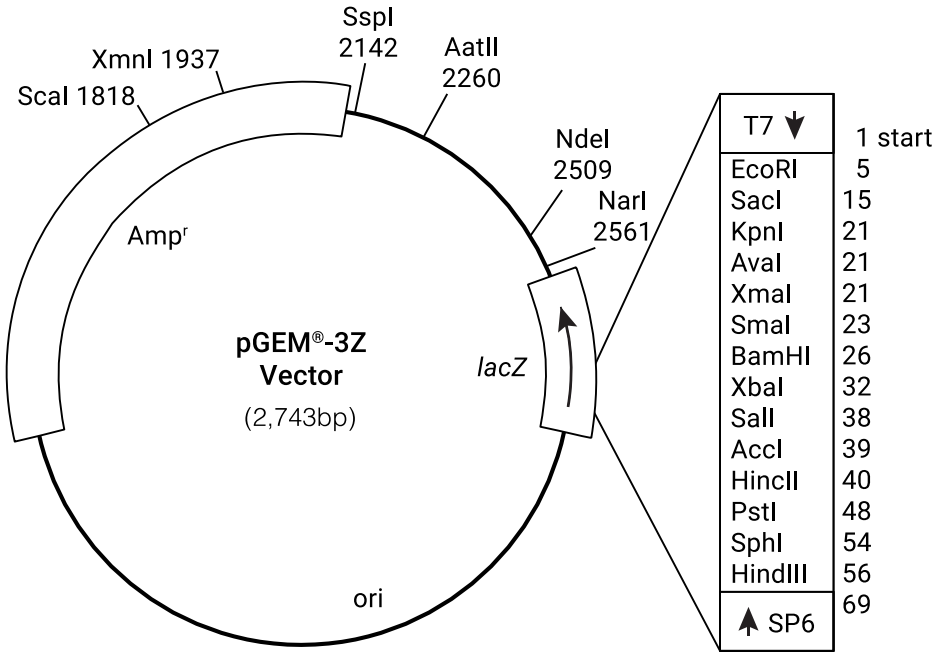

Fig. 4.2 Vector map of the pGEM-3Z plasmid (Source: Promega).

4.1.12. DNA & protein sequences

4.1.12.1. HLA-A*02:01 wild type heavy chain with C-termina BirA sequence

5'-

CATATGGGGTCACACAGTATGAGGTATTTCTTCACATCAGTTAGTAGGCCCGGAAGAGGGGAGCCGCGTTTCA
TTGCGGTGGGTTACGTTGACGACACCCAGTTCGTTCGTTTTGACAGCGATGCGGCGAGCCAACGTATGGAACC
GCGTGCGCCGTGGATTGAGCAGGAAGGTCCGGAGTACTGGGACGGCGAAACCCGTAAGGTTAAAGCGCACA
GCCAAACCCACCGTGTGGATCTGGGTACCCTGCGTGGCTGCTACAACCAGAGCGAGGCGGGTAGCCACACCG
TTCAACGTATGTATGGTTGCGACGTGGGCAGCGATTGGCGTTTCCTGCGTGGTTACCACCAGTACGCGTATGA
CGGCAAGGATTATATTGCGCTGAAAGAAGACCTGCGTAGCTGGACCGCGGCGGATATGTGCGCGCAAACCAC
CAAGCACAAATGGGAAGCGGCGCATGTTGCGGAACAGCTGCGTGCGTACCTGGAGGGTACCTGCGTGGAAT
GGCTGCGTCGTTATCTGGAGAACGGCAAGGAAACCCTGCAACGTACCGACGCGCCGAAAACCCACATGACCC
ACCATGCGGTGAGCGATCATGAGGCGACCCTGCGTTGCTGGGCGCTGAGCTTCTATCCGGCGGAGATCACCCT
GACCTGGCAGCGTGACGGCGAAGATCAGACCCAAGACACCGAGCTGGTTGAAACCCGTCCGGCGGGTGATG
GCACCTTTCAAAAGTGGGCGGCGGTGGTTGTGCCGAGCGGTCAGGAGCAACGTTATACCTGCCACGTGCAGC

ACGAAGGCCTGCCGAAACCGCTGACCCTGCGTTGGGAACCGGGTAGCGGTAGCGGCCTGAACGACATTTTTG
AAGCGCAGAAGATTGAGTGGCACGAATAAGGATCC-3‘

4.1.12.2. HLA-A*02:01 disulfide mutant heavy chain with C-terminal BirA sequence

5‘-
CATATGGGGTCACACAGTATGAGGTATTTCTTCACATCAGTTAGTAGGCCCGGAAGAGGGGAGCCGCGTTTCATTGCGGT
GGGTTACGTTGACGACACCCAGTTCGTTCGTTTTGACAGCGATGCGGCGAGCCAACGTATGGAACCGCGTGCGCCGTGG
ATTGAGCAGGAAGGTCCGGAGTACTGGGACGGCGAAACCCGTAAGGTTAAAGCGCACAGCCAAACCCACCGTGTGGATC
TGGGTACCCTGCGTGGCTGCTACAACCAGAGCGAGGCGGGTAGCCACACCGTTCAACGTATGTATGGTTGCGACGTGGG
CAGCGATTGGCGTTTCCTGCGTGGTTACCACCAGTACGCGTATGACGGCAAGGATTATATTGCGCTGAAAGAAGACCTGC
GTAGCTGGACCGCGGCGGATATGTGCGCGCAAACCACCAAGCACAAATGGGAAGCGGCGCATGTTGCGGAACAGCTGC
GTGCGTACCTGGAGGGTACCTGCGTGGAATGGCTGCGTCGTTATCTGGAGAACGGCAAGGAAACCCTGCAACGTACCGA
CGCGCCGAAAACCCACATGACCCACCATGCGGTGAGCGATCATGAGGCGACCCTGCGTTGCTGGGCGCTGAGCTTCTATC
CGGCGGAGATCACCCTGACCTGGCAGCGTGACGGCGAAGATCAGACCCAAGACACCGAGCTGGTTGAAACCCGTCCGGC
GGGTGATGGCACCTTTCAAAAGTGGGCGGCGGTGGTTGTGCCGAGCGGTCAGGAGCAACGTTATACCTGCCACGTGCAG
CACGAAGGCCTGCCGAAACCGCTGACCCTGCGTTGGGAACCGGGTAGCGGTAGCGGCCTGAACGACATTTTTGAAGCGC
AGAAGATTGAGTGGCACGAATAAGGATCC-3‘

4.1.12.3. HLA-A*02:01 disulfide mutant heavy chain with C-terminal His-Tag

5‘-
CATATGGGGTCACACAGTATGAGGTATTTCTTCACATCAGTTAGTAGGCCCGGAAGAGGGGAGCCGCGTTTCATTGCGGT
GGGTTACGTTGACGACACCCAGTTCGTTCGTTTTGACAGCGATGCGGCGAGCCAACGTATGGAACCGCGTGCGCCGTGG
ATTGAGCAGGAAGGTCCGGAGTACTGGGACGGCGAAACCCGTAAGGTTAAAGCGCACAGCCAAACCCACCGTGTGGATC
TGGGTACCCTGCGTGGCTGCTACAACCAGAGCGAGGCGGGTAGCCACACCGTTCAACGTATGTATGGTTGCGACGTGGG
CAGCGATTGGCGTTTCCTGCGTGGTTACCACCAGTACGCGTATGACGGCAAGGATTATATTGCGCTGAAAGAAGACCTGC
GTAGCTGGACCGCGGCGGATATGTGCGCGCAAACCACCAAGCACAAATGGGAAGCGGCGCATGTTGCGGAACAGCTGC
GTGCGTACCTGGAGGGTACCTGCGTGGAATGGCTGCGTCGTTATCTGGAGAACGGCAAGGAAACCCTGCAACGTACCGA
CGCGCCGAAAACCCACATGACCCACCATGCGGTGAGCGATCATGAGGCGACCCTGCGTTGCTGGGCGCTGAGCTTCTATC
CGGCGGAGATCACCCTGACCTGGCAGCGTGACGGCGAAGATCAGACCCAAGACACCGAGCTGGTTGAAACCCGTCCGGC
GGGTGATGGCACCTTTCAAAAGTGGGCGGCGGTGGTTGTGCCGAGCGGTCAGGAGCAACGTTATACCTGCCACGTGCAG
CACGAAGGCCTGCCGAAACCGCTGACCCTGCGTTGGGAACCGGGTAGCCACCACCACCACCACCACTAAGGATCC-3‘

4.1.12.4. β2m light chain

5‘-

CATATGATTCAGCGTACTCCGAAAATCCAGGTCTATTCCCGTCATCCAGCAGAAAACGGCAAATCCAACTTCCTGAACTGC
TACGTTTCTGGCTTTCATCCATCTGACATCGAAGTTGACCTCCTGAAAAACGGTGAACGCATCGAAAAAGTCGAACACTCT
GATCTGTCCTTCTCCAAAGACTGGTCTTTCTACCTCCTGTACTATACCGAGTTCACTCCAACTGAGAAAGACGAATACGCAT
GTCGTGTAAACCACGTAACTCTGTCTCAGCCGAAAATCGTGAAATGGGACCGTGATATGTGAGGATCC-3‘

4.1.12.5. 1G4 alpha chain

5‘-

ATGGAGACCCTCTTGGGCCTGCTTATCCTTTGGCTGCAGCTGCAATGGGTGAGCAGCAAACAGGAGGTGACACAGATTCC
TGCAGCTCTGAGTGTCCCAGAAGGAGAAAACTTGGTTCTCAACTGCAGTTTCACTGATAGCGCTATTTACAACCTCCAGTG
GTTTAGGCAGGACCCTGGGAAAGGTCTCACATCTCTGTTGCTTATTCAGTCAAGTCAGAGAGAGCAAACAAGTGGAAGAC
TTAATGCCTCGCTGGATAAATCATCAGGACGTAGTACTTTATACATTGCAGCTTCTCAGCCTGGTGACTCAGCCACCTACCT
CTGTGCTGTGAGGCCCACATCAGGAGGAAGCTACATACCTACATTTGGAAGAGGAACCAGCCTTATTGTTCATCCGTATAT
CCAGAACCCTGACCCTGCCGTGTACCAGCTGAGAGACTCTAAATCCAGTGACAAGTCTGTCTGCCTATTCACCGATTTTGA
TTCTCAAACAAATGTGTCACAAAGTAAGGATTCTGATGTGTATATCACAGACAAAACTGTGCTAGACATGAGGTCTATGG
ACTTCAAGAGCAACAGTGCTGTGGCCTGGAGCAACAAATCTGACTTTGCATGTGCAAACGCCTTCAACAACAGCATTATTC
CAGAAGACACCTTCTTCCCCAGCCCAGAAAGTTCCTGTGATGTCAAGCTGGTCGAGAAAAGCTTTGAAACAGATACGAAC
CTAAACTTTCAAAACCTGTCAGTGATTGGGTTCCGAATCCTCCTCCTGAAAGTGGCCGGGTTTAATCTGCTCATGACGCTG
CGGCTGTGGTCCAGCTGA-3’

4.1.12.6. 1G4 beta chain

5’-

ATGAGCATCGGCCTCCTGTGCTGTGCAGCCTTGTCTCTCCTGTGGGCAGGTCCAGTGAATGCTGGTGTCACTCAGACCCCA
AAATTCCAGGTCCTGAAGACAGGACAGAGCATGACACTGCAGTGTGCCCAGGATATGAACCATGAATACATGTCCTGGTA
TCGACAAGACCCAGGCATGGGGCTGAGGCTGATTCATTACTCAGTTGGTGCTGGTATCACTGACCAAGGAGAAGTCCCCA
ATGGCTACAATGTCTCCAGATCAACCACAGAGGATTTCCCGCTCAGGCTGCTGTCGGCTGCTCCCTCCCAGACATCTGTGT
ACTTCTGTGCCAGCAGTTACGTCGGGAACACCGGGGAGCTGTTTTTTGGAGAAGGCTCTAGGCTGACCGTACTGGAGGA
CCTGAAAAACGTGTTCCCACCCGAGGTCGCTGTGTTTGAGCCATCAGAAGCAGAGATCTCCCACACCCAAAAGGCCACAC
TGGTATGCCTGGCCACAGGCTTCTACCCCGACCACGTGGAGCTGAGCTGGTGGGTGAATGGGAAGGAGGTGCACAGTG
GGGTCAGCACAGACCCGCAGCCCCTCAAGGAGCAGCCCGCCCTCAATGACTCCAGATACTGCCTGAGCAGCCGCCTGAG
GGTCTCGGCCACCTTCTGGCAGAACCCCCGCAACCACTTCCGCTGTCAAGTCCAGTTCTACGGGCTCTCGGAGAATGACG
AGTGGACCCAGGATAGGGCCAAACCCGTCACCCAGATCGTCAGCGCCGAGGCCTGGGGTAGAGCAGACTGTGGCTTCAC
CTCCGAGTCTTACCAGCAAGGGGTCCTGTCTGCCACCATCCTCTATGAGATCTTGCTAGGGAAGGCCACCTTGTATGCCGT
GCTGGTCAGTGCCCTCGTGCTGATGGCCATGGTCAAGAGAAAGGATTCCAGAGGCTGA-3’

4.1.12.7. bs-868Z11-CD3 structure

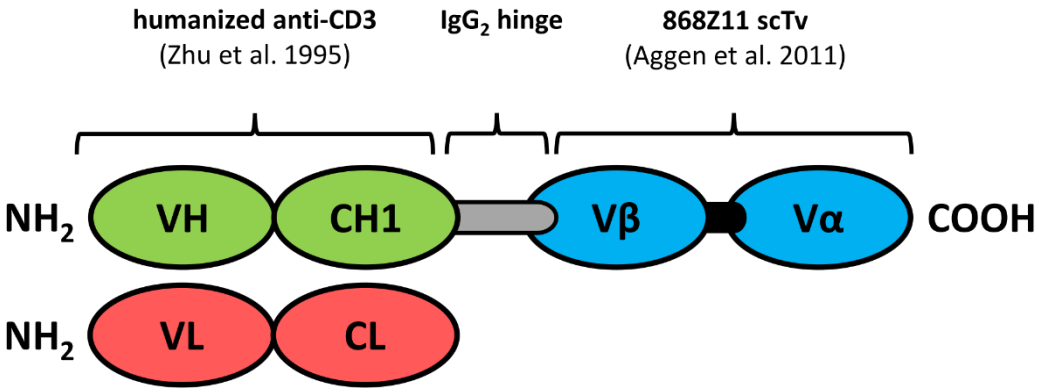

Fig. 4.3 Illustration of bsTCR bs-868Z11-CD3 construct.

The 868Z11 domain is based on the SLYNTVATL-reactive TCR 868 and incorporates affinity enhancing mutations in the CDR2β (YYEEEE to YVRGEE) and CDR3α region (CAVRTNSGYALN to CAVRGAHDYALN) identified by Varela-Rohena et al.(*106*). The Vβ and Vα domains of the affinity enhanced TCR were linked through a single chain linker (GSADDAKKDAAKKDGKS) and further modified with a surface stability conferring mutation in the Vα2 region (F49S) to allow for soluble expression by Aggen et al.(*107*). To create the bs-868Z11-CD3 molecule, this 868Z11 scTv domain was fused to the F(ab') heavy chain portion of a humanized anti-CD3 antibody through an IgG2 derived CH2 hinge domain (APPVAG) with two cysteine-knock-outs ($C_{226}S$ and $C_{229}S$), incorporated to prevent the formation of $F(ab)_2$ homodimers on expression.

4.1.13. Instruments

Table 4.19 List of instruments and the respective manufacturers used to conduct experiments.

Instrument name	Manufacturer
Snyergy2 Plate Reader	Biotek
Octet RED384	Molecular Devices (previously Fortébio)
AEKTA Pure	GE Healthcare
AEKTAprime plus	GE Healthcare
Syro II peptide synthesizer	Biotage
Viaflo 96/384 pipetting robot	Integra
iQue Screener flow cytometer	Intellicyt

Instrument name	Manufacturer
Nanodrop 8000 spectrophotometer	ThermoFisher Scientific
Table centrifuge 5425R for Eppendorf tubes	Eppendorf
Table centrifuge Megafuge 1.0R for conical tubes and plates	Heraeus
Superspeed centrifuge Sorvall Lynx 6000	ThermoFisher Scientific
Novaspec Plus Photometer	Amersham Biosciences
Chemidox XRS	Biorad
Minitron Incubation Shaker	Infors HT
Multitron Pro Incubation Shaker	Infors HT
Heratherm Oven	ThermoFisher Scientific
BBD6220 Incubator	ThermoFisher Scientific
Ultrafiltration stirred cell 8400	Merck Millipore
ECM 830 Square Wave Electroporation System	BTX
HT-200 Plate Handler	BTX
630B Safety Stand	BTX
ELx405 Plate Washer	Biotek
Veriti 96 well thermocycler	Applied Biosciences
QuadroMACS magnetic cell separator	Mylteni Biotec
E835 power supply	Consort
Xcell Sure Lock running chamber	ThermoFisher Scientific
366 nm UV lamp and chamber	CAMAG

4.1.14. Consumables

Table 4.20 List of consumables and the respecitve manufacturers used to conduct experiments.

Consumables name	Manufacturer
96 well plates round bottom	Corning, Cat. Nr. 3799
96 well plates flat bottom white	Brand,
96 well plates V-bottom	Greiner, Cat. Nr. 651201
96 well plate flat bottom black	
384 well plate tilted well	
Cell culture 24 well plates	Greiner, Cat. Nr. 662160
Cell culture flasks T25 / T75 / T125 / T175	Greiner, Cat. Nr.
Ultrafiltration membrane 30 kDa	Merck Millipore, Cat. Nr. PLTK07610
Steritop-GP Filtration Unit 250 ml/ 500 ml	Merck Millipore, Cat. Nr. SCGPT02RE / SCGPT05RE
Amicon Ultra-15 Ultracel 10K ultracentrifugation units	Merck Millipore, Cat. Nr. UFC903008
Vivaspin 15R, 30.000 MWCO Hydrosart	Sartorius, Cat. Nr. VS15RH21
Sartoclear Dynamics Lab V filtration kit	Sartorius, Cat. Nr. SDLV-0500-05C--2
Eppendorf tubes 1.5 / 2 / 5 ml	Eppendorf, Cat. Nr. 0030 120.159 / 0030 120.094 / 0030 119.401
15 ml conical tubes	Greiner, Cat. Nr. 227261
50 ml conical tubes	BD, Cat. Nr. 352096
Serological pipettes 5 / 10 / 25 / 50 ml	Corning, Cat. Nr. 4487/4488/4489/4490
BTX electroporation plates, 25-well	VWR, Cat. Nr. 732-0345
Electroporation cuvettes	VWR, Cat. Nr. 732-1137
LS columns	Miltenyi, Cat. Nr. 130-042-401

4.1.15. Software

Table 4.21 Software used for raw data collection, analysis and graphical display.

Software name	Developer
Prism 7	GraphPad
Data Analysis HT v11.0	Molecular Devices (previously Fortébio)
Data Acquisition v11.0	Molecular Devices (previously Fortébio)
Gen5 plate reader software	Biotek
Inkscape	-

4.1.16. Deposited structures

The crystal structure of the 1G4-DS-A*02:01-ESO-9V complex has been deposited in the Protein Data Bank under the accession number 6Q3S.

4.2. Chemical Methods

4.2.1. Peptide Synthesis

Peptides used for the described experiments were either produced in house (all wild type peptides, UV-cleavable peptide ligand, pSL9 PSL, peptides predicted to be cross-reactive for bs-868Z11-CD3, healthy tissue-based peptides) or obtained from Pepscan (pESO9V PSL, PS-SCL).

All peptides produced in house were synthesized using standard Fmoc chemistry with a Syro II peptide synthesizer. Peptides were subsequently analyzed using HPLC and had an average purity of 74%.

UV-light sensitive peptides contained a light-sensitive building block with a 2-nitrophenylamino acid residue.

Before use, peptides were dissolved in DMSO with 0.5% TFA at concentrations ranging from 2 mg ml^{-1} to 4 mg ml^{-1} depending on the desired use case, based on an average yield value determined previously for similar synthesis reactions.

All peptides obtained by Pepscan were delivered as crude lyophilized peptides with spot-checked HPLC analysis for the pESO9V PSL. Before use, peptides were dissolved in DMSO with 0.5% TFA at concentrations ranging from 2 mg ml^{-1} to 10 mg ml^{-1} depending on the desired use case, assuming an average 1.75 mg yield from a 2 µmol synthesis.

The dipeptide H-Gly-Met-OH (GM) was procured from Bachem, Cat. Nr.4001203.0025.

4.3. Molecular Biology Methods

4.3.1. *In Vitro* Transcription

For expression of desired T cell receptors in CD8+ T cells or Jurkat-NFAT effector cells, alpha and beta chain encoding mRNA was produced using amplified DNA templates and an *in vitro* transcription reaction. All steps were performed in matching PCR or RNA workstations using DEPC-treated nuclease free water.

The template DNA for 1G4 alpha and beta chain was amplified using a Takara Primestar HS DNA polymerase kit from the respective sequences previously cloned into the pGEM-3Z vector, including a Kozak sequence between the T7 promoter and the TRAV or TRBV sequence (in-house development). A 64 bp poly-A tail was added through the reverse primer.

Table 4.22 List of primers and their respective sequence used for template DNA amplification of 1G4 sequences. Primers synthesized by Sigma.

Primer name	Sequence
Forward-Primer 1G4 alpha	5'-AATAATACGACTCACTATAGGGAGAGCCGCCACCATGGAGACCCTCTTGGGCCTG-3'
Forward-Primer 1G4 beta	5'-AATAATACGACTCACTATAGGGAGAGCCGCCACCATGAGCATCGGCCTCCTGTG-3'
Reverse-Primer 1G4	5'-$(T)_{64}$CCTAGGTGCATCACGTGTGC-3'

Table 4.23 Composition of template DNA amplification mix.

Component	Volume (µl)
5X PrimeSTAR Buffer (Mg^{2+} plus (5mM))	10.2
dNTPs (2.5 mM each)	4
F-Primer alpha oder beta (10 µM)	1
R-Primer (10 µM)	1
PrimeSTAR HS DNA Polymerase (2.5 U $µl^{-1}$)	0.5
DNA Template (2 ng $µl^{-1}$)	1
DEPC-H_2O	33.3

Table 4.24 PCR protocol for template DNA amplification.

Step	Time (s)	Temperature (°C)	Cycle number
Denaturation and polymerase activation	60	98	1
Denaturation	15	98	5
Annealing	5	54	
Elongation	70	72	
Denaturation	15	98	30
Annealing	5	60	
Elongation	70	72	
Cooling	∞	4	1

After the amplification, the remaining plasmid DNA was digested by adding 10 µl of the restriction enzyme DpnI diluted in Cut Smart Buffer according to manufacturer's instruction to each PCR reaction and incubating for 1 h at 37°C. Template DNA was then isolated using ethanol precipitation: 6 µl of NaOAc, 3M pH 4.5-5.2 was added to each digestion following 167.5 µl 96% ethanol solution prechilled to -20°C and then incubated for at least 30 minutes or over-night at -20°C. Following the incubation, samples were centrifuged at 4°C for 20 to 30 min at 16000 x g. Supernatant was carefully removed and 150 µl prechilled 70% ethanol solution added, mixed and once more centrifuged for 20 to 30 min at 16000 x g. Supernatant was removed and pellet air dried before resuspension in DEPC-H_2O. DNA concentration was measured on a Nanodrop 8000 using the DNA-50 program. Obtained templated DNA was also analyzed using agarose electrophoresis with a 1% gel and 1 µl of DNA template with 5 µl Orange G loading buffer.

In vitro transcription was performed using the mMESSAGE mMACHINE T7 transcription kit, containing the T7 enzyme matching the T7 promoter present in the DNA template. For each *in vitro* transcription reaction mix, 0.3 to 1 µg of template DNA was added.

Table 4.25 Composition *in vitro* transcription mix.

Component	Volume (µl)
DEPC-H_2O (µl)	4
2x NTP/CAP (µl)	10
10x Reaction Buffer (µl)	2
Template DNA (µl)	2
T7 Enzyme Mix (µl)	2

Reaction mixtures were incubated for 2 hours at 37˚C. Afterwards, template DNA was digested by adding 1 µl of TURBO DNase to each sample and further incubation at 37˚C for 15 minutes. Produced mRNA was then isolated by adding 30 µl of the LiCl precipitation solution to each samples and incubation at -20˚C for at least 20 minutes or over-night. Following the incubation, samples were centrifuged at 4°C for 20 to 30 min at 16000 x g. Supernatant was carefully removed and 150 µl prechilled 70% ethanol solution added, mixed and once more centrifuged for 20 to 30 min at 16000 x g. Supernatant was removed and pellet air dried before resuspension in DEPC-H_2O. FNA concentration was measured on a Nanodrop 8000 using the RNA-40 program. Obtained templated DNA was also analyzed using denaturing agarose electrophoresis with a 1% gel and 1 µl of RNA product with 5 µl Gel loading buffer II.

4.4. Cell Biology Methods

4.4.1. T cell activation assays

4.4.1.1. Cultivation of T2 target cell line

The TAP-deficient HLA-A*02:01-expressing cell line T2 was procured from ATCC (CRL-1992) at passage number 2 and cultured in Jurkat Assay Medium. Assuming a 24-hour doubling rate, individual flasks were split to remain below a $2x10^6$ cells ml^{-1} concentration before the next split and receive a media exchange at least every 4 days. Cells were kept in culture up until passage number 16 before fresh culture start from a passage 6 working bench.

4.4.1.2. Cultivation of Jurkat-NFAT effector cell line

The GloResponse NFAT-RE-luc2 Jurkat cell line (Jurkat-NFAT) was procured from Promega (Cat. Nr. CS1764) at passage number 6 and cultured in Jurkat Culture Medium, which included hygromycin B to ensure ongoing expression of the reporter gene.

Assuming a 24-hour doubling rate, individual flasks were split to remain below a $2x10^6$ cells ml^{-1} concentration before the next split and receive a media exchange at least every 4 days. Cells were kept in culture up until passage number 14 before fresh culture start from a passage 9 working bench.

4.4.1.3. Freezing and thawing of Jurkat-NFAT or CD8+ T cells

For thawing of Jurkat-NFAT cells, PBMCs or CD8+ T cells, cryotubes were removed from liquid nitrogen and stored on dry ice until quick thawing at 37°C in a water bath. Thawed cell suspensions were transferred quickly to 15 ml conical tubes containing CTL-Wash buffer supplemented with 0.1% L-Glutamine 200 nM and 50 U ml^{-1} benzonase.

4.4.1.4. Cellularly expressed T cell receptors

4.4.1.4.1. T cell receptor expression and activation using Jurkat-NFAT cell line

4.4.1.4.1.1. Electroporation of Jurkat T cells

For expression of desired TCRs in Jurkat-NFAT effector cells using mRNA, Jurkat-NFAT T cells were electroporated in presence of respective alpha and beta chain encoding mRNA mixtures. To that end, Jurkat-NFAT cells were either harvested from ongoing cell culture or directly after thawing from -80°C storage. After washing twice with PBS, the cells were resuspended in prechilled X-Vivo as electroporation buffer to achieve a final concentration of 2×10^7 cells ml^{-1}. Shortly before the electroporation, 250 µl cell suspension each were mixed with the mRNA cocktail, prepared containing roughly 7 µg mRNA per chain and prepared in a separate RNA workstation, and electroporated using a 500 V and 3 ms long pulse on an ECM830 square wave electroporator. Electroporation was either performed in single cuvettes or using 25 well electroporation plates. Individual cell suspensions were then transferred into 24 well plates, each well containing 1.5 ml pre-warmed JAM with 1 µg ml^{-1} DNase. Plates were incubated for 18-20 h at 37°C, 5% CO_2 before harvesting to assemble coincubation experiments.

In the case of mock electroporations serving as controls, X-Vivo was supplemented in place of the mRNA cocktail. All steps were performed under sterile conditions in a laminar flow hood.

4.4.1.4.1.2. Coincubation

To perform coincubation experiments using either TCR expressing or mock Jurkat-NFAT cells, T2 cells were harvested from continuous cell culture, washed and resuspended in T2 culture medium at a concentration of 1×10^6 cells ml^{-1} and transferred to 96 well round bottom plates. Peptides solved in DMSO, 0.5% TFA were added to desired final concentration and the suspension incubated for 2 to 3 hours at 37°C, 5% CO_2.

After peptide loading, T2 cells were resuspended and 50 µl distributed to white 96 well flat bottom plates. 50µl of the respective Jurkat-NFAT cells were then added at a concentration of 1 x 10^6 cells ml^{-1} for a final effector to target ratio of 1:1 (50.000 cells each). Fully assembled plates were mixed for 5 minutes at 300 rpm on a plate shaker and the incubated for 18 to 20 hours at 37°C, 5% CO_2.

4.4.1.4.1.3. Luciferase Readout

After the incubation period, 50 µl of Bio-Glo luciferase reagent was added to each well and the plates incubated for 5 minutes at 300 rpm on a plate shaker in the dark before reading luminescence as relative light units (RLU) at a 0.5 second integration time with a Synergy2 plate reader.

4.4.1.4.2. T cell receptor expression and activation using CD8+ T cells

4.4.1.4.2.1. PBMC isolation

PBMCs from HLA-A*02:01 positive donors were isolated from leukapheresis products procured directly after collection from the DRK Mannheim. Received samples were diluted at a 1:1 ratio with DPBS and carefully layered on 15 ml Biocoll separating solution for density gradient separation. Samples were centrifuged carefully without brake for 20 minutes at 800 g and room temperature. Afterwards, plasma was discarded, and the interphase transferred to 50 ml conical tubes. Interphase was washed once, and the supernatant discarded. Pellets were resuspended in DPBS, 1% HAS and counted using a Neubauer counting chamber and Tuerk's solution and trypan blue to determine cell numbers. Isolated PBMCs were then used directly for CD8+ T cell isolation or prepared for prior freezing.

In the case of freezing, the samples were pelleted once more, discarding the supernatant and resuspending in RPMI1640, 11.5% HSA. Shortly before aliquoting and freezing, RPMI1640, 11.5% HSA, 20% DMSO was added dropwise to the cell suspension at 1:1 volume to volume ratio. Cell solutions were then distributed into cryotubes and frozen at -80°C in Mr. Frosty isopropanol freezing containers before transfer to liquid nitrogen storage.

4.4.1.4.2.2. CD8+ T cell isolation by MACS enrichment

Isolation of CD8+ T cells from PBMCs by MACS enrichment was performed according to manufacturer's instructions. In short, cell suspensions were washed once with cold Auto-MACS buffer. After centrifugation, supernatant was discarded, and pellets resuspended in Auto-MACS buffer containing Anti-CD8 MACS beads in the refrigerator for 15 minutes. After the incubation, cells were washed once and then resuspended in Auto-MACS buffer and transferred to pre-equilibrated LS enrichment columns placed in a Quadro MACS.

Individual columns where washed three times with 3 ml Auto-MACS buffer each before elution into 15 ml conical tubes using 5 ml buffer and the provided plungers.

4.4.1.4.2.3. Stimulation and electroporation of CD8+ T cells

For expression of desired TCRs in CD8+ T cells using mRNA, CD8+ T cell samples isolated from PBMC samples of healthy donors were subjected to two different incubation and stimulation steps before electroporation in presence of respective alpha and beta chain encoding mRNA mixtures. To that end, CD8+ T cell samples were thawed as described previously and subjected to an over-night resting phase in TCM with 0.1 µl ml^{-1} IL-2 at a concentration of 1 x 10^7 cells ml^{-1} and 37°C, 5% CO_2. After the resting phase, the samples were transferred into cell culture flasks or 24 well plates previously coated with an anti-CD3 antibody. Coating was performed at 4°C over-night with 10 µg ml^{-1} antibody in PBS and wells or flasks were washed three times with PBS before transfer of the cell suspensions. For the stimulation, soluble anti-CD28 antibody at 0.1 µg ml^{-1} and 30 U ml^{-1} IL-2 were also added to the cell suspension. Stimulation was carried out for 3 days at 37°C, 5% CO_2 and 1 x 10^7 cells ml^{-1}. After stimulation, cell suspensions were harvested, washed in PBS with 1% HSA, resuspended in prechilled X-Vivo as electroporation buffer to achieve a final concentration of 2 x 10^7 cells ml^{-1}. Shortly before the electroporation, 250 µl cell suspension each were mixed with the mRNA cocktail, containing roughly 7 µg mRNA per chain and prepared in a separate RNA workstation, and electroporated using a 500 V and 3 ms long pulse on an ECM830 square wave electroporator. Electroporation was either performed in single cuvettes or using 25 well electroporation plates. Individual cell suspensions were then transferred into 24 well plates, each well containing prewarmed 1.5 ml TCM with 1 µg ml DNase I and 0.1 µl ml IL-2. Plates were incubated for 18-20 h at 37°C, 5% CO_2 before harvesting to assemble coincubation experiments.

In the case of mock electroporations serving as controls, X-Vivo was supplemented in place of the mRNA cocktail. All steps were performed under sterile conditions in a laminar flow hood.

4.4.1.4.2.4. Coincubation

To perform coincubation experiments using either TCR expressing or mock CD8+ T cells, T2 cells were harvested from continuous cell culture, washed and resuspended in T2 culture medium at a concentration of 1 x 10^6 cells ml^{-1} and transferred to 96 well round bottom plates. Peptides solved in DMSO, 0.5% TFA were added to desired final concentration and the suspension incubated for 2 to 3 hours at 37°C, 5% CO_2. After peptide loading, T2 cells were resuspended and 50 µl distributed to white 96 well flat bottom plates. 50 µl of the respective Jurkat-NFAT cells were then added at a concentration of 1 x 10^6 cells ml^{-1} for a final effector to target ratio of 1:1 (50.000 cells each).

Fully assembled plates were mixed for 5 minutes at 300 rpm on a plate shaker and the incubated for 18 to 20 hours at 37°C, 5% CO_2. After incubation, cells were pelleted by centrifuging for 2 min at 677 x g, 2 x 75 µl supernatant transferred into 96 well V-bottom plates and frozen at -80°C until ELISA readout.

4.4.1.4.2.5. IFN-gamma ELISA

IFN-gamma ELISA readout to determine concentration in harvested supernatant was performed using an ELISA MAX Deluxe IFN-gamma kit according to manufacturer instructions with minor modifications. Washing steps were performed using an ELx405 plate washer. The IFN-gamma standard delivered with the kit was replaced with recombinant human IFN-gamma protein procured separately from Abcam and the standard concentration range extended, from 2000 pg ml^{-1} to 15.6 pg ml^{-1} in a 1:2 dilution series. Supernatant samples were diluted 1:5 in assay diluent before incubation and the HRP reaction stopped by addition of 2N H_2SO_4. Standard curve was calculated for each plate individually based on IFN-gamma standard duplicates with a 4PL curve fit using the Gen5 software.

4.4.1.5. Bispecific T cell engager analysis using Jurkat-NFAT cell line

4.4.1.5.1. Coincubation

To perform coincubation experiments using bs-868Z11-CD3, T2 cells were harvested from continuous cell culture, washed and resuspended in T2 culture medium at a concentration of 3.3 x 10^6 cells ml^{-1} and transferred to 96 well round bottom plates. Peptides solved in DMSO, 0.5% TFA were added to desired final concentration and the suspension incubated for 2 to 3 hours at 37°C, 5% CO_2. After peptide loading, T2 cells were resuspended and 25 µl distributed to the white 96 well flat bottom plates with bsTCR dilutions and GloResponse™ NFAT-luc2 Jurkat cells for a final effector to target ratio of 1:1 (75.000 cells each). Fully assembled plates were mixed for 5 minutes at 300 rpm on a plate shaker and the incubated for 18 to 20 hours at 37°C, 5% CO_2.

4.4.1.5.2. Luciferase Readout

After the incubation period, 75 µl of Bio-Glo luciferase reagent was added to each well and the plates incubated for minutes at 300 rpm on a plate shaker in the dark before reading luminescence as relative light units (RLU) at a 0.5 second integration time with a Synergy2 plate reader.

4.4.1.6. Flow cytometric T2 peptide binding assay

T2 cells were harvested from continuous cell culture, washed and resuspended in T2 culture medium at a concentration of 3.3 x 10^6 cells ml^{-1} and transferred to 96 well round bottom plates.

Peptide in DMSO, 0.5% TFA was added to a final concentration of 10 µM and the suspension incubated for 2 hours 37˚C, 5% CO_2. Plates were washed twice with PFEA before addition of 50 µl PE labelled anti-human HLA-A2 per well diluted 1:250 with PFEA to a final concentration of 0.8 µg/ml. Plates were incubated at 4˚C for 30 minutes before being washed twice with PFEA. Finally, cells were resuspended in fixation solution (PFEA, 1% formaldehyde) and kept at 4˚C before analysis using an iQue Screener. T2 cells were gated based on the FSC-A/SSC-A signal and doublets removed using an FSC-H/FSC-A doublet exclusion. The PE channel positive gate coordinates were based on an unstained control. Data was plotted using GraphPad Prism v7.

4.5. Biochemical Methods

4.5.1. Protein biochemistry

4.5.1.1. MHC complex production

4.5.1.1.1. Inclusion body production & purification

Recombinant heavy chains for either HLA-A*02:01 wild type or disulfide mutants, containing a C-terminal BirA signal sequence or a His-tag, as well as human β_2m light chain were produced in *E. coli* as inclusion bodies and purified as previously described (*94*). In short, the respective chains embedded in a pET-3a vector were transfected into competent BL21(DE3)pLysS by heat shock transformation and positive clones picked after selective growth over night at 37˚C on ampicillin and chloramphenicol containing LB-agar plates. Clones were used to inoculate low-salt LB medium with the same antibiotics for an over-night preculture in an incubation shaker. The next day, 20 ml preculture was transferred into 1 l medium in culture flasks and further incubated. OD_{600} was measured to identify the reach of a mid-log growth phase, between 0.5 and 0.6, the preferred starting point for inclusion body production by IPTG addition. 5 hours after IPTG addition, cells were harvested using superspeed centrifugation, pellets resuspended in cold DPBS and frozen at -80˚C for at least overnight. Cell suspension were then homogenized using an ultrasound device. After centrifugation, resulting pellets were cleared of cell debris through five washing steps with triton wash buffer, resuspension and repeated centrifugation. After removal of all debris, remaining inclusion bodies washed once more with resuspension buffer and the remaining pellets incubated in urea buffer overnight. Concentration of the final product was determined using the Nanodrop 8000 and the specific extinction coefficient based on the primary amino acid sequence, purity was confirmed using SDS-PAGE.

4.5.1.1.2. Wild type HLA-A*02:01 refolding

HLA-A*02:01 complex refolding reactions were performed as previously described with minor modifications(*94*).

In brief, wild type HLA-A*02:01 heavy chain, β_2m light chain, and peptide were diluted in MHC injection buffer, injected using a syringe into MHC refolding buffer. Refolding reactions were incubated for 2 to 8 days at 4°C while stirring and then concentrated using ultrafiltration stirred cells and 30 kDa filtration membranes. The concentrate was then purified by size exclusion chromatography (SEC) with TBSA SEC running buffer on an AEKTAprime plus system using a HiLoad 26/600 75 pg column. Protease inhibitors PSMF, leupeptin and pepstatin were added to combined monomer fractions and subsequently concentrated to 2000 µg ml^{-1} with Amicon Ultra-15 ultracentrifugation units, aliquoted and frozen at -80°C or biotinylated by BirA biotin-protein ligase either overnight at 4°C or 27°C according to the manufacturer's instructions and subjected to a second gel-filtration before concentration and aliquotation.

For the wild type HLA-A*02:01 peptide-MHC complexes, either nonameric and HLA-A*02:01 associated peptides or UV light-sensitive full-length peptides were added to the refolding buffer at a concentration of 30 µM.

4.5.1.1.3. Disulfide-stabilized HLA-A*02:01 refolding

HLA-A*02:01 refoldings using the disulfide mutant heavy chains were performed similarly to the wild type refoldings. For the disulfide-stabilized refoldings, the dipeptide GM was added to the refolding buffer at a concentration of 10 mM.

4.5.1.1.4. Peptide loading

Peptide loading reactions with functionally empty DS-A2 MHC complexes were performed by addition of desired peptides to a monomer solution kept on ice with at least a 100:1 molar ratio of peptide to MHC complex. After addition, solutions were mixed immediately, removed from ice and incubated for at least 5 minutes at room temperature. MHC complex concentrations during loading ranged from 25 to 500 µg ml^{-1}.

4.5.1.1.5. UV exchange

Peptide exchange reactions with UV light-cleavable peptides were performed as previously described(*100*). In short, desired nonameric peptides were mixed with biotinylated UV light-sensitive pMHC complexes at 100:1 molar ratio and subjected to at least 30 minutes of 366 nm UV light.

4.5.1.2. Soluble TCR production

4.5.1.2.1. Inclusion body production & purification

1G4 TCR alpha chain was mutated at position 48 by replacing a threonine with a cysteine and TCR beta chain at position 57 by replacing a serine with a cysteine to form an inter-chain disulfide bond as previously described (*108*, *109*). Gene fragments were ordered and ligated into the pET-3a vector by Genscript using Bam HI and Nde I restriction sites. Prior to refolding, TCR alpha and TCR beta chain were produced separately in as inclusion bodies and purified similarly to the process for HLA-A*02:01 heavy and light chain.

4.5.1.2.2. Soluble TCR refolding

Soluble TCRs were produced as previously described (X). In short, purified 1G4 alpha and beta chain were diluted in TCR injection buffer and injected using a syringe into TCR refolding buffer. TCR refoldings were incubated over night at 4˚C while stirring and then transferred into dialysis membranes for dialysis against MilliQ-H_2O. After 24 hours, MilliQ-H_2O was exchanged with 10 mM Tris, pH 8 buffer and incubated for another 24 hours. The TCR refolding was then filtrated using Steritop filter cups and concentrated on an AEKTAprime plus system using a POROS HQ 50 µM anion exchange column. Concentrated protein was eluted using a 1.2M NaCl in 10 mM Tris, pH 8 gradient and further concentrated to 5 ml or less for SEC with Amicon Ultra-15 ultracentrifugation units. After SEC using a HiLoad 26/600 75 pg column, monomer fractions were combined, further concentrated again and the buffer exchanged for a HEPES/Tween buffer during that step. Aliquots were frozen at –80˚C with concentrations between 2 and 10 mg ml^{-1}. Protein concentration was determined using a Nanodrop 8000 and a protein specific extinction coefficient determined with ExPASy ProtParam based on the primary amino acid sequence.

4.5.1.3. Bispecific T cell engager production

The bs-868Z11-CD3 molecule was generated by linking the scTv 868Z11 to the C terminus of the F(ab')-domain of a humanised anti-CD3 antibody (*110*). To this end, the V_β domain of the scTv was directly fused to the upper CH2 region derived from human IgG_2 (APPVAG). Cysteine-knockouts $C_{226}S$ and $C_{229}S$ were introduced in the hinge to prevent the formation of $F(ab)_2$ molecules.

4.5.1.3.1. CHO expression

HCMV promoter-driven expression vectors pMH2 (in-house construct of standard genetic elements) containing either the sequence for the construct described above or the light chain of the humanised anti-CD3 antibody were procured from Genscript and transiently co-transfected in ExpiCHO cells according to the manufacturer's instructions.

24 hours after transfection, feed was added and cells were incubated at 32°C, 5% CO_2 in manufacturer recommended Corning shake flasks. After 12 days, the supernatant was harvested and filtered using a Sartoclear Dynamics Lab V filtration kit with 0.22 µm filters after addition of 0.1% NaN_3.

4.5.1.3.2. bsTCR purification

The cleared supernatant was processed by tandem affinity chromatography on an AEKTApure chromatography system: protein was first captured using a HiTrap Protein L column and, after elution with 84.4 mM citrate, 31.2 mM Na_2HPO_4, pH 2.8, automatically loaded onto a Superdex 200 pg 16/600 column equilibrated with DPBS. Monomer fractions were pooled and further concentrated using Vivaspin 15R, 30.000 MWCO Hydrosart centrifugal concentrators. After 0.22 µm filtration of the concentrate, protein concentration was determined using a Nanodrop 8000 and a protein specific extinction coefficient determined with ExPASy ProtParam based on the primary amino acid sequence.

4.5.1.4. Protein crystallography and imaging

The DS-A2/pESO9V complex and the 1G4 TCR were concentrated and mixed in a 1:1 ratio to achieve a concentration of 7 mg ml^{-1} for crystallization. A sitting drop vapor diffusion experiment resulted in crystals in the presence of a mother liquor containing 0.1 M ammonium acetate, 0.1 M bis-tris pH 5.5, 17% PEG 10.000. A single crystal was transferred to a cryo-protectant solution containing 0.1 M ammonium acetate 0.1 M bis-tris pH 5.5, 20% (w/v) PEG 10.000, and 10% glycerol. The crystal was mounted and cryo-cooled to 100 K on the EMBL P14 beamline at DESY containing an EIGER 16M detector. An X-ray data set was collected to a resolution of 2.5 Ångström (Table S1). The data were processed with XDS and scaled with AIMLESS(*111*, *112*). Molecular replacement was performed using MOLREP with the coordinates of the TCR portion of the native complex first, followed by the peptide/MHC complex (PDB 2BNR), and the structure was refined with REFMAC5(*113*, *114*). The engineered disulphide bond was manually built with Coot(*115*). The structure was refined to an R factor of 22.9% (Rfree 27.3%). Molprobity was used to validate the geometry and indicated 93.9% of the residues were in the allowed regions of the Ramachandran plot (with one glycine residue (Gly 143) in the disallowed regions)(*116*).

4.5.1.5. Gel electrophoresis

4.5.1.5.1. SDS PAGE

To perform denaturing SDS PAGE, 4 µg of each MHC monomer were mixed with 12 µl TBSA, 2.2 µl NuPAGE LDS sample reducing agent 10x and 5.4 µl NuPAGE LDS sample buffer 4x and incubated for 10 min at 95°C before cooling to room temperature for 5 minutes. Precast NuPAGE 10% Bis-Tris gels were mounted in the running chamber, loaded with MES SDS Running buffer 1x and 15 µl of the

denatured sample added to the respective well. 10 µl SeeBlue Plus2 Prestained Standard 1x was loaded as well and a 200 V current applied for 20 minutes. Afterwards, gels were washed for 10 minutes in deionized water, then stained using 30 ml Coomassie staining solution by quick heating in the microwave and 30 to 60 min incubation on room temperature, then washed quickly in deionized water and destained through multiple incubation steps in destaining solution (10% glacial acetic acid, 40% ethanol and 50% deionized water). After desired staining was achieved, gels were analyzed on a ChemiDoc XRS+ system using Image Lab software.

4.5.1.5.2. Native PAGE

To perform a native PAGE, 4 µg of the respective monomers were either mixed with 12 µl TBSA or 12 µl streptavidin and incubated for 1 h at room temperature. Afterwards, 14 µl Novex Tris-Glycine Native Sample Buffer 2x was added and 15 µl loaded into wells of a precast Novex WedgeWell 10-20% Tris-Glycine Mini gel mounted in a running chamber loaded with Novex Tris-Glycine Native Running Buffer 1x. 10 µl SeeBlue Plus2 Prestained Standard 1x was loaded as well and a 125 V current applied for 4 h. Afterwards, gels were washed and stained identically to SDS PAGE experiments.

4.5.1.5.3. Agarose gel electrophoresis

To perform agarose gel electrophoresis, a 1% agarose gel was cast by adding 100 ml 1x TAE buffer to 1 g agarose and heating in a microwave until solved. After cooling to 60˚C, 4 µl PeqGREEN dye was added, the solution well mixed and transferred to a gel carrier with combs. After solidifying, individual chambers were loaded with 7 µl sample in Orange G loading buffer or 7 µl 1 kb DNA ladder. Gels were transferred into running chamber with 1x TAE running buffer and 10V cm^{-1} voltage applied for 20 minutes. Gels were analyzed on a ChemiDoc XRS+ system using Image Lab software.

4.5.1.5.4. Denaturing agarose gel electrophoresis

To perform denaturing agarose gel electrophoresis, a 1% denaturing agarose gel was cast by adding 72 ml 1x TAE buffer to 1 g agarose and heating in a microwave until solved. After initial cooling, 10 ml 10x MOPS buffer and 18 ml formaldehyde, 37% was added as well as 4 µl PeqGREEN dye. The solution well mixed and transferred to a gel carrier with combs. After solidifying, individual chambers were loaded with 7 µl sample in Gel loading buffer II or 5 µl peqGOLD High Range RNA ladder. Before loading, samples were denatured by incubation for 10 min at 75˚C and 2 minutes cooling on ice. Gels were transferred into running chamber with 1x MOPS running buffer and 7V cm^{-1} voltage applied for 30 minutes. Gels were analyzed on a ChemiDoc XRS+ system using Image Lab software.

4.5.2. Bio-layer Interferometry Measurements

The affinity of sTCR or bsTCR molecules for different pMHC complexes was measured on an Octet RED384 system using kinetic or steady state binding analysis. All analytes or ligands were diluted to their final concentration in kinetics buffer (PBS, 0.1% BSA, 0.05% Tween-20) if not specified otherwise. All biosensors were hydrated for at least 10 minutes in kinetics buffer before use. Loadings and measurements were performed in 384 tilted well plates with at least 40 µl at a 3 mm sensor offset. Plate temperature was set at 25˚C and shaker speed at 1000 rpm. To allow inter-step correction, baselines before association phases and the following dissociation phase were performed in the same well. Kinetics buffer was used as dissociation buffer with DMSO at an appropriate concentration added if necessary, to match the analyte composition. All sensorgrams were analyzed using the Octet RED384 system software "Data Analysis HT" version 11.0. Raw sensor data was aligned at the Y axis by aligning the data to the end of the baseline step, and inter-step correction was used to align the start of the dissociation to the end of the association phase. No Savitzky-Golay filtering was applied. Resulting sensorgrams were then fitted using a 1:1 Langmuir kinetics binding model.

4.5.2.1. Streptavidin immobilization

In the case of pMHC immobilization using biotin-streptavidin interaction, dip and read streptavidin (SA; Pall Fortébio Cat. Nr. 18-5021) biosensors were used to immobilize biotinylated pMHC monomers at a presumed concentration of 25 µg ml^{-1} for 60 seconds followed by a 60 second baseline and association and dissociation phases of 60 seconds each if not specified otherwise.

4.5.2.2. Anti-FAB2G immobilization

In the case of bsTCR immobilization, dip and read anti-human Fab-CH1 2nd generation (FAB2G; Pall Fortébio Cat. Nr. 18-5127) biosensors were used to immobilize bsTCR molecules at a concentration of 100 µg ml^{-1} for 60 seconds followed by a 15 second baseline and 60s phases of association and dissociation each if not specified otherwise. FAB2G biosensors were regenerated up to 4 times by incubating the loaded biosensor for 5 seconds each in 10 mM Glycine pH1.5 and kinetics buffer consecutively for three times. FAB2G were also pre-conditioned that way before their first ligand immobilization.

4.5.3. Data plotting and statistical analysis

All data was plotted using the GraphPad Prism software version 7. Correlation between x and y data sets were calculated by computing the Pearson correlation coefficient and are reported as r squared using the GraphPad Prism software version 7.

5. Results

5.1. Disulfide-stabilized HLA-A2 molecules as novel tool for pMHC complex generation

5.1.1. Introduction

This chapter describes the production of a functionally empty HLA-A*02:01 mutant stabilized by an artificially introduced disulfide bridge and focuses on the characterization of said mutant as a suitable tool to generate peptide-MHC libraries representative of wild type complexes. This work was performed in close collaboration with Prof. Sebastian Springer and his group at the Jacobs University Bremen, who conceptualized the disulfide bridge and provided an initial refolding protocol.

5.1.2. Inclusion body preparation and refolding of disulfide-stabilized HLA-A*02:01 molecules

A disulfide bond was introduced into the MHC class I HLA-A*02:01 peptide binding cleft F-pocket by mutation of the tyrosine residue Y84 and alanine residue A139 to cysteine respectively. The sequence containing the mutated positions and the target sequence for the biotinylating enzyme was cloned into the pET3a vector (Genscript) and transfected into BL21(DE3) competent *E. coli* by heat shock transformation. After IPTG induced protein expression, inclusion body collection and purification, a significantly enriched protein fraction compared to a pre-induction sample with an expected size of roughly 38 kDa could be obtained (Fig. 5.1).

The obtained HLA-A*02:01 Y84C / A139C heavy chain was used with similarly produced β_2m in a refolding reaction without peptide to produce empty disulfide-stabilized HLA-A*02:01 molecules (DS-A2). While aggregates could be observed by size exclusion chromatography (SEC) of the refolding reaction, no UV peak was observed at the expected elution volume compared to a conventional refolding, using the wild type heavy chain and a 9 amino acid long full-length peptide. In contrast, a refolding reaction with the mutated heavy chain and the HLA-A*02:01 presented peptide EBV BLMF-$1_{280\text{-}288}$ GLCTLVAML (pEBV) produced similar results compared to the wild type refolding (Fig. 5.2 a).

Based on previous discovery by Sebastian Springer, the dipeptide H-Gly-Met-OH (GM) was added to the refolding reaction as refolding assistant to facilitate the refolding without full length peptide(*98*).

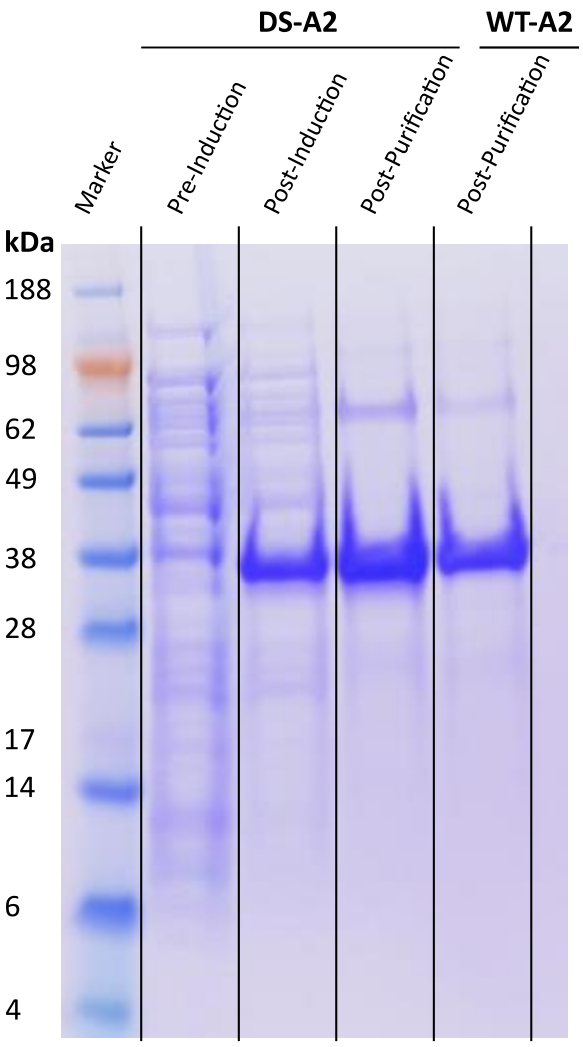

Fig. 5.1 SDS-Page analysis of *E. coli* culture samples during various stages of inclusion body production.

SEC purification of this refolding attempt revealed a UV peak at elution volumes indicative of correctly refolded HLA-A*02:01 monomers. This was the case for purification of the refolding reaction on a FPLC system with a high concentration of dipeptide in the SEC buffer, maintaining this aspect of the refolding reaction, and a system without added dipeptide (Fig. 5.2 b). Purified monomer from both purifications with and without dipeptide in the SEC buffer were harvested and biotinylated overnight at 27˚C using the BirA enzyme. Second SEC purification yielded monomer associated peaks only for the purification with dipeptide present, albeit with a significant aggregate peak at an earlier elution volume, and only an aggregate peak for the purification strategy without dipeptide in the SEC buffer (Fig. 5.2 c).

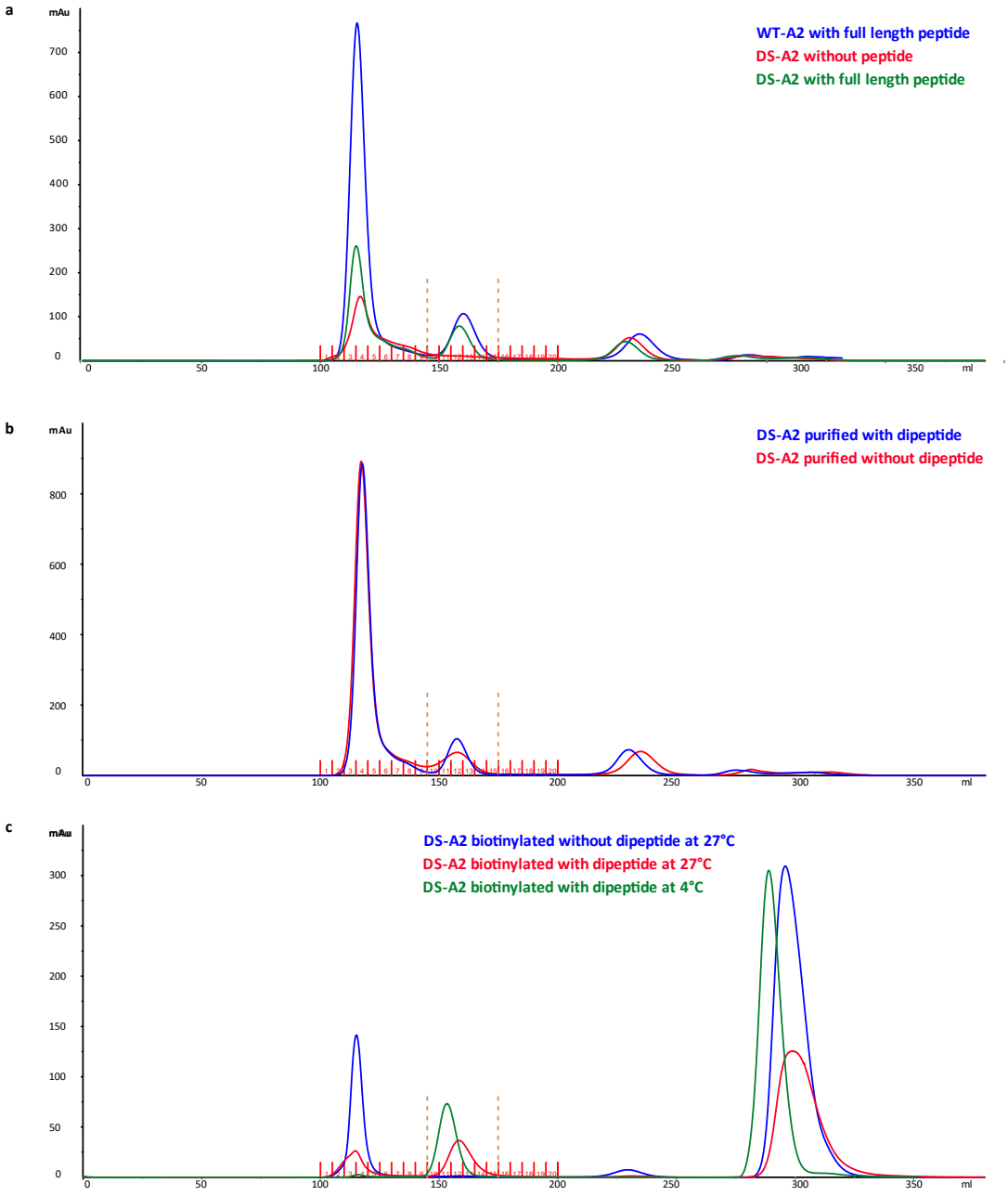

Fig. 5.2 SEC elution profiles of HLA-A*02:01 refoldings using different heavy chain constructs and peptides. Dotted lines mark collected monomer fractions. (a) Comparison of SEC elution profiles for wild type HLA-A*02:01 refolded with a nonameric full-length peptide antigen and DS-A2 mutant with and without full length peptide. (b) Comparison of SEC elution profiles between DS-A2 initially refolded with dipeptide and then purified with or without dipeptide in the SEC buffer. (c) Comparison of SEC elution profiles after biotinylation using either a 27°C protocol with or without dipeptide and a 4°C protocol with dipeptide present in the reaction mixture.

Under the assumption that a correctly folded monomer was obtained with both primary purification attempts, but stability at room temperature was decreased for the dipeptide free purification of a then presumably empty HLA-A*02:01 monomer, dipeptide was added directly to the biotinylation reaction of a previously dipeptide free purified monomer. In addition, the biotinylation was performed at a lower temperature of 4°C and a higher BirA concentration. This strategy resulted in a much higher monomer yield and less visible aggregation based on the SEC purification results. Collected fractions were further concentrated and stored at -80°C.

To confirm that the collected fractions contained purified biotinylated HLA-A*02:01 monomers, Native PAGE was performed using the DS-A2 mutant, either refolded with full length peptide or dipeptide and biotinylated with the 27°C or revised 4°C biotinylation protocol.

A conventional wild type HLA-A*02:01 monomer refolded with the HLA-A*02:01 presented 10mer peptide Melan-A $MART1_{26-35}$ ELAGIGILTV (pMLA) served as control. All monomers were loaded onto the gel directly or after a 30 min incubation with streptavidin (Fig. 5.3).

Bands correlating with the expected size of 47 kDa could be detected for the full-length peptide refoldings, but only a diffuse band pattern resulted from the dipeptide refoldings. Since the temperature significantly increases during the gel electrophoresis run due to the applied voltage, it was hypothesized that this might cause degradation of the presumably-empty monomer similar to the behaviour observed after biotinylation.

To test this hypothesis and check whether the presumably empty DS-A2 was able to bind a peptide ligand after refolding, the peptides pEBV and pMLA previously used for refolding were added to different samples prior to native PAGE. The band patterns resulting from this peptide loading attempt were very similar to those from the wild type monomer sample, supporting the temperature degradation hypothesis and hinting that the presumably empty state of the monomer could be regarded as functionally empty.

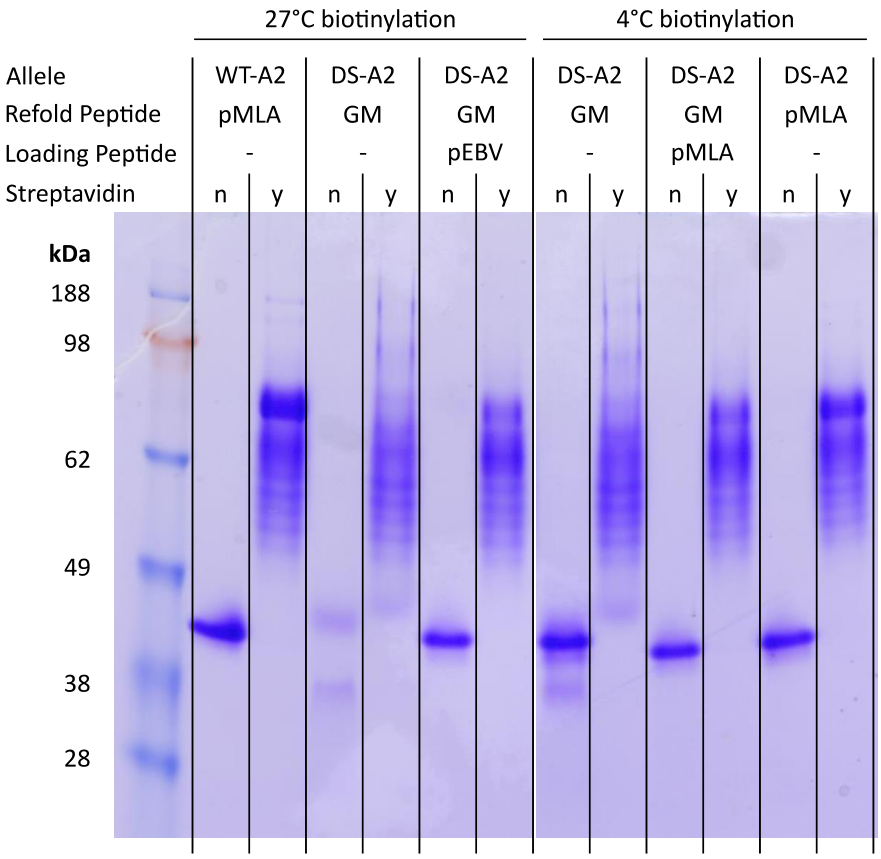

Fig. 5.3 Native-Page analysis of collected and concentrated monomer fractions after biotinylation of various refolded MHC complexes. Streptavidin was added to produce multimers, preferentially tetramers. Loading peptide represents addition of the respective 9mer peptide to presumably-empty DS-A2 refoldings to retroactively produce peptide-MHC complexes.

5.1.3. Comparison of TCR binding kinetics with wild type and disulfide-stabilized pMHC complexes

To further corroborate whether the presumably empty HLA molecule could be regarded as functionally-empty and to identify potential consequences of the introduced disulfide bond if present, its interaction as peptide-MHC complex with the TCR compared to wild type HLA-A*02:01 complexes was examined.

For this purpose, the 1G4 TCR, which demonstrates a strong binding affinity for the HLA-A*02:01 presented NY-ESO-$1_{157\text{-}165}$ peptide SLLMWITQC (pESO9C) or its synthetic variant SLLMWITQV (pESO9V), was produced as soluble TCR (sTCR) by expression of disulfide bridge stabilized version the alpha and beta chains as inclusion bodies in *E. coli* and refolding based on the work by Boulter et al. (Fig. 5.4)(*108*, *117*).

The purified sTCR was then used for kinetic analysis of the interaction with pESO9V peptide-MHC complexes, either as a conventionally refolded wild type HLA-A*02:01 molecule or as DS-A2 molecule peptide loaded after refolding.

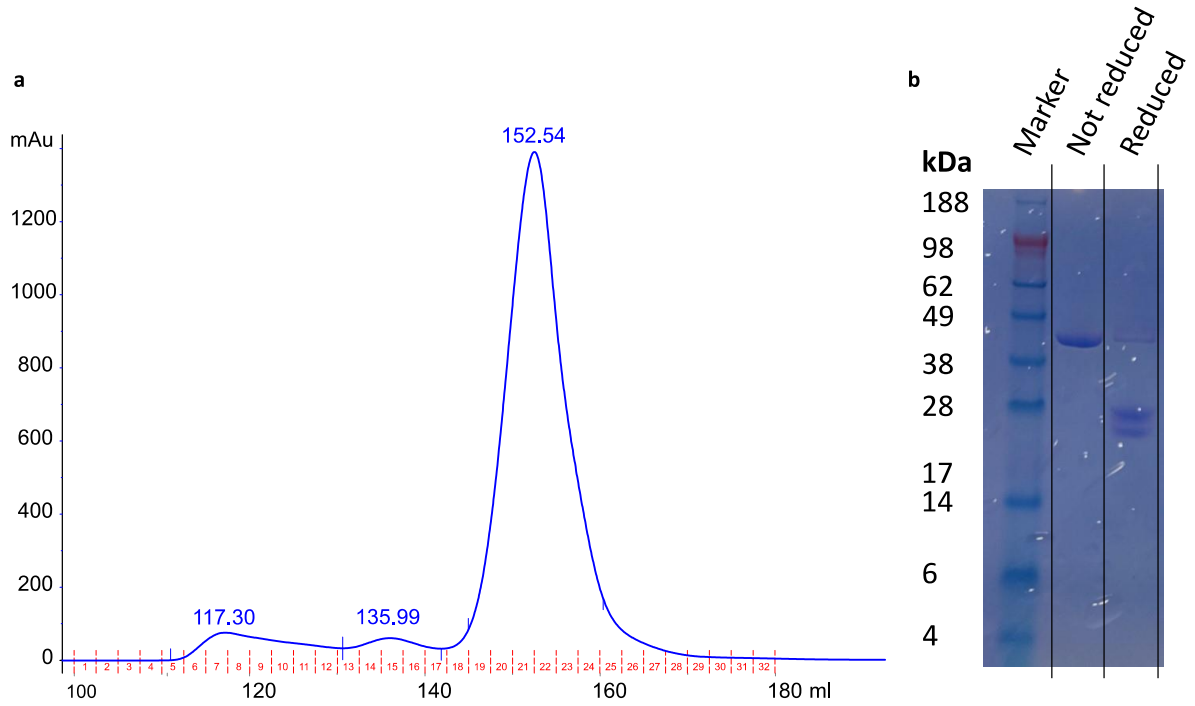

Fig. 5.4 Analysis of soluble TCR refolding for 1G4. (a) SEC elution profile of soluble TCR refolding. The peak with the mean elution volume of 152.54 ml was collected as monomer fraction. (b) SDS-PAGE analysis of the monomer fraction. Bands matching the theoretical sizes of the individual chains, 23 kDa for the alpha chain and 29 kDa for the beta chain, could be detected in the reduced sample.

Binding kinetics measurements were performed by bio-layer interferometry (BLI) on an Octet RED384 using the as soluble analyte. Biotinylated DS-A2 was immobilized on streptavidin-coated biosensors after 5 minutes of incubation with the peptide ESO 9V. Wild type ESO 9V, non-peptide loaded DS-A2 and the non 1G4 recognized HLA-A*02:01 presented epitope HIV-1 p17 $GAG_{77\text{-}85}$ SLYNTVATL (pSL9) were similarly immobilized and binding kinetics measured for all across a 1:2 dilution series of 1G4 concentrations (24 µM to 375 nM).

1G4 TCR binding to either DS-A2 or WT-A2 pESO9V was very similar with respect to sensorgrams and dissociation constants (K_D) identified by curve fittings, indicating successful peptide loading as well as no interference of the disulfide bridge with TCR binding (Fig. 5.5 a and b). A weak binding signal (but no dissociation) could be detected for the functionally-empty immobilized DS-A2 monomer at high concentrations of 1G4 (Fig. 5.5 c) which was not observed for the negative control pHIV1 pMHC (Fig. 5.5 d).

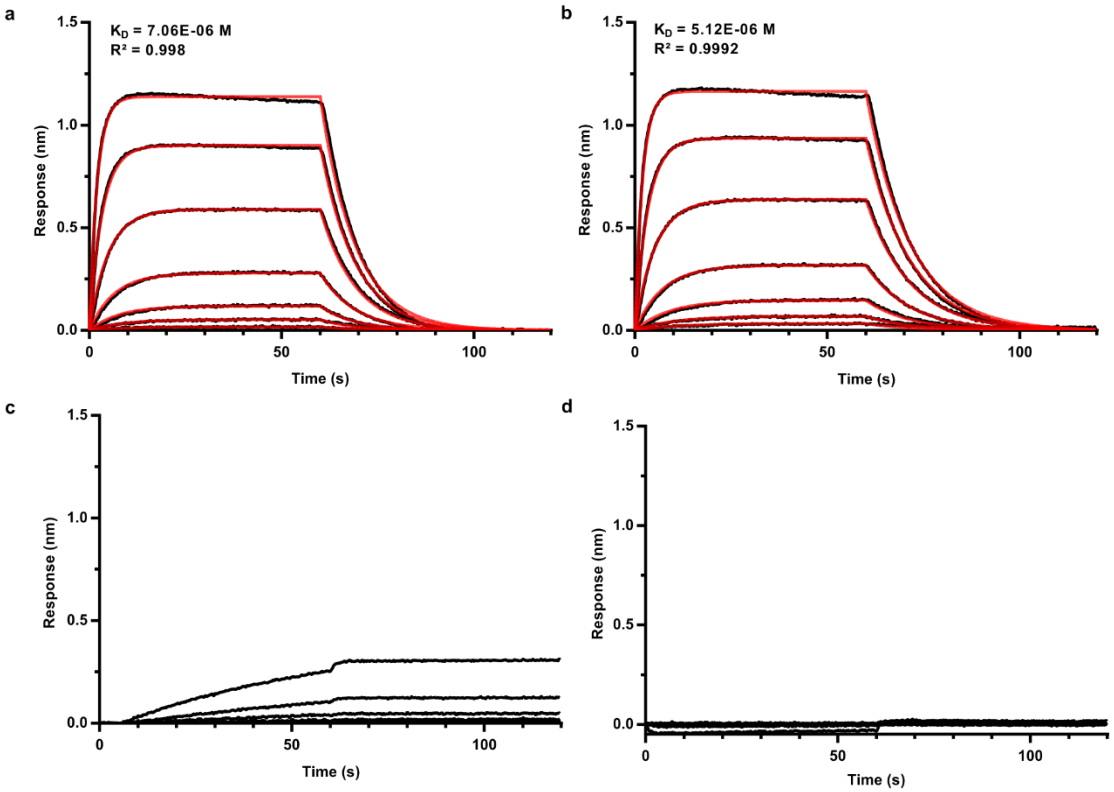

Fig. 5.5 Association and dissociation behavior of the 1G4 sTCR with different pMHC complexes. Raw data is displayed in black, curve fittings in red. All measurements performed as 1:2 analyte dilution series starting at 24 µM. (a) Binding curve of the 1G4 TCR against immobilized pESO9V DS-A2 pMHC. (b) Binding curve of the 1G4 TCR against immobilized pESO9V WT-A2 pMHC. (c) Binding curve of the 1G4 TCR against immobilized empty DS-A2. (d) Binding curve of the 1G4 TCR against immobilized pSL9 DS-A2 pMHC.

While these measurements hinted at the existence of the introduced disulfide bond, explaining its retained stability and peptide loading capacity, they presented only indirect evidence. To directly visualize the disulfide bond, crystallization and structural analysis of the complex between DS-A2 pESO9V peptide-MHC and the 1G4 sTCR was attempted. To that end, multiple conditions screened using a 1:1 pMHC to sTCR ratio and sitting vapor drop diffusion experiment at the EMBL Outstation in Hamburg. A single crystal from one successful condition was then analyzed at the EMBL P14 beamline, yielding an X-ray dataset with a resolution of 2.5 Ångström.

The disulfide bridge linking both alpha helices of the peptide binding pocket could be observed, and the peptide was situated similarly in the binding pocket compared to a WT-A2 ESO 9V structure deposited in the PDB. Overall, comparison of the crystal structures revealed a high degree of structural overlap between both the pESO9V WT-A2 and DS-A2 complexes: The backbone of both HLA-A*02:01 molecules aligned almost perfectly with a rmsd value of 1.14 Å calculated over C_α (Fig. 5.6 a). The same was true for both bound peptides including their side chains with a rmsd value of 1.27 Å calculated over all atoms, even when in close vicinity to the disulfide bond (Fig. 5.6 b).

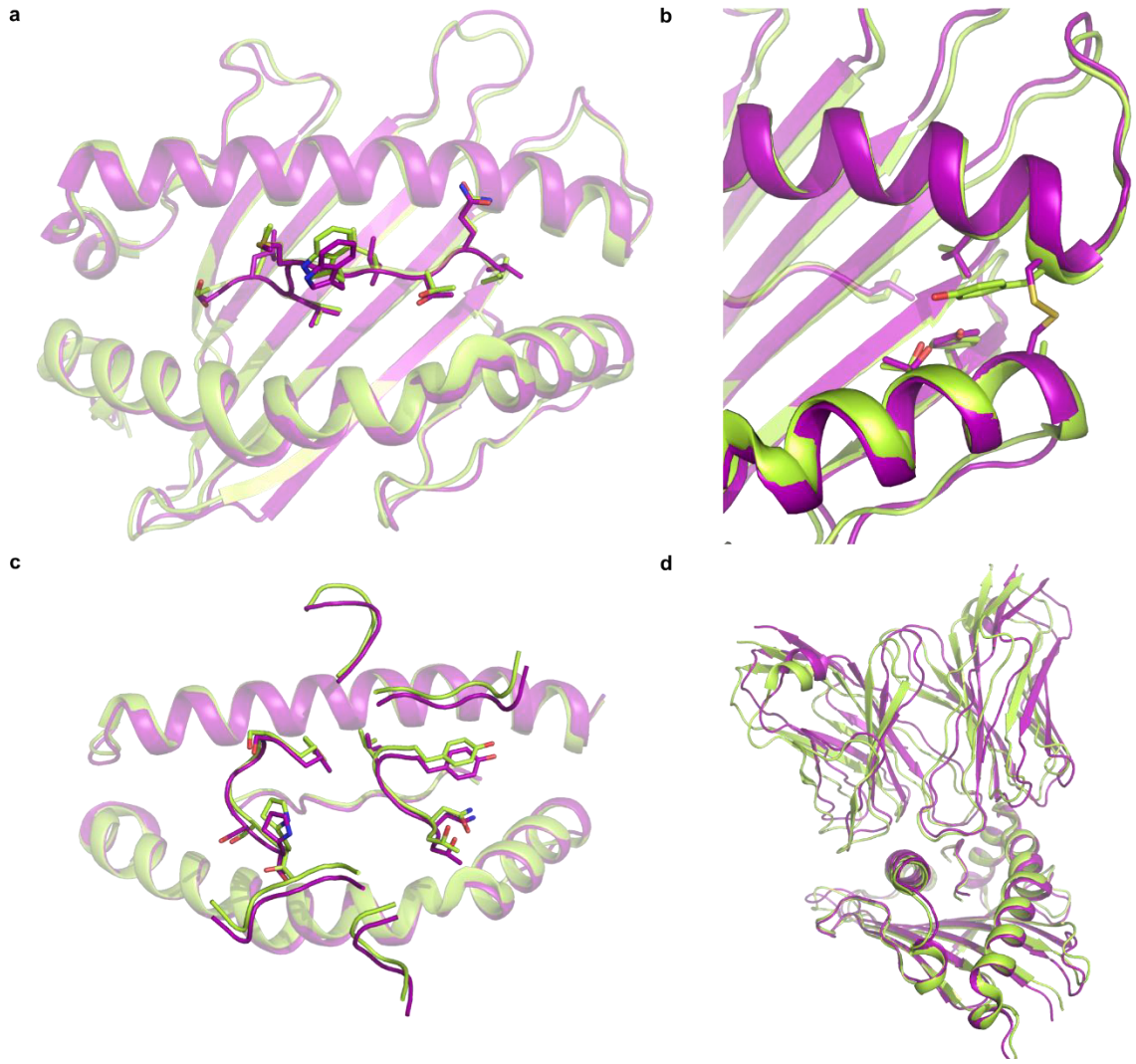

Fig. 5.6 Crystal structure of pESO9V DS-A2 and pESO9V WT-A2 in complex with 1G4. (a) Overlay of WT and DS-A2 structure with focus on peptide and amino acid side chain orientation. (b) Closeup of the F-pocket and the introduced disulfide bond between α_1 and α_2. (c) Overlay of the 1G4 CDR loops interacting with the peptide and the MHC backbone. (d) Overlay of both crystal structures from a lateral perspective.

Similar conclusions could be made for the interaction with the 1G4 TCR. The CDR loop regions interacting with the peptide and the MHC backbone did show slight deviations of the interface and a small change in the docking angle of 4.13, when comparing pESO9V-WT-A*02:01-1G4 with the pESO9V-DS-A*02:01-1G4 crystal structure. This shift was still within the range of expected deviations for the same complex when crystallized repeatedly (Fig. 5.6 c and d).

Although the crystal structure offered no evidence that the introduction of the disulfide bond had implications for the interaction with a TCR, altering the kinetics compared to a wild type peptide-MHC, this could very well be different with other peptide ligands or TCRs. To expand this comparison towards a higher number of peptides covering a broader range of binding affinity constants the bsTCR bs-868Z11-CD3 was employed as a second soluble TCR analyte. This molecule is comprised of the single chain TCR 868Z11, an affinity maturated TCR recognizing the HLA-A*02:01 presented peptide pSL9 with antibody-like affinity, linked to a humanized anti-CD3 antibody functioning as T cell engaging domain.

First, binding kinetics measurements were performed to analyze binding of bs-868Z11-CD3 to the designated pSL9 pMHC target complex. Conventionally refolded WT-A2 pSL9 peptide-MHC molecules or pSL9 peptide-loaded DS-A2 molecules were immobilized on streptavidin biosensors and binding kinetics measured with soluble bs-868Z11-CD3. Binding affinity for pSL9 DS-A2 pMHC was similar to the pSL9 WT-A2 pMHC with 2.35 nM and 3.24 nM, respectively (Fig. 5.7 a and b).

In a second step, a positional scanning library was synthesized based on the peptide pSL9, resulting in 162 distinct peptides that were to result in a broad range of different binding affinities by bs-868Z11-CD3 when displayed as peptide-MHC complexes. These were created using the respective peptides by either peptide loading onto DS-A2 or by performing an UV light-mediated peptide ligand exchange. The peptide-MHC complexes generated with the respective methods were then immobilized onto streptavidin biosensors and binding kinetics measured using two bs-868Z11-CD3 concentrations.

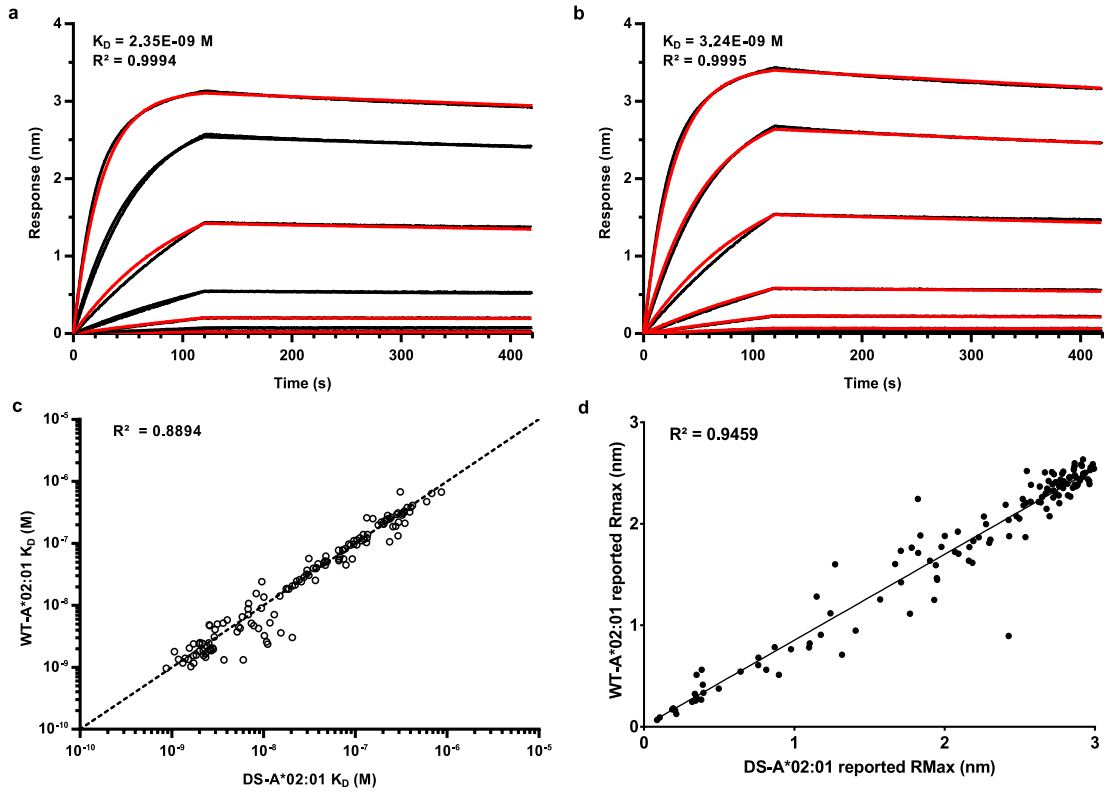

Fig. 5.7 Binding kinetics screening results of the pSV9 specific bs-868Z11-CD3 bsTCR with different MHC monomers and peptide ligands. (a) Binding curve of bs-868Z11-CD3 against immobilized pSL9 DS-A2 pMHC. Raw data is displayed in black, curve fittings in red. Measured using 1:2 analyte dilution series starting at 500 nM. (b) Binding curve the bs-868Z11-CD3 against immobilized pSL9 WT-A2 pMHC. Raw data is displayed in black, curve fittings in red. Measured using 1:2 analyte dilution series starting at 500 nM. (c) Correlation between affinities measured using DS-A2 pMHCs or WT-A2 pMHC complexes generated using UV-exchange. K_Ds were plotted for 140 different peptide ligands generated using both methods and measured during successive experiments. K_Ds were fitted using 500 nM and 158 nM analyte concentrations. Peptides were included if peak signal levels reached at least 0.05 nM for both concentrations and individual fits had a R^2 above 0.9. The in-picture R^2 is the calculated correlation coefficient, dashed line represents optimal 1:1 ratio. (d) Correlation between Rmax values reported using DS-A2 pMHCs or WT-A2 pMHC complexes generated using UV-exchange.

The measurements revealed binding affinities covering a 1000-fold range from single digit nM to single digit µM K_ds, reaching the lower sensitivity threshold of this measurement setup. To compare the affinity constants calculated with DS-A2 or WT-A2 generated for each respective peptide, all measurements were selected for curve fitting that had evaluable curves at both analyte concentrations and curve fitting results accompanied by R^2 values of at least 0.9. K_D values for the resulting 140 peptide ligands correlated well across the whole range (Fig. 5.7 c, Table S2, Table S3).

Discrepancies were within 2-fold range for over 90% of the pMHC pairs and 6.82-fold differences at most. Within the group with higher than 2-fold changes, a trend towards a larger dissociation constant for measurements with the DS-A*02:01 molecule was observed. The amount of functional pMHC immobilized on each biosensor expressed by the reported Rmax value was equally comparable for both wild type and disulfide-stabilized pMHCs (Fig. 5.7 d).

5.1.4. Summary

Based on the results of the performed experiments, the production of the disulfide-stabilized HLA-A*02:01 complex using the dipeptide assisted was successful, yielding a molecule capable to perform quick and refolding independent peptide loading reactions as well as to generate relevant kinetic interaction data with TCR ligands compared to the wild type molecule.

5.2. Characterization of the peptide-MHC binding preferences of cellularly expressed T cell receptors

5.2.1. Introduction

This chapter describes and evaluates different experimental strategies to characterize TCR candidates with respect to their peptide-MHC binding when cellularly expressed. Focus was on identifying a suitable effector cell type for expression of TCRs as well as selection of an appropriate readout and as cross-reactivity screening strategies suitable for routine practical application.

5.2.2. Screening of T cell receptors using cellular expression and T cell activation assays with peptide loaded target cells

5.2.2.1. Comparison of a CD8+ T cell assay and Jurkat-NFAT reporter assay system

Expression of a TCR of interest in a vehicle closely matching the intended therapeutic application and measuring its response to a stimulus through an appropriate readout is probably the most common way to analyze and characterize TCRs. Selection of these four variables, effector cell type, means of TCR expression, target cell type and readout, is of crucial importance as it significantly influences the feasibility and possible scope of experiments as well as the significance of the results for the intended purpose.

To enable quick screening of multiple TCR candidates in an early development phase, effector cell generation by electroporation of TCR alpha and beta chain encoding mRNA was combined with target cell generation by peptide pulse loading of HLA-A*02:01 positive T2 cells. In a first step, the well-established approach of using CD8+ T cells as effector cells, isolated by CD8-targeted magnetic activated sorting (MACS) from donor PBMC samples and combined with an IFN-g ELISA readout, was compared to a T cell activation assay using the genetically engineered Jurkat T cell line (Jurkat-NFAT), which expresses a luciferase reporter gene activated by an NFAT-response element and can be easily cultivated(*118*).

To compare both strategies with respect to sensitivity of detection and quantification of T cell activation in response to peptide-MHC stimulation as well as ranking of the strength of the interaction, the 1G4 TCR was selected for both assays and tested against 12 different peptides, consisting of pESO9V and 11 variants carrying different single amino acid substitutions. These peptides were expected to result in a broad range of T cell activation based on previous assays. Jurkat-NFAT cells were directly electroporated either after thawing or harvesting from ongoing cell cultures whereas isolated CD8+ T cells were subjected to a 3-day anti-CD3/CD28 stimulation beforehand.

For both approaches, roughly 7 µg of TCR alpha and beta chain encoding mRNA each were electroporated per 5 million effector cells. CD8+ T cells from two different donors were tested to identify donor specific effects, e.g. by native TCRs. After electroporation, both effector cell types were incubated for 18h with T2 cells, loaded with 6 different concentrations for each peptide, in a 1:1 effector to target ratio.

The luciferase readout was performed directly after the incubation period whereas the supernatant of the CD8+ cell coincubations was harvested, frozen at -80°C and later analyzed using an IFN-g ELISA. For both Jurkat-NFAT and CD8+ T cells, mock electroporations containing no mRNA were used as negative control.

Overall, responses covering a broad spectrum of T cell activation, characterized by different absolute activation levels as well as peptide loading concentration dependent changes of T cell activation, could be detected in all three assays (Fig. 5.8). For some interactions, T cell activation was notably lower at higher peptide loading concentrations, a potential sign of overstimulation and anergy caused by high affinity interactions. The CD8+ T cell-based assays were very sensitive, with activation detectable at concentration levels as low as 10 pM, e.g. for the interaction with pESO9V.

In comparison, the Jurkat-NFAT assay was slightly less sensitive, roughly matching the activation pattern of the CD8+ assay offset by one peptide dilution step. On the flipside, the background generated by the mock electroporation when judged as fold increase compared to the 1G4 electroporations was significantly lower compared to the CD8+ approach. Here, IFN-g secretion was actually increased in some of the mock controls compared to the 1G4 electroporations at lower peptide loading concentrations. The mock electroporations of donor HBC-657 did also exhibit stimulation by the 9I, 9C and 5G amino acid substitution variants.

To compare how the responses would have been ranked according to strength in each separate assay, the interactions were sorted based on either the EC50 values determined using a nonlinear regression 4PL curve fit or based on the response at one peptide loading concentration selected to be equally meaningful (Table 5.1).

Based on the fitted EC50 values, ranking by strength of the TCR-pMHC interaction would have been similar with both CD8+ and Jurkat-NFAT based approaches, despite the higher sensitivity of the CD8+ T cell-based assay. Changes in position were mostly limited to increases or decreases by one rank in the direct comparison, but this behaviour was in line with the changes observed within the CD8+ based approach when using cells from different donors.

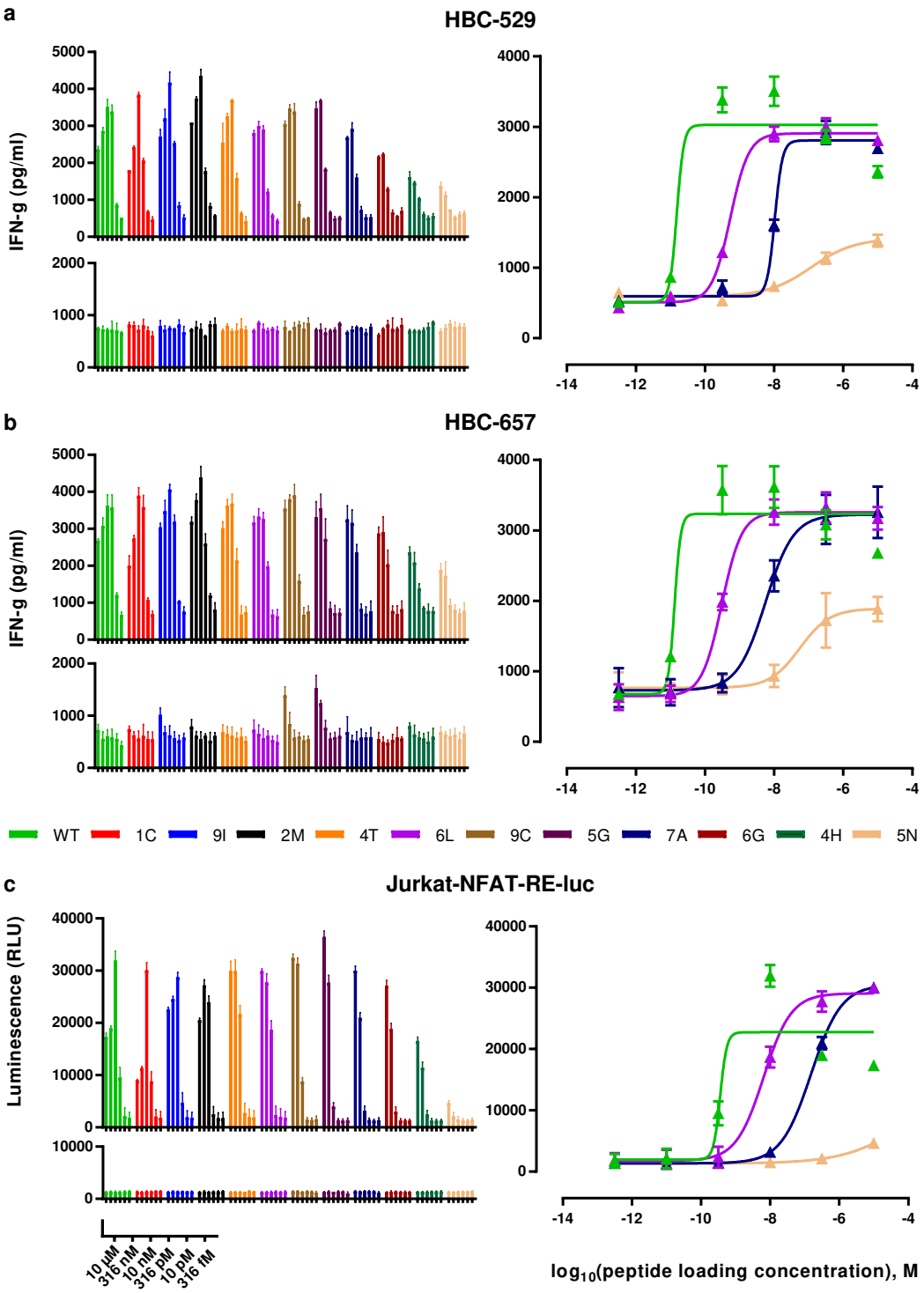

Fig. 5.8 1G4-mediated T cell activation in response to 12 different peptides loaded on target cells determined using CD8+ T cells and IFN-g ELISA or a Jurkat-NFAT luciferase reporter assay. HBC-657 and Jurkat-NFAT data represent biological triplicates, HBC-529 data biological duplicates. Peptides were loaded at 6 different concentrations, individual bars for each peptide are sorted in decreasing concentration. (a) IFN-g secretion of electroporated CD8+ T cells from PBMC donor HBC-529. CD8+ T cells were electroporated in presence of 1G4 mRNA (top left) or with electroporation buffer as mock control (bottom left). Example for IFN-g secretion plotted against log-transformed peptide loading concentrations for 4 peptides used for EC50 curve fitting (right). (b) IFN-g secretion analysis for CD8+ T cells from donor HBC-657. (c) Luciferase produced luminescence readout of electroporated Jurkat-NFAT cells.

Table 5.1 Ranking of 1G4-mediated T cell activation by the 12 peptide sample dataset from high to low activation based on the individual assays.

		WT	1C	9I	2M	4T	6L	9C	5G	7A	6G	4H	5N
HBC-529	EC50	1.5 E-11	2.5 E-10	2.2 E-10	3.6 E-10	3.2 E-10	5.4 E-10	4.7 E-10	1.1 E-08	1.0 E-08	1.1 E-08	1.3 E-08	1.2 E-07
	EC50 ranking	**1**	**3**	**2**	**5**	**4**	**6**	**7**	**10**	**8**	**9**	**11**	**12**
	Response 316 pM (pg/ml)	3384	2062	2530	1778	1585	1217	895	665	722	663	614	533
	Response ranking	**1**	**3**	**2**	**4**	**5**	**6**	**7**	**9**	**8**	**10**	**11**	**12**
HBC-657	EC50	1.3 E-11	1.3 E-11	5.9 E-11	3.0 E-10	3.1 E-10	3.1 E-10	3.9 E-10	4.3 E-09	5.6 E-09	8.2 E-09	2.4 E-08	5.5 E-08
	EC50 ranking	**2**	**1**	**3**	**4**	**6**	**5**	**7**	**8**	**9**	**10**	**11**	**12**
	Response 316 pM (pg/ml)	3532	3711	3239	2690	2087	2017	1615	873	775	742	861	766
	Response ranking	**2**	**1**	**3**	**4**	**5**	**6**	**7**	**8**	**10**	**12**	**9**	**11**
Jurkat	EC50	3.6 E-10	3.3 E-10	4.7 E-10	7.3 E-10	5.1 E-09	6.5 E-09	2.5 E-08	1.1 E-07	1.5 E-07	1.5 E-07	1.6 E-07	9.2 E-05
	EC50 ranking	**2**	**1**	**3**	**4**	**5**	**6**	**7**	**8**	**9**	**10**	**11**	**12**
	Response 10 nM (RLU)	32859	29976	28302	23520	21991	17984	8471	3622	2752	2585	2070	1185
	Response ranking	**1**	**2**	**3**	**4**	**5**	**6**	**7**	**8**	**9**	**10**	**11**	**12**

As an alternative to the calculation of the EC50 value, which requires a relatively large range of concentrations and is also not entirely ideal due to the observed inhibition at higher peptide loading concentrations, ranking by the response to the 10 nM peptide loading concentration for the Jurkat-NFAT assay and 316 pM for the CD8+ assay produced similar results.

Due to the similar ranking results compared to the established assay combined with its practical advantages, the Jurkat-NFAT assay was selected as effector cell and readout combination for the cross-reactivity screenings.

5.2.2.2. Strategies to identify pMHC-TCR binding patterns

Various cross-reactivity screening strategies have been suggested in the literature to improve the safety before *in vivo* clinical use. Employing the 1G4 TCR, three of these strategies were tested using the previously outlined screening system to directly compare their results.

5.2.2.2.1. Alanine Scanning

To perform the alanine screening, the pESO9V peptide as well as the 9 single alanine substitution peptides were incubated at three concentrations with T2 target cells and incubated with 1G4 expressing Jurkat-NFAT cells as previously described (Fig. 5.9).

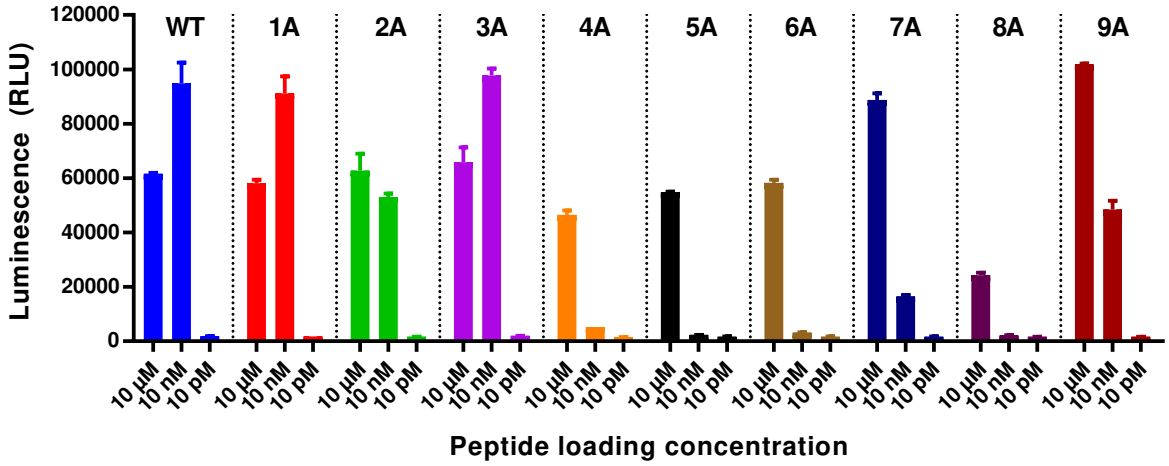

Fig. 5.9 Activation of Jurkat-NFAT effector cells expressing the 1G4 TCR in response to alanine scanning peptides based on the pESO9V peptide. Numbers represent position of alanine substitution. Dataset represents biological duplicates.

T cell activation could be detected in response to all peptides at the highest 10 µM peptide loading concentration. Responses at positions 4, 5, 6 and 8 was not sustained at lower concentrations though, whereas it still measurable or actually increased for other peptides, for example the wild type. Based on these patterns or the 10 nM responses, interaction with 1A, 2A and 3A would have been identified as strong, 7A and 9A as moderate and 4A, 5A, 6A and 8A as weak. Thus, using the methodology of the alanine scanning, positions 4, 5, 6 and 8 of pESO9V would have been declared important for 1G4-mediated T cell activation.

5.2.2.2.2. Positional Scanning Library

When excluding the potential combinations already covered by pESO9V and the alanine scanning, a positional scanning library based on pESO9V sequence contains 163 additional peptides. These peptides were synthesized and tested for activation of 1G4 expressing Jurkat-NFAT cells in an identical fashion compared to the alanine scanning approach (Fig. 5.10).

In response to the pESO9V positional scanning library, a broad range of 1G4 mediated responses was generated by the Jurkat cells. In principle, the observed activation levels were in line with the alanine scanning results: especially at position 4, 5, 6 and 8, activation at 10 nM or even at 10 µM was reduced for many substitutions.

Some substitutions had a less significant impact though compared to others at this position, e.g. 6L or 6M, potentially offering a more nuanced binding motif. In contrast, some substitutions were not well tolerated at positions which saw no changes with the alanine substation, for example 1D.

5.2.2.2.3. Positional Scanning Synthetic Combinatorial Peptide Library

For screening of the 1G4 TCR against the positional scanning synthetic combinatorial peptide library, peptide loading was performed at 100 µg/ml of each individual pool based on the scientific literature. All other experiment parameters of the Jurkat-NFAT readout were kept identical compared to the alanine scanning and PSL screen (Fig. 5.11).

Overall, the responses were limited in number and strength: the 8Q peptide pool showed the largest luminescence signal at an 5573 RLU median value, very low compared to the T cell activation when stimulated with the positional scanning library. A pESO9V peptide loading control used as an intra-assay control did not show significantly weaker responses compared to the previously shown data. While some of the positions of the pESO9V target were notably among the higher responses, e.g. 5W, 7T and 8Q, the PS-SCL dataset did result in a clear binding pattern of the 1G4 TCR.

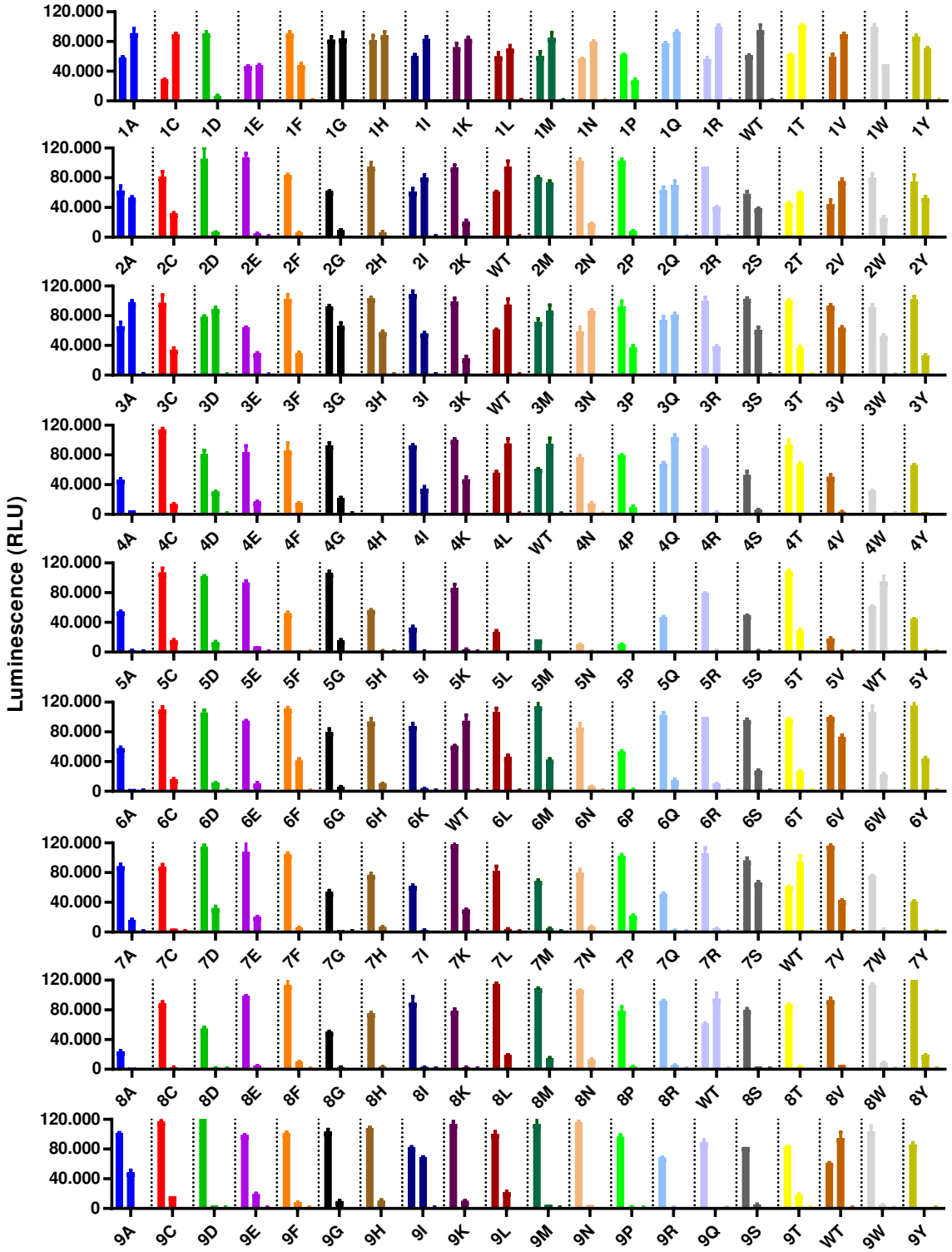

Fig. 5.10 Activation of Jurkat-NFAT effector cells expressing the 1G4 TCR in response to PSL peptides based on the pESO9V peptide. Numbers represent position of the substitution, letters the single letter amino acid code. Each peptide was loaded at 10 µM, 10 nM and 10 pM and bars are sorted with decreasing concentration. Dataset represents biological duplicates.

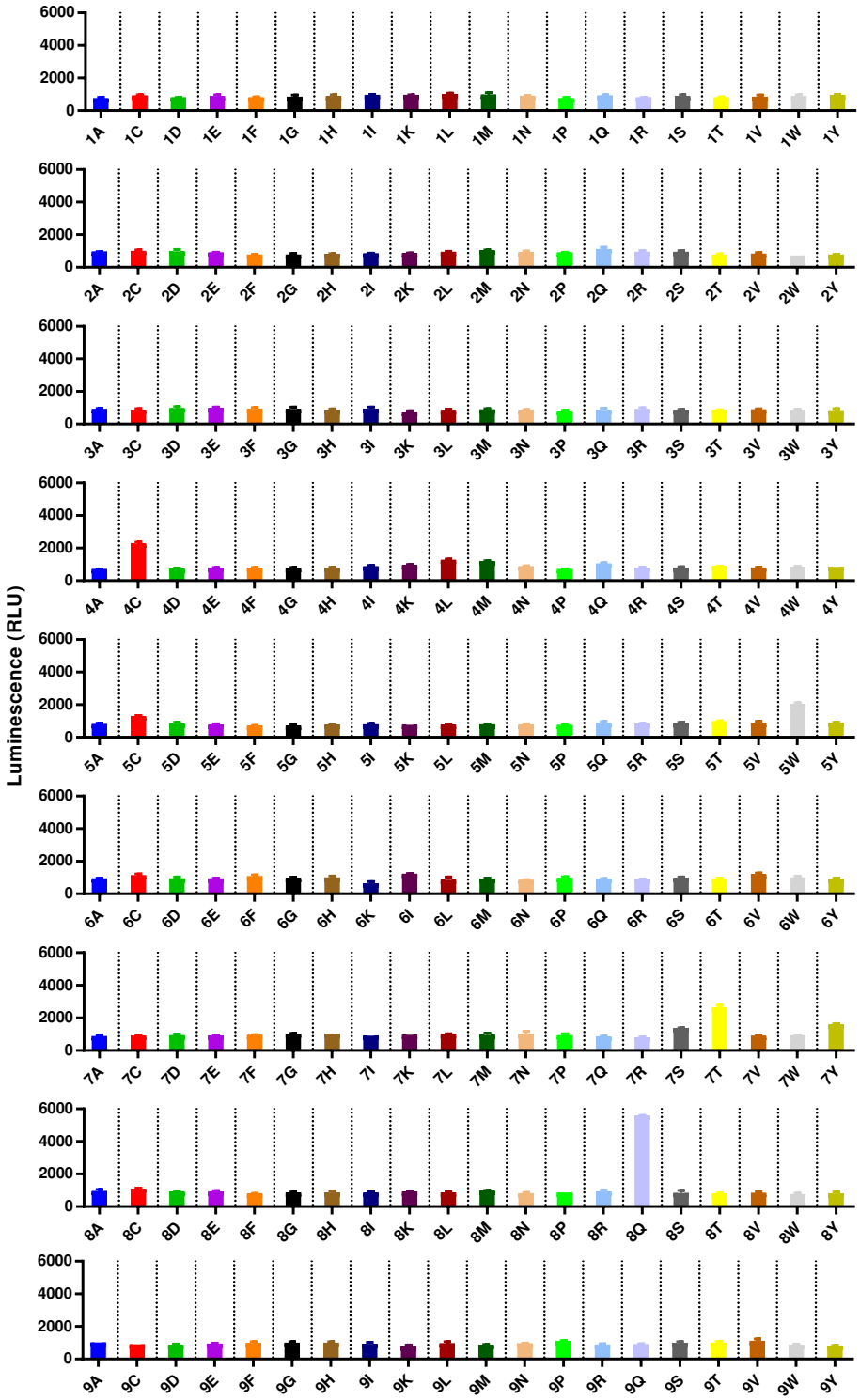

Fig. 5.11 Activation of Jurkat-NFAT effector cells expressing the 1G4 TCR in response to individual PS-SCL peptide pools. Numbers represent position of the defined amino acid in the pool, letters the single letter amino acid code. Dataset represents biological duplicates.

5.2.3. Screening of T cell receptors using soluble molecules and binding kinetics measurements

While measuring T cell activation using a cellular screening system stands to reason for investigating a TCR intended for that use, directly measuring the underlying binding affinity could offer additional information and process advantages. Using the soluble preparation of the 1G4 TCR and the BLI measurement system, the binding kinetics for the alanine scanning and the complete positional scanning library were measured.

5.2.3.1. Alanine Scanning

Peptide-MHC complexes were prepared using the pESO9V peptide as well as the 9 alanine scanning peptides by peptide loading reactions with DS-A2 molecules and immobilized on streptavidin biosensors. Binding kinetics were measured using six concentrations of the 1G4 sTCR as soluble analyte with a 1:3.16 dilution series from 50 µM to 500 nM. For curve fitting, all curves with a signal of at least 0.035 nm were included.

Robust binding kinetics could be obtained for 8 out of the 10 peptides, with K_D values ranging from 1.5 nM to 256 µM. No binding signals were obtained for the alanine exchanges at position 5 and 8. Based on the sensitivity of the affinity measurements, the K_Ds for these peptides were assigned a value of "> 300 µM". (Fig. 5.12, Table 5.2).

Table 5.2 Binding affinity constants for the interaction between the 1G4 sTCR and the pESO9V alanine scanning peptides. Determined using curve fitting of Octet RED384 recorded sensorgrams.

	pESO9V	1A	2A	3A	4A	5A	6A	7A	8A	9A
K_D	1.90E-06	1.50 E-06	1.79 E-06	2.71 E-06	3.94 E-05	>3.0 E-04 (n.d.)	2.57 E-04	1.31 E-05	>3.0 E-04 (n.d.)	4.97 E-06
k_{on}	4.39 E+04	4.41 E+04	2.88 E+04	4.12 E+04	2.28 E+04		3.50 E+03	2.73 E+04		4.22 E+04
k_{off}	8.35 E-02	6.61 E-02	5.15 E-02	1.12 E-01	8.99 E-01		8.98 E-01	3.57 E-01		2.10 E-01
R^2	0.9941	0.9919	0.9935	0.9961	0.9831		0.9600	0.9796		0.9896

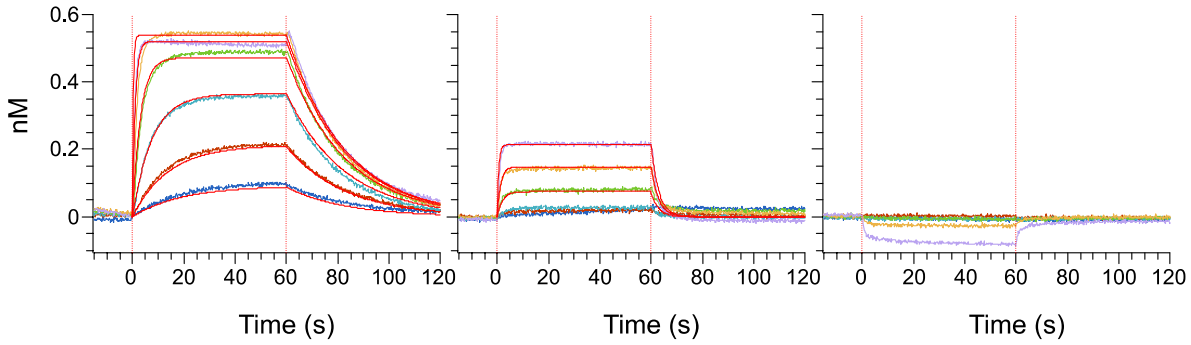

Fig. 5.12 Sensorgrams and curve fitting results for selected peptides from the pESO9V alanine scanning performed on the Octet RED384. Interactions ranging from very strong in the triple digit nanomolar range (left) to average (middle) to no observable binding (right) were detected.

By expressing each alanine scanning interaction as ratio compared to the pESO9V binding affinity, a binding pattern that exhibited similarities to the binding pattern depicted by the cellular alanine scanning result could be obtained (Fig. 5.13).

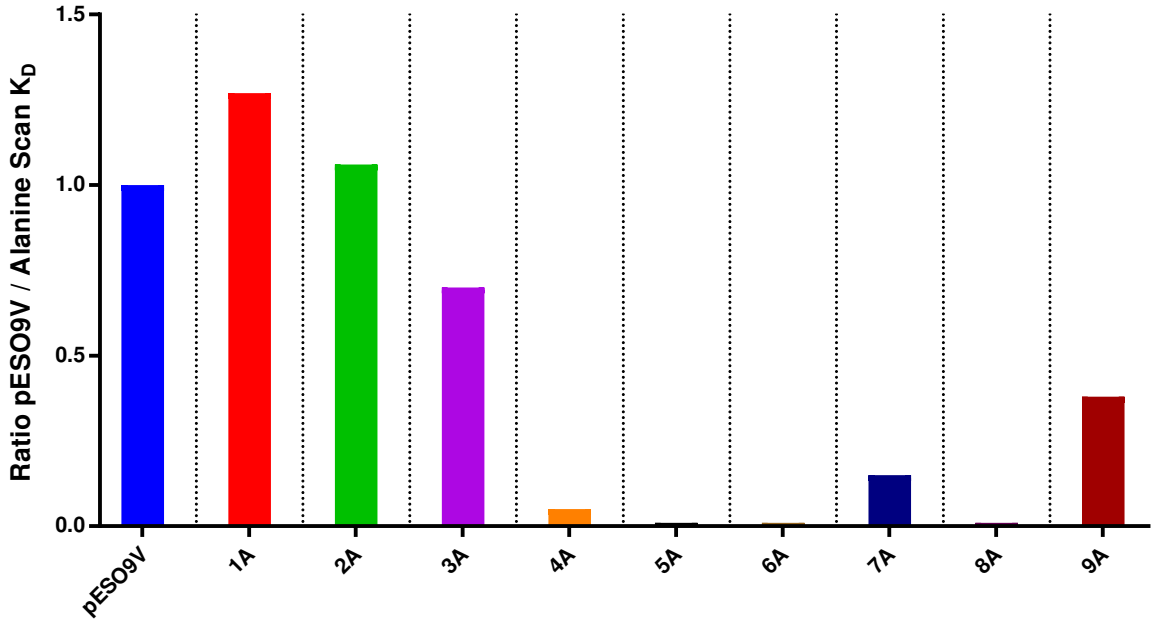

Fig. 5.13 Alanine scanning based binding motif of the 1G4 sTCR, displayed as ratio between the wild type and respective alanine scanning peptide K_D.

5.2.3.2. Positional Scanning Library

The peptide-MHC complexes for the positional scanning library were produced and binding kinetics measured for the 1G4 sTCR on the Octet RED384 with an identical setup compared to the alanine scanning measurements. Among the additional 163 peptides, no fittable binding was detected for 57 interactions, mostly peptides with substitutions at position 4, 5, 6 and 8.

The highest detected binding affinity was measured at 791 nM. The fitted K_Ds were used to generate a heatmap with color coding, transitioning from red to yellow to green to indicate increasing K_D values, to illustrate the overall binding trend at each position across the peptide (Table 5.3).

The connection between the alanine scanning and the PSL results was reminiscent of the link between both assays in the cellular screening system: while positions with weak binding to alanine substitutions tended to produce weak binding affinities with differently substituted peptides at the same position, outliers like 6L or 6M were detectable in this assay as well.

Table 5.3 PSL matrix and heatmap depicting 1G4 K_Ds against single amino acid substitutions based on the pESO9V peptide.

	A	C	D	E	F	G	H	I	K	L	M	N	P	Q	R	S	T	V	W	Y
1	1.50 E-06	1.26 E-06	1.74 E-06	7.91 E-07	4.44 E-06	2.75 E-06	3.28 E-06	1.23 E-06	1.54 E-06	1.05 E-06	1.22 E-06	2.00 E-06	1.50 E-06	1.77 E-06	1.41 E-06	1.90 E-06	1.59 E-06	1.52 E-06	4.81 E-06	3.72 E-06
2	1.79 E-06	1.41 E-06	1.91 E-06	2.00 E-06	1.39 E-06	2.41 E-06	2.83 E-06	1.85 E-06	3.27 E-06	1.90 E-06	3.77 E-06	3.04 E-06	4.42 E-06	4.89 E-06	3.52 E-06	1.51 E-06	1.02 E-06	1.73 E-06	3.04 E-06	2.66 E-06
3	2.71 E-06	5.27 E-06	5.97 E-06	3.52 E-06	6.22 E-06	8.72 E-06	1.01 E-05	5.42 E-06	1.88 E-05	1.90 E-06	3.47 E-06	2.17 E-06	9.33 E-06	3.87 E-06	8.05 E-06	7.81 E-06	1.02 E-05	4.18 E-06	4.84 E-06	1.40 E-05
4	3.94 E-05	1.81 E-05	2.85 E-05	>3.0 E-04	>3.0 E-04	>3.0 E-04	2.23 E-05	2.12 E-06	1.60 E-05	1.13 E-06	1.90 E-06	2.45 E-05	>3.0 E-04	2.79 E-06	>3.0 E-04	6.01 E-05	9.22 E-06	>3.0 E-04	>3.0 E-04	>3.0 E-04
5	>3.0 E-04	>3.0 E-04	>3.0 E-04	>3.0 E-04	>3.0 E-04	>3.0 E-04	>3.0 E-04	>3.0 E-04	>3.0 E-04	>3.0 E-04	>3.0 E-04	>3.0 E-04	>3.0 E-04	>3.0 E-04	>3.0 E-04	>3.0 E-04	>3.0 E-04	>3.0 E-04	1.90 E-06	>3.0 E-04
6	>3.0 E-04	2.09 E-05	>3.0 E-04	>3.0 E-04	1.02 E-05	2.73 E-05	3.67 E-05	1.90 E-06	>3.0 E-04	8.71 E-06	1.36 E-05	4.29 E-05	3.23 E-05	>3.0 E-04	>3.0 E-04	2.82 E-05	2.44 E-05	5.22 E-06	1.53 E-05	2.10 E-05
7	1.31 E-05	1.15 E-05	8.86 E-06	6.14 E-06	>3.0 E-04	1.61 E-05	3.13 E-05	>3.0 E-04	>3.0 E-04	>3.0 E-04	>3.0 E-04	1.56 E-05	8.72 E-06	>3.0 E-04	>3.0 E-04	2.47 E-06	1.90 E-06	1.25 E-06	>3.0 E-04	>3.0 E-04
8	>3.0 E-04	>3.0 E-04	>3.0 E-04	>3.0 E-04	>3.0 E-04	1.43 E-05	4.80 E-06	>3.0 E-04	>3.0 E-04	>3.0 E-04	>3.0 E-04	>3.0 E-04	>3.0 E-04	1.90 E-06	>3.0 E-04	>3.0 E-04	>3.0 E-04	>3.0 E-04	2.26 E-06	>3.0 E-04
9	4.97 E-06	4.59 E-06	2.53 E-06	5.26 E-06	2.76 E-06	3.97 E-06	2.16 E-06	2.90 E-06	2.42 E-06	8.33 E-06	1.22 E-05	5.01 E-06	2.62 E-06	2.00 E-06	1.53 E-06	4.37 E-06	2.71 E-06	1.90 E-06	3.32 E-06	1.18 E-06

5.2.4. Comparison of cellular and biochemical measurements

Having measured T cell activation as well as the binding affinity to the PSL, a comparison plot was used to evaluate whether a positive correlation between both assays could be observed. Since Jurkat-NFAT activation to the 10 nM peptide loading concentration produced a similar ranking as the EC50 calculation for the tested peptides, this dataset was selected for comparison the K_D values (Fig. 5.14).

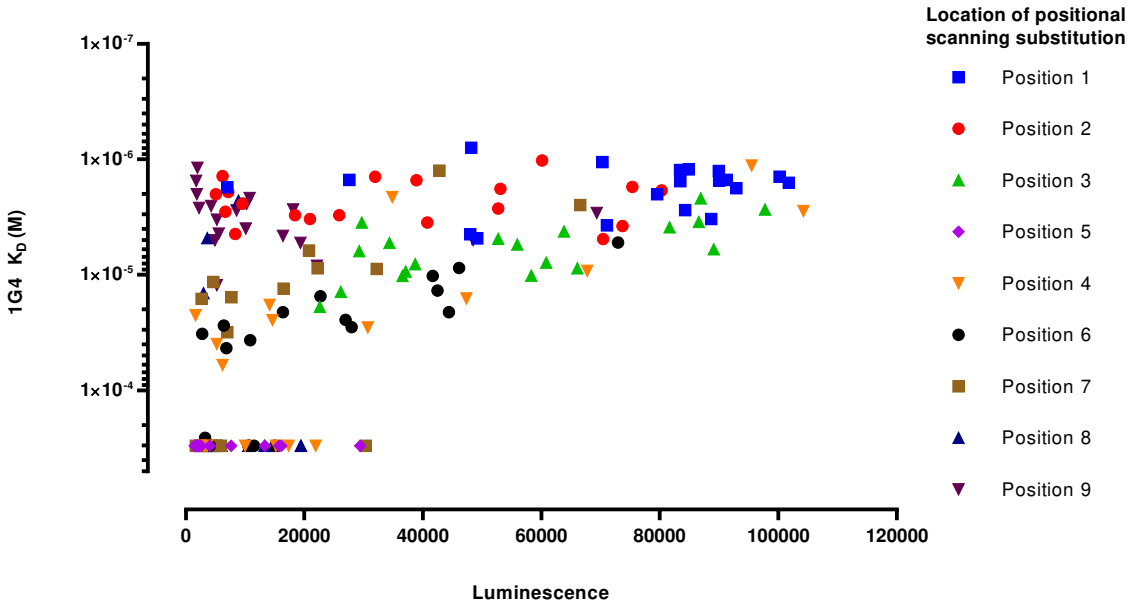

Fig. 5.14 Comparison of the calculated 1G4 sTCR K_Ds against the PSL and the 1G4-mediated Jurkat-NFAT activation induced with 10 nM peptide loading of T2 target cells. Color and symbols represent position of the PSL directed peptide substitution.

Based on visual inspection of the plot, three groups could be identified: Group 1 contained peptides that decreased or increased in cellular activity in agreement with the K_D values measured. Group 2 consisted of peptides with strong binding affinities but that did produce weak or no T cell activation at 10 nM peptide loading of the target cells. These peptides mostly carried substitutions at position 2 or position 9. Group 3 belonged to the peptides that had no measurable interaction with the 1G4 TCR in the binding affinity assay but at least in part did produce T cell activation, indicating that their affinity was outside of the sensitivity of the kinetic screening with the employed setup.

Due to characteristics of group 2, a second plot containing information of the assumed affinity of the peptide for binding to the HLA-A*02:01 complex was created (Fig. 5.15). This was based on the hypothesis that the weak binding affinity of a peptide to the peptide-MHC complex would negatively influence presentation during the coincubation and thus mask the affinity of the TCR for this peptide. The binding affinity was predicted using the NetMHC4.0 algorithm and was presented as rank, with peptides of rank 2 or larger typically considered as weak to strong HLA-A*02:01 binders.

Among the peptides with a predicted NetMHC rank of 1 or lower, T cell activation seemed to correlate with the measured binding affinity in general. Above rank 1, this connection was no longer apparent, but no real pattern could be identified upon visual inspection within that group.

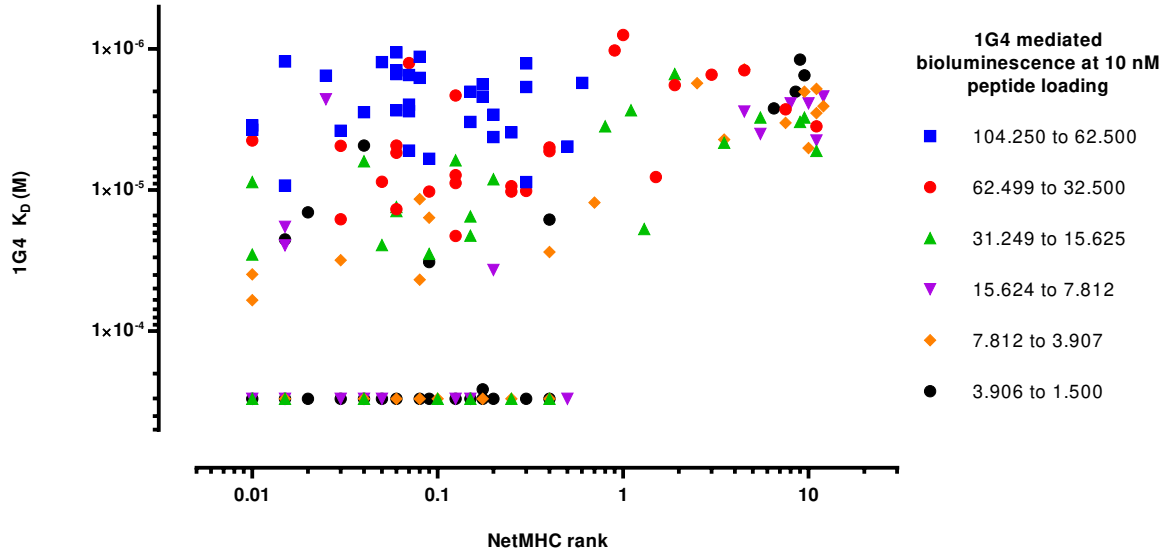

Fig. 5.15 Comparison of the calculated 1G4 sTCR K_Ds against the PSL and the NetMHC4.0 predicted affinity of the respective peptides for the peptide-MHC complex, depicted as NetMHC ranks. Color and symbols represent categorization into different T cell activation groups based on the magnitude of luminescence detected after stimulation with 10 nM peptide loaded T2 target cells.

5.2.5. Summary

In summary, the Jurkat-NFAT assay was identified as capable system for TCR-pMHC interaction characterization and quantification. The assay was used to depict TCR binding motifs using various screening strategies, of which alanine scanning and PSL were most efficient. Using the same approaches with soluble TCR refoldings and a kinetic screening system was possible as well but was less sensitive compared to the cellular screening approach.

5.3. Strategies to interrogate T cell receptor cross-reactivity for T cell engaging bispecific molecules

5.3.1. Introduction

This chapter describes strategies to measure bsTCR binding affinities or T cell activation mediated by these molecules and the potential use case of such datasets to characterize their peptide-MHC binding preferences and identify potential cross-reactive peptide ligands.

5.3.2. Screening of bispecific T cell receptors using the Jurkat-NFAT T cell activation assay with peptide loaded target cells

5.3.2.1. Screening Setup

Whereas modification of the peptide loading concentration was the only way to introduce a controllable titration into the screening assays using cellularly expressed TCRs, altering the concentration of the bsTCR concentration is a second and very relevant option in that setting.

To compare the effects of both strategies, the bsTCR bs-868Z11-CD3 was incubated at 6 different concentrations (1:10 dilution from 10 nM to 0.1 pM) with Jukrat-NFAT cells as well as pSL9 loaded target cells in a 1:1 effector to target cell ratio.

The peptide loadings were also performed at 6 different concentration levels, yielding 36 different combinations. In addition, peptide loading with 3 washing steps before addition of the target cells to the Jurkat-NFAT cells and bsTCRs was tested against a simple resuspension without washing step to ensure that no background increases or activation decreases were caused by the omission (Fig. 5.16).

Both peptide loading concentration as well as bsTCR concentration had a detectable effect on the Jurkat-NFAT cell response. Absence of washing steps did not have a negative effect on the background levels or induce large EC50 shifts.

The bsTCR concentration was selected as variable since it was more relevant to the question of bsTCR activity against a defined target and because fits were slightly better as a plateau could be reached at higher bsTCR concentrations. Due to the ease of use and potential throughput increase, omission of the washing step was selected combined with 100 nM peptide loading, as this concentration is more likely to result in peptide presentation levels comparable to antigen levels encountered *in vivo.*

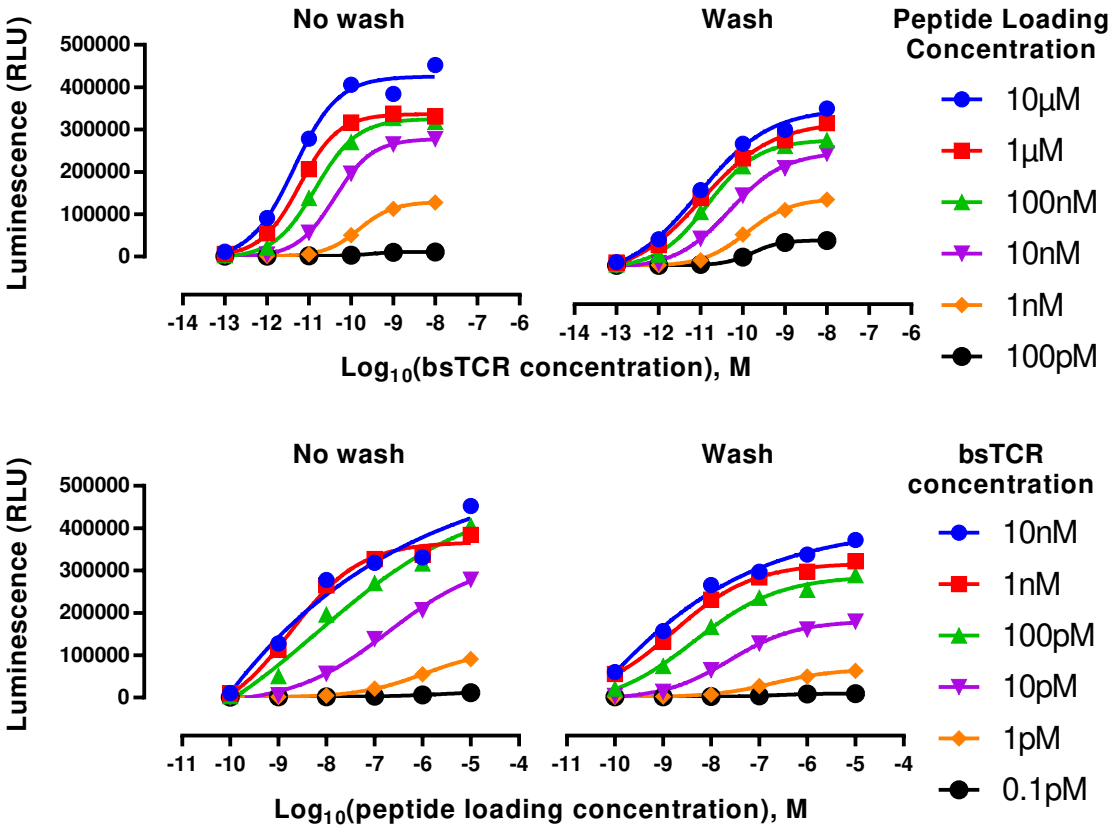

Fig. 5.16 Comparison of different Jurkat-NFAT and bsTCR activation assay experimental strategies. (a) Nonlinear regression fitting of Jurkat-NFAT activation for peptides loaded at fixed concentration without washing incubated with a bsTCR dilution series. (b) Same analysis as (a) with washing step between peptide loading and coincubation. (c) Nonlinear regression fitting of Jurkat-NFAT incubation with fixed bsTCR concentration against a titration series of the peptide loading concentration without washing. (d) Same analysis as (c) with washing step between peptide loading and coincubation.

5.3.2.2. Alanine Scanning

With the established setup, alanine screening was performed by loading T2 target cells with 100 nM of peptide for 2 hours. Target cells were then combined with Jurkat-NFAT effector cells and bs-868Z11-CD3 at one of the previously used 6 concentration levels without washing. The coincubations were incubated for 18h and then analyzed using the luciferase readout. Since pSL9 already contains an alanine at position 7, glycine was used as alternative substitution (Fig. 5.17).

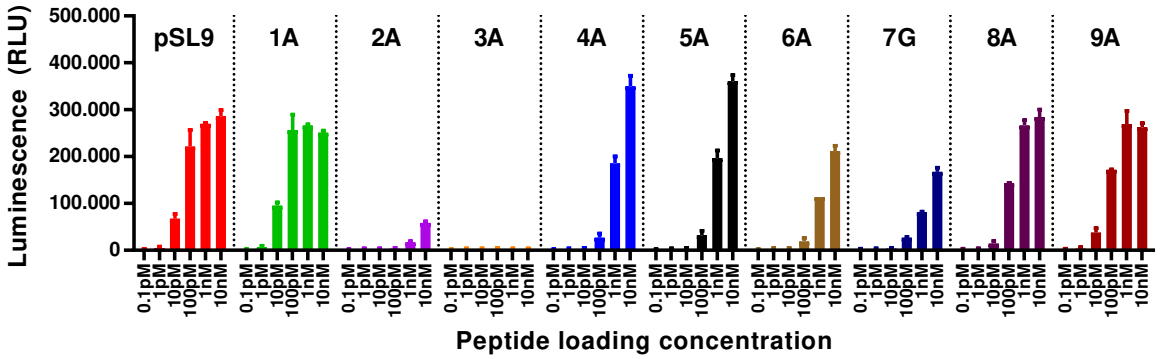

Fig. 5.17 Activation of Jurkat-NFAT effector cells incubated with different bs-868Z11-CD3 concentrations in response to alanine scanning peptides based on the pSL9 peptide loaded on T2 target cells. Numbers represent position of alanine substitution. Dataset represents biological duplicates.

EC50 concentrations could be fitted for most interactions with good fitting values, with a nearly 250-fold difference between the weakest and strongest fitable response. The response against the 3A substituted peptide was the only exception and was assigned a >10 nM value due to the employed concentration range (Fig. 5.18, Table 5.4).

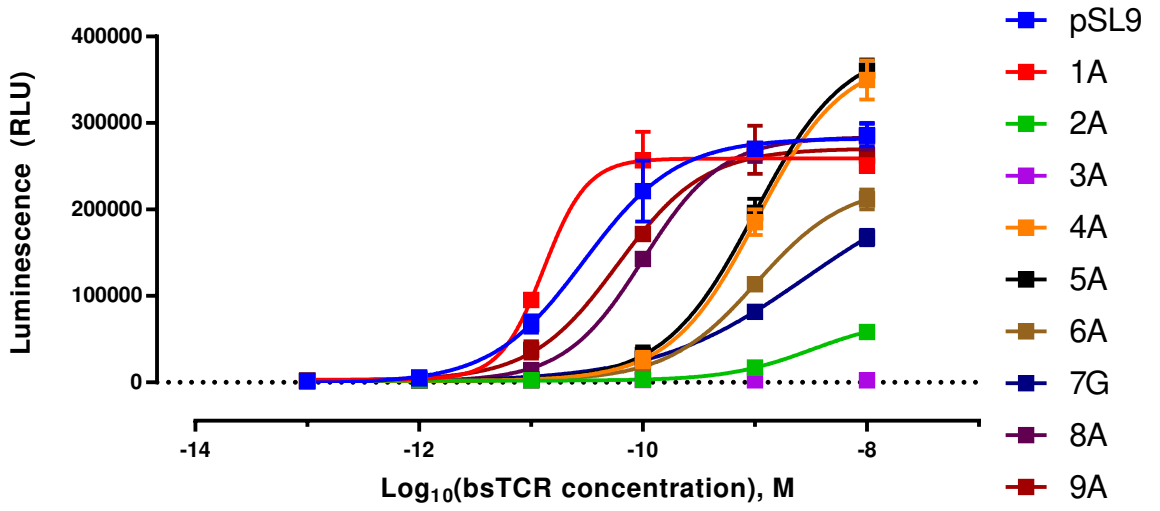

Fig. 5.18 Nonlinear regression curve fittings of Jurkat-NFAT activation in response to the pSL9 peptide and alanine scanning peptides.

Table 5.4 Nonlinear regression curve fitting results Jurkat-NFAT activation in response to the pSL9 peptide and alanine scanning peptides.

	pSL9	1A	2A	3A	4A	5A	6A	7G	8A	9A
EC50	2.97 E-11	1.29 E-11	3.17 E-09	>1.0 E-08	1.04E-09	9.97 E-10	1.03 E-09	2.86 E-09	1.01 E-10	5.95 E-11
R^2	0.9907	0.9913	0.9941		0.996	0.9975	0.9972	0.9973	0.9975	0.992

A binding motif based on the Jurkat-NFAT alanine screening would have identified position 3 as particularly crucial and 2, 4, 6 and 7 as considerably important for recognition by bs-868Z11-CD3.

5.3.2.3. Positional Scanning Library

An identical setup was used for screening against the positional scanning library. In contrast to the 1G4 PSL library, cysteine substitutions were omitted due to potentially increased background caused by dimerized cysteine disulfide bridge byproducts previously observed.

A broad spectrum of activation levels against the positional scanning library, ranging from no detectable T cell activation with any bsTCR concentration to strong bioluminescence signals starting at low bsTCR concentrations, e.g. for the wild type peptide.

Peptides that did not result in significant activation above background with at least 3 concentrations produced fittings with insufficient goodness of fit and were thus assigned the same >10 nM value previously assigned to the 3A substitution (Fig. 5.19, Table 5.5).

When comparing the alanine scanning result to the additional PSL substitutions, multiple pronounced differences could be detected. While the 2A and 3A substitution themselves were not tolerated at all, other amino acid substitutions at these positions led to strong. In contrast, many PSL positions were less favorable than the alanine substitutions at these positions, for example at position 4.

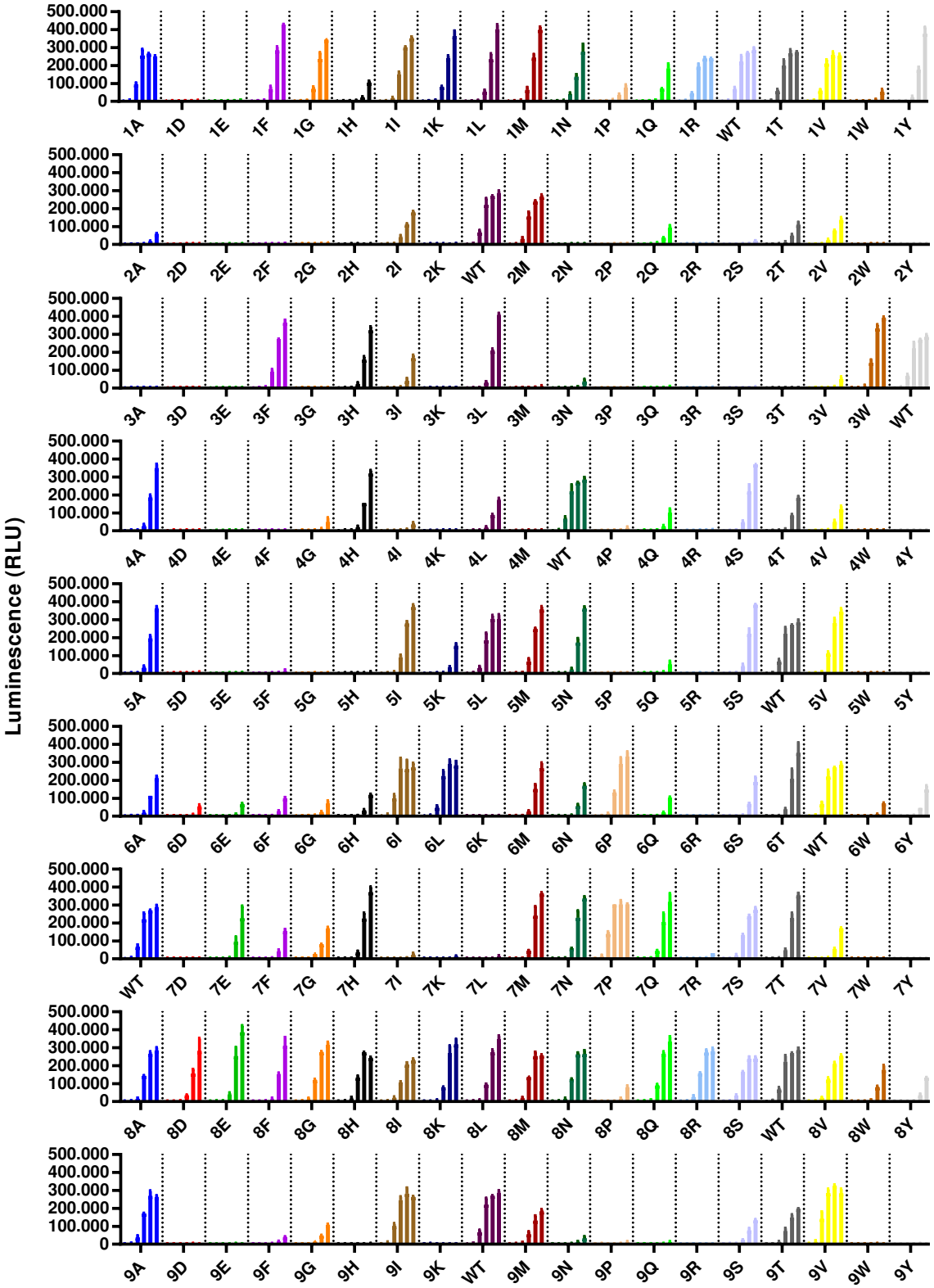

Fig. 5.19 Activation of Jurkat-NFAT effector cells incubated with different bs-868Z11-CD3 concentrations in response to T2 cells loaded with PSL peptides based on the pSL9 sequence. Numbers represent position of the substitution, letters the single letter amino acid code. 6 different concentrations were used in a 1:10 dilution series, ranging from 0.1 pM to 10 nM, and bars are sorted with increasing concentration. Dataset represents biological duplicates.

Table 5.5 PSL matrix and heatmap depicting bs-868Z11-CD3 mediated EC50 values in the Jurkat-NFAT activation assay against single amino acid substitutions based on the pSL9 peptide.

	G	P	A	V	L	I	M	F	Y	W	H	K	R	Q	N	E	D	S	T	G
1	5.08 E-10	1.77 E-09	1.29 E-11	2.80 E-11	8.90 E-10	1.45 E-10	7.86 E-10	5.88 E-10	1.29 E-09	1.00 E-08	3.92 E-09	5.98 E-10	3.34 E-11	1.47 E-09	1.91 E-09	1.00 E-08	1.00 E-08	2.97 E-11	3.83 E-11	5.08 E-10
2	1.00 E-08	1.00 E-08	3.17 E-09	1.16 E-09	2.97 E-11	8.45 E-10	7.06 E-11	1.00 E-08	1.00 E-08	1.00 E-08	1.00 E-08	1.00 E-08	1.00 E-08	2.72 E-09	1.00 E-08	1.00 E-08	1.00 E-08	1.00 E-08	2.33 E-09	1.00 E-08
3	1.00 E-08	1.00 E-08	1.00 E-08	1.00 E-08	1.12 E-09	2.68 E-09	1.00 E-08	3.63 E-10	2.97 E-11	1.81 E-10	1.21 E-09	1.00 E-08	1.00 E-08	1.00 E-08	1.00 E-08	1.00 E-08	1.00 E-08	1.00 E-08	1.00 E-08	1.00 E-08
4	1.00 E-08	1.00 E-08	1.04 E-09	1.43 E-09	1.26 E-09	1.00 E-08	1.00 E-08	1.00 E-08	1.00 E-08	1.00 E-08	1.21 E-09	1.00 E-08	1.00 E-08	2.87 E-09	2.97 E-11	1.00 E-08	1.00 E-08	8.26 E-10	1.21 E-09	1.00 E-08
5	1.00 E-08	1.00 E-08	9.97 E-10	2.33 E-10	7.11 E-11	3.59 E-10	5.10 E-10	1.00 E-08	1.00 E-08	1.00 E-08	1.00 E-08	2.80 E-09	1.00 E-08	1.00 E-08	1.26 E-09	1.00 E-08	1.00 E-08	8.75 E-10	2.97 E-11	1.00 E-08
6	2.36 E-09	1.54 E-10	1.03 E-09	2.97 E-11	3.74 E-11	1.28 E-11	9.06 E-10	2.14 E-09	1.88 E-09	8.37 E-09	2.17 E-09	1.00 E-08	1.00 E-08	2.85 E-09	1.59 E-09	5.80 E-09	9.51 E-09	1.56 E-09	8.47 E-10	2.36 E-09
7	2.86 E-09	1.11 E-11	2.97 E-11	1.89 E-09	1.00 E-08	1.00 E-08	6.17 E-10	2.24 E-09	8.42 E-09	1.00 E-08	7.75 E-10	1.00 E-08	1.00 E-08	6.42 E-10	5.42 E-10	1.26 E-09	1.00 E-08	1.15 E-10	6.69 E-10	2.86 E-09
8	1.65 E-10	3.57 E-09	1.01 E-10	1.24 E-10	2.86 E-10	1.23 E-10	9.43 E-11	1.11 E-09	2.20 E-09	1.25 E-09	1.00 E-10	2.57 E-10	8.32 E-11	2.86 E-10	1.09 E-10	6.43 E-10	1.02 E-09	5.15 E-11	2.97 E-11	1.65 E-10
9	2.38 E-09	4.35 E-09	5.95 E-11	1.11 E-11	2.97 E-11	1.56 E-11	3.77 E-10	1.89 E-09	1.00 E-08	1.00 E-08	1.00 E-08	1.00 E-08	1.00 E-08	7.42 E-09	2.07 E-09	1.00 E-08	1.00 E-08	1.10 E-09	2.62 E-10	2.38 E-09

5.3.2.4. Positional Scanning Synthetic Combinatorial Peptide Library

For screening of the bs-868Z11-CD3 bsTCR against the positional scanning synthetic combinatorial peptide library, peptide loading was again performed using 100 µg/ml of each individual pool. All other experiment parameters of the Jurkat-NFAT readout were kept identical compared to the alanine scanning and PSL screening (Fig. 5.20).

In comparison to the PSL results, only weak levels of Jurkat-NFAT activation were measurable. In addition, most peptide pools did not produce any activation. Amongst the pools that did result in increased luminescence signals, most had the amino acid fixed position that matched the pSL9 peptide. Only the 4L pool was slightly more active in relation to the other observed responses compared to the same substitution in the PSL.

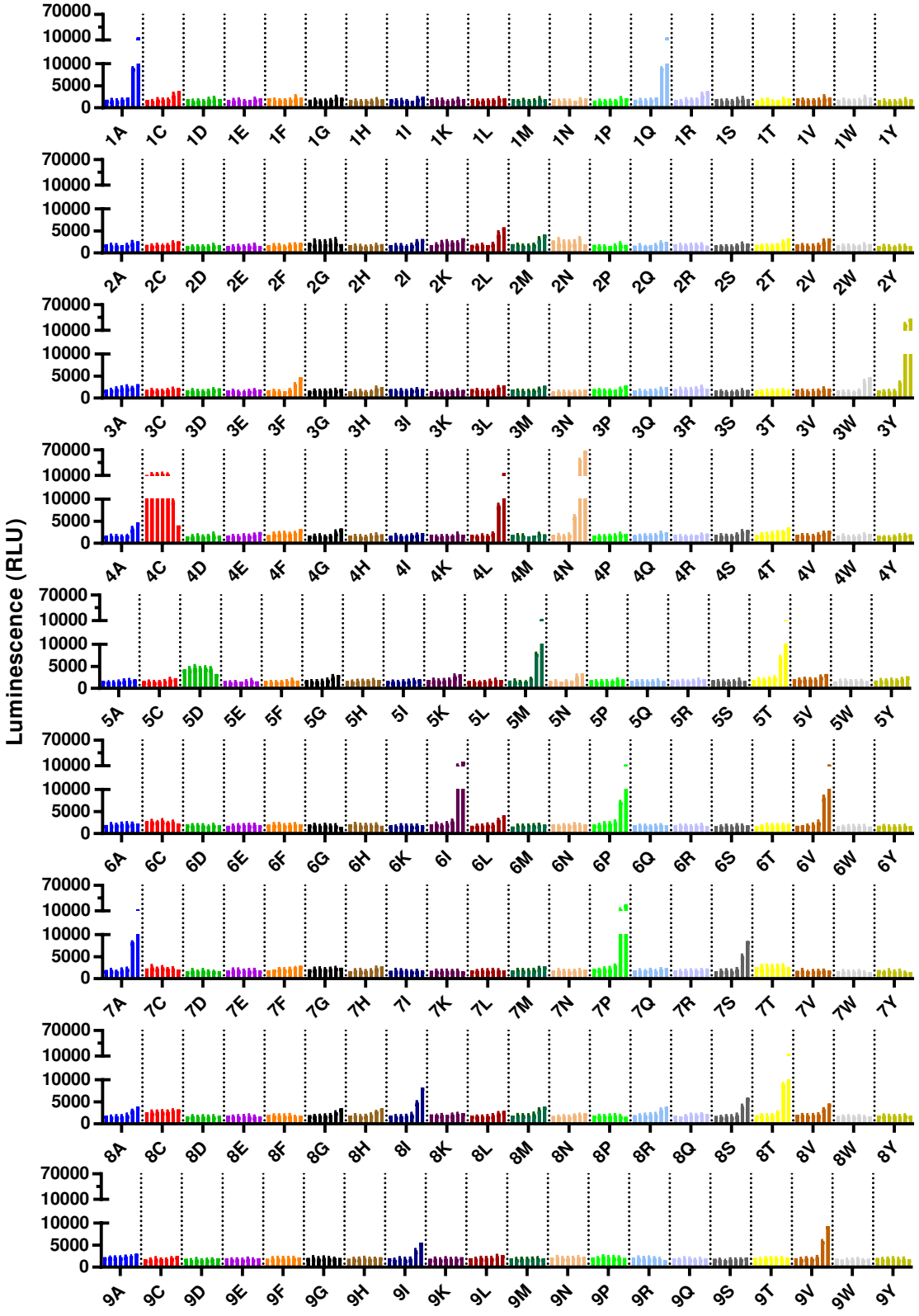

Fig. 5.20 Activation of Jurkat-NFAT effector cells incubated with different bs-868Z11-CD3 concentrations in response to individual PS-SCL peptide pools. Numbers represent position of the defined amino acid in the pool, letters the single letter amino acid code. 7 different concentrations were used in a 1:10 dilution series, ranging from 0.1 pM to 100 nM, and bars are sorted with increasing concentration. Dataset represents biological duplicates from 0.1 pM to 10 nM and single experiment results for the 100 nM concentration.

5.3.3. Single chain T cell receptor binding kinetics screening

Measuring binding affinity for pMHC targets with bispecific TCRs to predict their functionality presents a logical alternative to cellular testing due to the affinity range and the antibody-like interaction mode.

In comparison to refolded soluble TCRs, bispecific constructs using antibody fragments allow for a much more economical setup, as biosensors which bind F(ab) fragments in a reversible and regeneratable manner exist for example. This is important as binding by affinity maturated TCRs may often reach half times in the double-digit minute or hour range, which makes waiting for full dissociation to reuse impractical. When the bsTCR is immobilized and the peptide-MHC is employed as soluble analyte, one also repeatedly immobilizes a ligand with known reactivity, which makes it easier to judge the curve fitting result due to more precise knowledge of the Rmax value.

To use these advantages in the bsTCR screening setup, regenerable Anti-F(ab) sensors were used together with soluble peptide loaded DS-A2 preparations to analyze the bs-868Z11-CD3 bsTCR interactions with pSL9 derived alanine scan or positional scanning library.

5.3.3.1. Alanine Scanning

To perform the alanine scanning method using binding kinetics screening, the bsTCR bs-868Z11-CD3 was immobilized on Anti-F(ab) sensors and association and dissociation measured against soluble peptide loaded DS-A2 samples at 4 concentrations, starting at 500 nM with a 1:3.16 dilution series, on the Octet RED384. The sensors were regenerated after each dissociation step and reloaded with bs-868Z11-CD3 before the next cycle. Kinetic binding constants were fitted for peptide-MHCs that had at least two curves reaching peak signals of 0.05 nM or more. Samples that did not fulfil that criteria were assigned a >5.0 µM based on the assumed sensitivity range of the setup.

Binding affinities could be determined for 8 of the alanine substitutions peptides, with a 30-fold difference between the highest and lowest constants. A weak binding signal but no good curve fitting could be detected for the 3A substitution (Fig. 5.21, Table 5.6).

In comparison to the EC50 based binding motif, the kinetic approach would have conveyed a less important role of position 2 and 7 but also highlighted the importance of positions 3 to 6 (Fig. 5.22).

Table 5.6 Binding affinity constants for the interaction between the bs-868Z11-CD3 bsTCR and the pSL9 based alanine scanning peptides. Determined using curve fitting of Octet RED384 recorded sensorgrams.

	pSL9	1A	2A	3A	4A	5A	6A	7G	8A	9A
K_D	3.81E-09	5.82 E-09	1.00 E-08	>5.0 E-06	1.15 E-07	9.66 E-08	5.48 E-08	8.29 E-09	8.50 E-09	6.74 E-09
k_{on}	1.03 E+05	1.04 E+05	1.02 E+05	n.d.	1.40 E+05	1.27 E+05	1.10 E+05	8.24 E+04	1.14 E+05	1.13 E+05
k_{off}	1.53 E-05	6.0 4E-04	1.02 E-03	n.d.	1.60 E-02	1.22 E-02	6.05 E-03	6.83 E-04	9.69 E-04	7.61 E-04
R^2	0.9993	0.9969	0.9995	n.d.	0.9952	0.995	0.9967	0.996	0.9991	0.9904

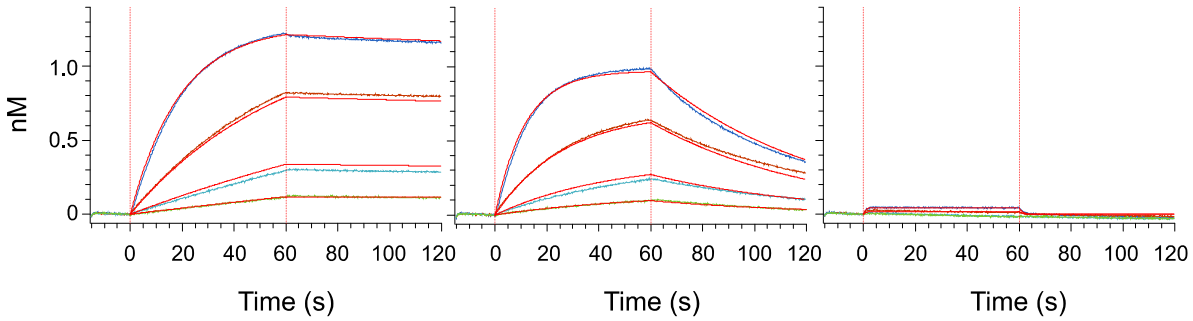

Fig. 5.21 Sensorgrams and curve fitting results for selected peptides from the pSL9 alanine scanning experiment performed on the Octet RED384. Detected interactions ranging from very strong in the single digit nM range (left) to average in the triple digit nM (middle) to detectable but too weak for accurate fitting (right) were detected.

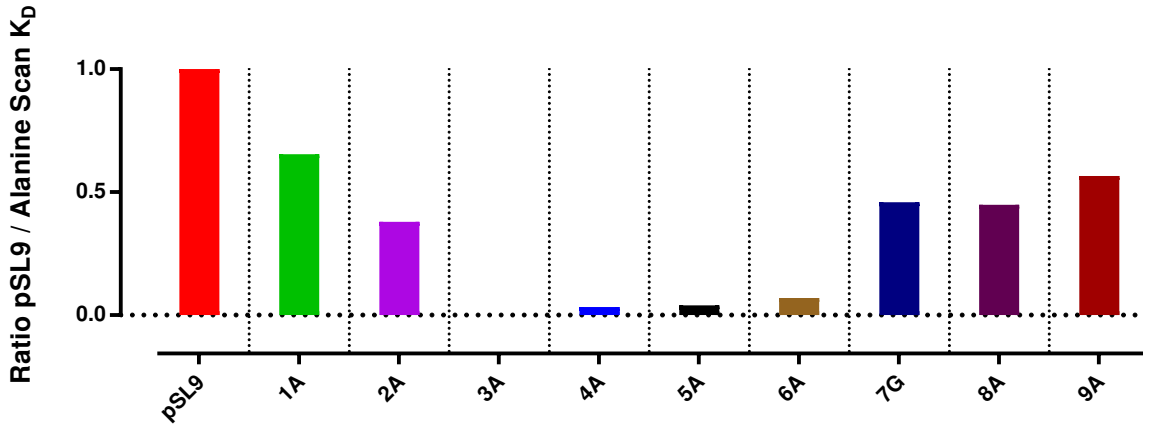

Fig. 5.22 Alanine scanning based binding motif of the bs-868Z11-CD3 bsTCR, displayed as ratio between the wild type and respective alanine scanning peptide K_Ds.

5.3.3.2. Positional Scanning Library

The peptide-MHC complexes for the positional scanning library were produced and binding kinetics measured for the bs-868Z11-CD3 bsTCR with an identical setup on the Octet RED384 compared to the alanine scanning measurements (Table S4).

The obtained K_Ds were used once more to generate a colour coded heatmap, transitioning from red to yellow to green to indicate increasing K_D values, illustrating the overall binding trend at each position across the peptide (Table 5.7).

The resulting binding motif indicated strong preference for the pSL9 amino acids on position 3, 4 and 5 and more flexibility at other positions, similar to the EC50 based analysis.

Table 5.7 PSL matrix and heatmap depicting bs-868Z11-CD3 K_Ds for interactions with the single amino acid substitutions based on the pSL9 peptide.

	G	P	A	V	L	I	M	F	Y	W	H	K	R	Q	N	E	D	S	T
1	3.05 E-08	8.54 E-09	5.82 E-09	5.74 E-09	4.99 E-08	1.35 E-08	4.19 E-08	5.22 E-08	1.24 E-07	4.62 E-07	3.43 E-07	1.91 E-08	4.42 E-09	1.38 E-07	3.13 E-08	4.85 E-07	4.49 E-08	3.81 E-09	6.94 E-09
2	1.86 E-08	1.65 E-07	1.00 E-08	8.47 E-09	3.81 E-09	8.68 E-09	6.55 E-09	8.52 E-09	3.26 E-08	8.16 E-08	2.73 E-08	7.43 E-08	1.02 E-07	9.41 E-09	2.45 E-08	4.09 E-08	1.01 E-07	8.17 E-09	5.41 E-09
3	>5.0 E-06	>5.0 E-06	>5.0 E-06	5.11 E-07	1.32 E-07	4.77 E-07	1.07 E-06	3.47 E-08	3.81 E-09	3.36 E-08	9.09 E-08	>5.0 E-06	5.55 E-07	6.29 E-07	4.74 E-07	>5.0 E-06	>5.0 E-06	>5.0 E-06	3.01 E-06
4	5.33 E-07	5.54 E-07	1.15 E-07	1.80 E-07	6.70 E-08	5.25 E-07	1.88 E-06	>5.0 E-06	>5.0 E-06	>5.0 E-06	8.11 E-08	>5.0 E-06	>5.0 E-06	2.84 E-07	3.81 E-09	>5.0 E-06	>5.0 E-06	5.95 E-08	1.61 E-07
5	6.03 E-07	>5.0 E-06	9.66 E-08	3.07 E-08	1.46 E-08	4.85 E-08	4.26 E-08	7.26 E-07	4.60 E-06	>5.0 E-06	6.23 E-07	2.24 E-07	7.78 E-07	4.72 E-07	1.19 E-07	>5.0 E-06	3.91 E-05	6.91 E-08	3.81 E-09
6	1.34 E-07	1.54 E-08	5.48 E-08	3.81 E-09	9.08 E-09	8.74 E-09	2.72 E-08	5.79 E-07	4.43 E-07	1.74 E-05	1.75 E-07	>5.0 E-06	>5.0 E-06	2.71 E-07	1.79 E-07	1.43 E-06	6.04 E-07	1.66 E-07	3.37 E-08
7	8.29 E-09	3.71 E-09	3.81 E-09	5.99 E-07	>5.0 E-06	>5.0 E-06	1.02 E-07	5.14 E-07	>5.0 E-06	>5.0 E-06	1.14 E-07	1.20 E-06	1.28 E-06	5.38 E-08	4.11 E-08	1.61 E-06	>5.0 E-06	1.04 E-08	6.90 E-08
8	1.14 E-08	2.34 E-07	8.50 E-09	6.98 E-09	1.58 E-08	4.16 E-09	7.69 E-09	1.93 E-07	4.00 E-07	2.09 E-07	1.09 E-08	1.73 E-08	7.93 E-09	1.59 E-08	1.08 E-08	4.73 E-08	2.12 E-08	4.68 E-09	3.81 E-09
9	7.71 E-09	5.03 E-08	6.74 E-09	8.41 E-09	3.81 E-09	6.70 E-09	7.45 E-09	1.19 E-08	1.02 E-08	3.32 E-08	1.37 E-08	4.57 E-08	5.71 E-09	5.88 E-09	9.10 E-09	6.96 E-06	7.18 E-06	7.19 E-09	5.66 E-09

5.3.4. Comparison of cellular and biochemical approaches

The PSL interaction datasets generated using the cellular approach, specifically the fitted EC50 values, were compared to the measured binding affinities to analyze how predictive the latter values were for the *in vitro* function of the bsTCR (Fig. 5.23)

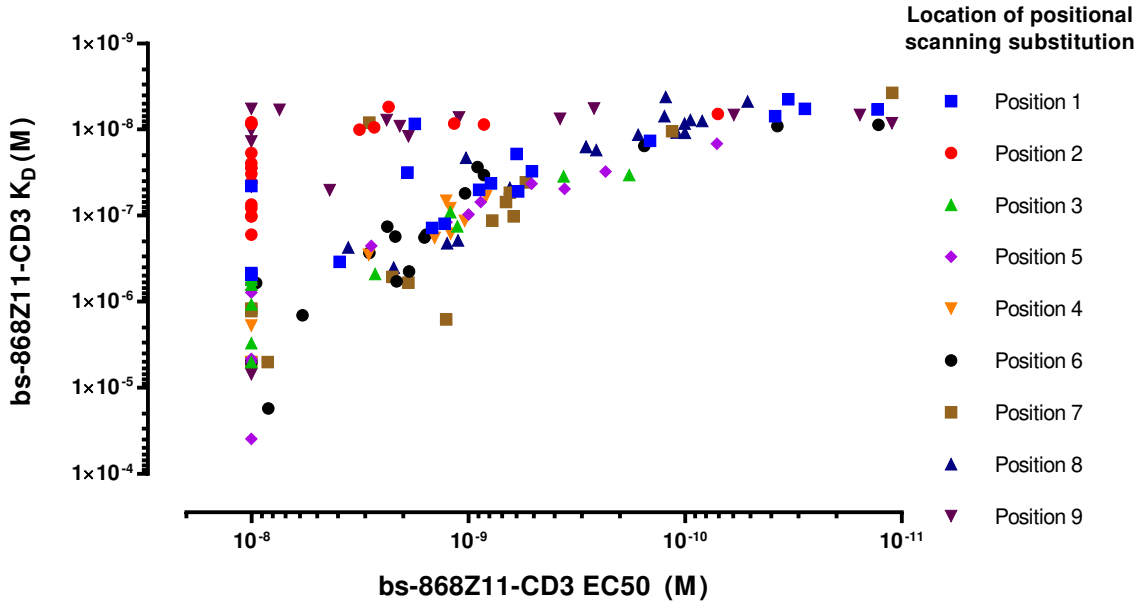

Fig. 5.23 Comparison of the measured bs-868Z11-CD3 bsTCR K_{DS} against the pSL9 PSL and the Jurkat-NFAT activation assay determined EC50 concentrations. Color and symbols represent position of the PSL directed peptide substitution.

Overall, a robust connection between the binding affinities and EC50 concentrations determined using the Jurkat-NFAT based assay was detected. Two cases of outliers were apparent: the first was one peptide with a slightly larger dissociation constant in comparison to its EC50 value. When compared to the rest of the peptides, it was identified as an outlier with a relatively slow on rate but slow off rate. Correlating with the k_{off} value instead brought this interaction into the expected range while being equally effective for the other peptides (Fig. 5.24)

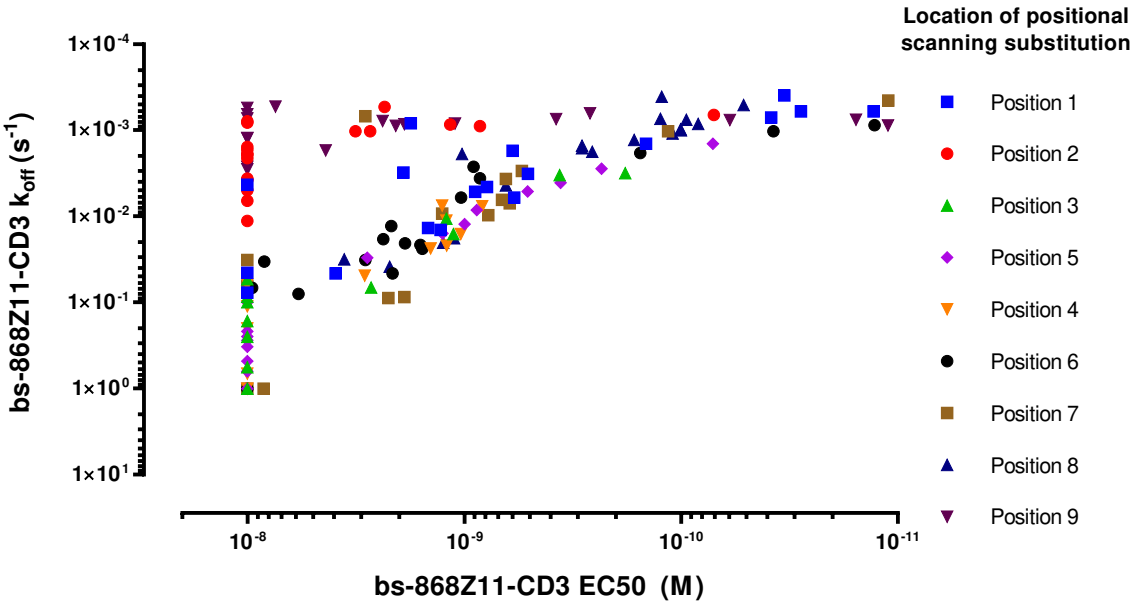

Fig. 5.24 Comparison of the measured bs-868Z11-CD3 bsTCR k_{off} constants against the pSL9 PSL and the Jurkat-NFAT activation assay determined EC50 concentrations. Color and symbols represent position of the PSL directed peptide substitution.

The second case was a group of outliers displayed strong pMHC-bsTCR binding affinities but weaker T cell activation than expected when compared to the overall trend. These peptides were mostly substituted at position 2 and 9, indicating a connection to the peptide-MHC complex stability similar to the 1G4 comparison: lower affinities for the peptide-MHC complex could result in decreased presentation levels of the respective pMHC complexes on the target cells after the exogenous loading. These levels might in turn influence pMHC-bsTCR complex numbers and ultimately Jurkat-NFAT effector cell activation.

To investigate this theory, the peptides were combined into groups roughly representing the strength of the cellular activation, based on the lowest bsTCR concentration leading to a 3-fold luminescence signal increase above background. The individual K_D values were then plotted against the NetMHC 4.0 assigned rank (Fig. 5.25).

For peptides below rank 2, a pattern suggesting a connection between increasing affinity constants and increasing bsTCR concentrations necessary to reach the activation threshold emerged. Above this rank, the activation threshold values decreased in accordance with the NetMHC prediction.

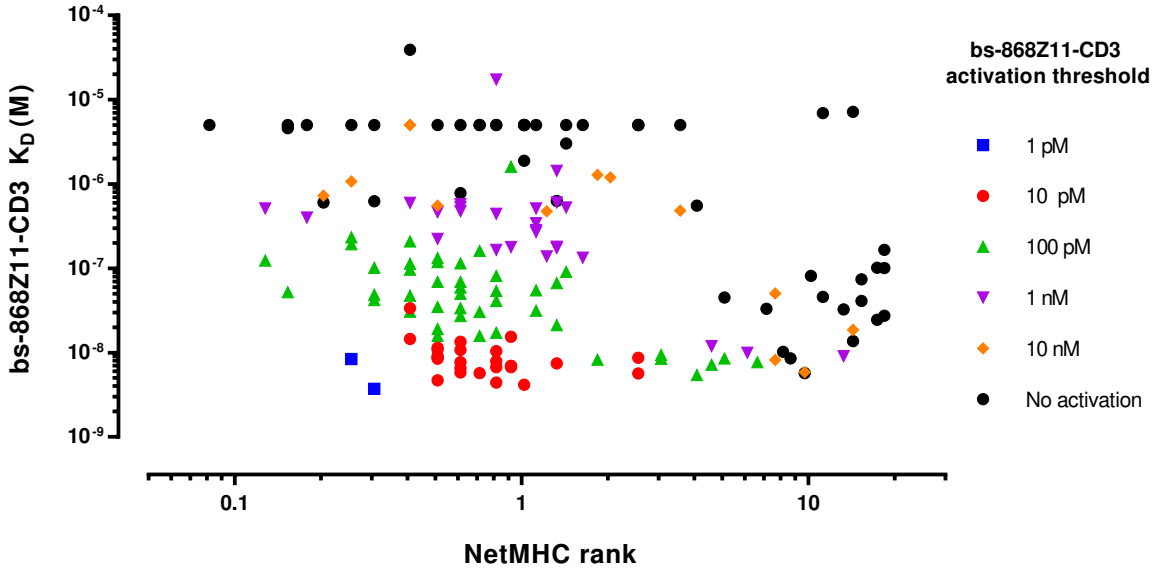

Fig. 5.25 Comparison of the measured bs-868Z11-CD3 bsTCR K_Ds against the pSL9 PSL and the NetMHC4.0 predicted affinity of the respective peptides for the peptide-MHC complex, depicted as NetMHC ranks. Color and symbols represent categorization into different T cell activation groups based on the bs-868Z11-CD3 concentration necessary to achieve a 3-fold luminescence increase over background.

To provide more direct evidence for the hypothesis and corroborate the NetMHC predictions, a flow cytometric peptide binding assay was performed by 10 µM peptide loading of T2 target cells and HLA-A*02 surface level detection using a PE-labelled anti-HLA-A2 antibody. Only weakly elevated HLA-A2 surface levels were detected after peptide loading for peptides with lower predicted binding affinities compared to unloaded T2 cells, especially for NetMHC ranks of 2 and above, supporting the hypothesis (Fig. 5.26).

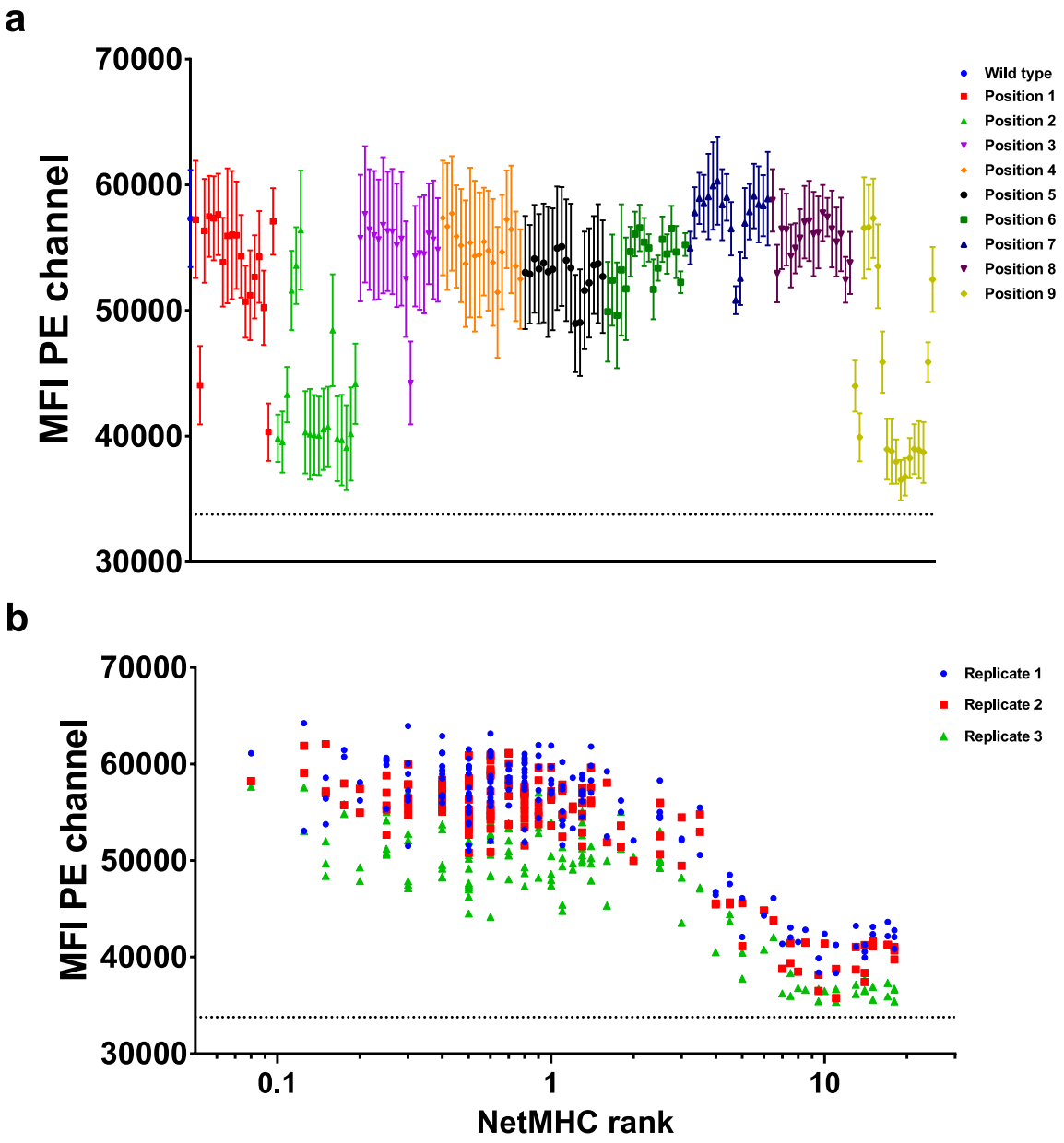

Fig. 5.26 Flow cytometric peptide binding assay with an anti-human HLA-A2 antibody staining of T2 cells after exogenous peptide loading. (a) PE channel MFI of T2 cells loaded individually with one specific peptide from the pSL9 PSL for 2 hours and stained afterwards using a PE labelled anti-human HLA-A2 antibody. Results are colored based on the position of the substitution compared to the wild type sequence. Error bars represent technical triplicates. (b) Comparison of PE channel MFI measured after peptide loading and antibody staining and NetMHC predicted peptide affinity for the MHC.

5.3.5. Prediction and identification of off-target peptides based on positional scanning libraries

To explore whether a PSL dataset derived binding motif could be used to identify relevant peptides, a peptide ligand search motif from the binding affinity dataset was created using an experimental K_D threshold of 50 nM: all single amino acid substitutions increasing the bs-868Z11-CD3 K_D above that threshold were excluded from the motif (Table 5.8).

Table 5.8 pSL9 PSL derived binding motif used for protein sequence database search.

Peptide Position	Permitted Amino Acids
1	GPAVLIMKRNDST
2	GAVLIMFYHQNEST
3	FYW
4	N
5	VLIMT
6	PVLIMT
7	GPANS
8	GAVLIMHKRQNEDST
9	GAVLIMFYWHKRQNST

Based on this motif, a search in the NCBI human non-redundant protein sequence database for nonameric peptide sequences matching combinations allowed by the motif was performed without any filters regarding predicted affinity for the peptide-MHC complex or detected presentation on healthy tissue. The search identified over 400 hits within the proteome, with sequence identity compared to pSL9 ranging from 1 to 6 identical positions. 140 peptides were selected, sampled to be representative of the sequence identity distribution in the larger group, synthesized and used for binding kinetics measurements as well as Jurkat-NFAT activation assays.

Single digit µM K_Ds or less could be determined for 91 of those peptides (Table S5). From this group, 24 peptides were able to induce a 3-fold T cell activation over background with at least one of the supplied bsTCR concentrations and 11 of them as early as 10 or 100 pM (Fig. 5.27 a). A similar connection was found between binding affinities and T cell activation compared to the results obtained with the positional scanning library (Fig. 5.27 b) with one outlier. NetMHC4.0 analysis revealed a peptide binding affinity with a rank of 7, indicating that low presentation by the T2 cells could play a role.

One of the peptides, ALYNVLAKV, was worth of special notice as it is presented on the cell surface of multiple human tissue samples according to the XPRESIDENT immunopeptidomics database, a high-throughput technology platform based on mass spectrometry (LC-MS/MS) which is coupled a with an immunoinformatics platform to identify HLA-bound peptides presented on tumor cells or normal tissues(*11*, *119*). The peptide is derived from intermediate filament family orphan 1 or 2 (IFFO1/2) and was detected on multiple healthy tissue and tumor tissue samples, ranging from head and neck, spleen, or kidney to non-small cell lung carcinoma or renal cell carcinoma. It produced robust T cell activation and the K_D of the interaction was 65.9 nM (Fig. 5.27 c and d). A second LC-MS detected peptide, KTFNLIPAV, with a lower K_D of 413 nM which was previously detected on 3 tumor tissue samples was also identified-

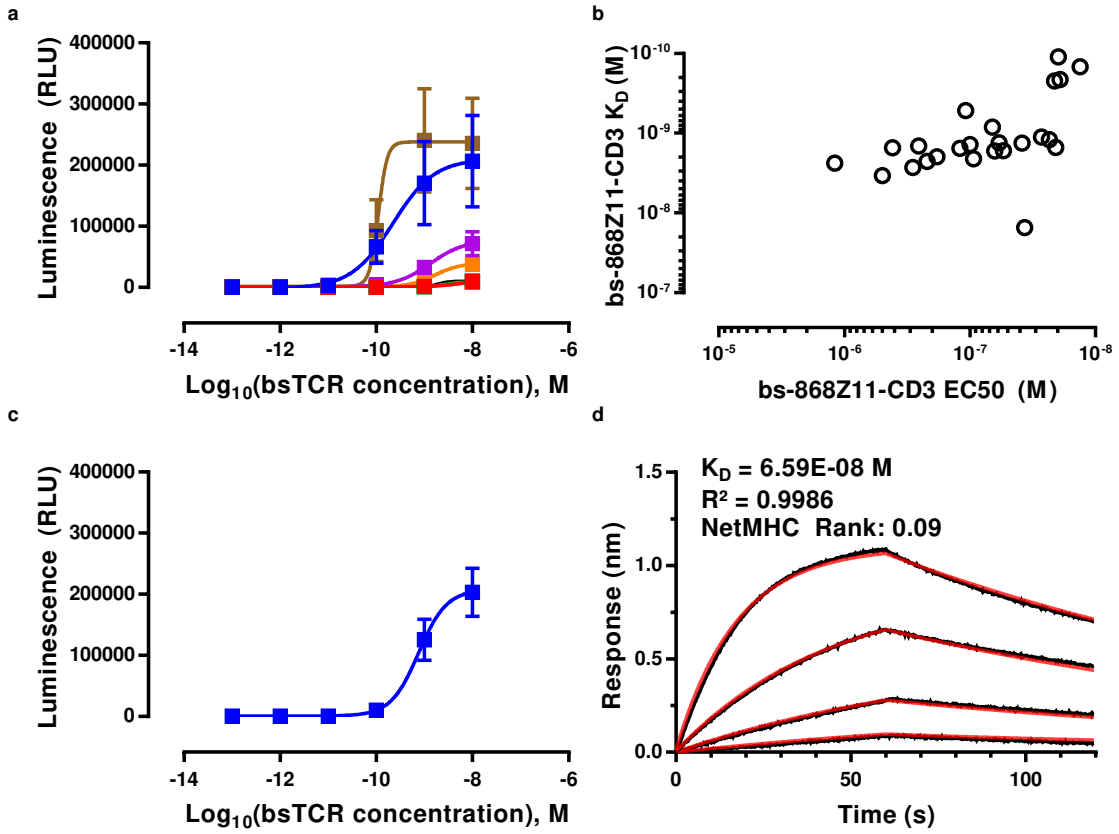

Fig. 5.27 T cell activation and binding of peptides predicted to be recognized by bs-868Z11-CD3. (a) Nonlinear regression curve fitting of T cell activation mediated by bs-868Z11-CD3 for exemplary peptides from the predicted binder pool. (b) Comparison of fitted EC50 and measured bs-868Z11-CD3 K_D for the 24 peptides positive in both assays. (c) Jurkat-NFAT activation by bs-868Z11-CD3 and 100 nM ALYNVLAKV-loaded T2 target cells. (d) Sensorgram for immobilized bs-868Z11-CD3 binding to soluble ALYNVLAKV-loaded DS-A2 peptide-MHC complexes measured on the Octet RED384.

It was further analyzed how the initially permitted amino acids for the search motif were distributed with respect to frequency at the respective position within the initially selected 140 peptide pool and whether this frequency changed for sub pools selected based on bs-868Z11-CD3 binding affinity (Fig. 5.28).

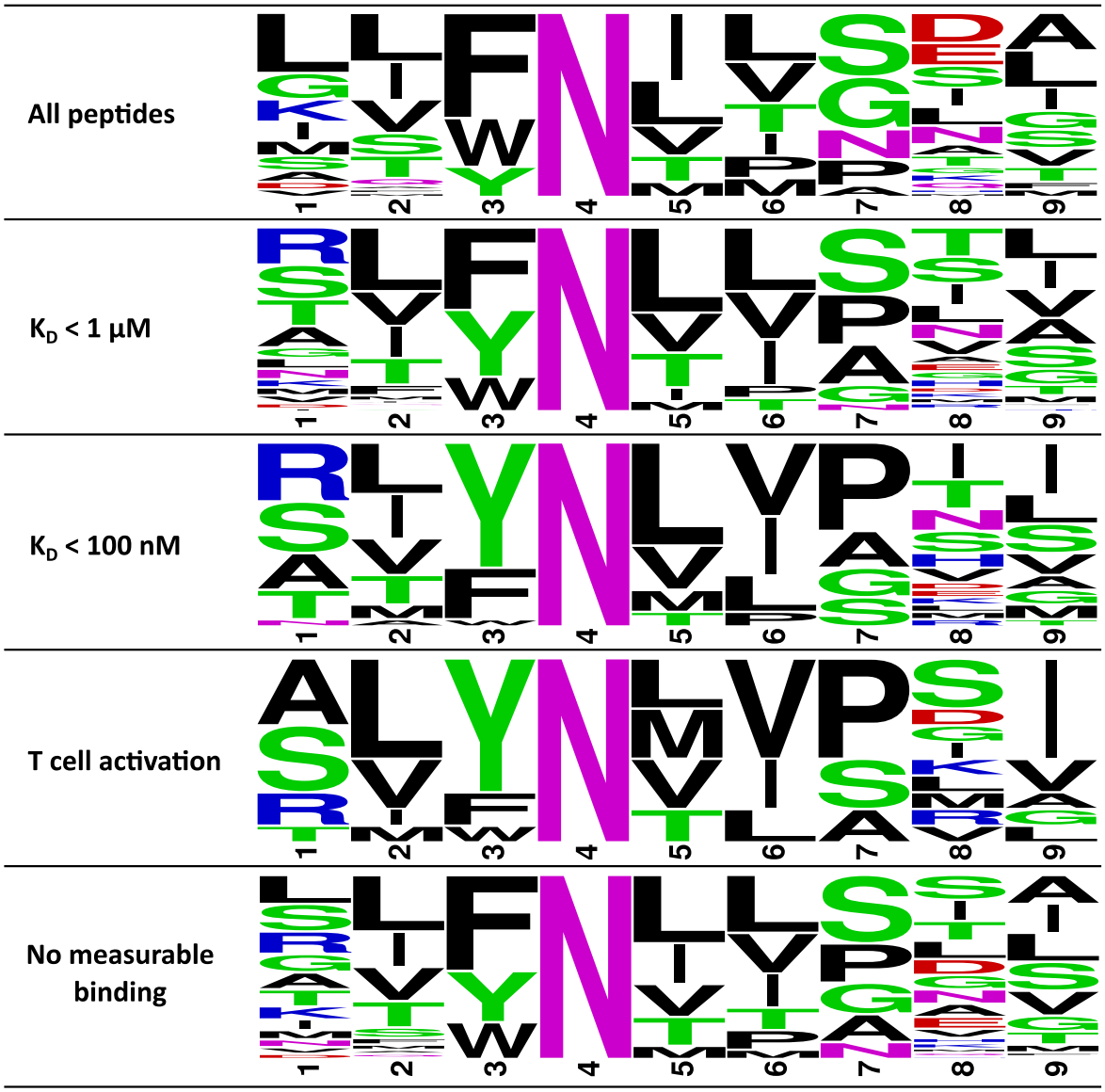

Fig. 5.28 WebLogo representation of amino acid distribution within the 140 peptide pool as well as differently defined sub pools. Individual letter sizes at each position are representative of the prevalence of the respective amino acid compared to the others at the same position within the pool. Amino acids were colored according to their chemical properties: polar amino acids (G,S,T,Y,C,Q,N) are green, basic (K,R,H) blue, acidic (D,E) red and hydrophobic (A,V,L,I,P,W,F,M) amino acids are black

As no initial filter besides amino acid occurrence was applied, e.g. a removal of predicted A*02:01 weak or no binders, nearly every peptide permitted was present in some form in the final library. With increasing binding affinity, a more pSL9 pattern seems to be beneficial, with especially serine at position 1 and tyrosine at position 3 increasing in prominence.

In contrast, tyrosine position 5 seems less preferred within the allowed combinations. Expectedly, position 2 and position 9 amino acids are much more restricted within the pool of peptides inducing Jurkat-NFAT activation, matching the amino acids preferred by HLA-A*02:01 at these anchor positions.

While the K_D cutoff approach used was suitable to identify an initial test peptide set, employing a similar strategy for a TCR during clinical development should be much more nuanced, as the cutoff strategy is likely disconnected from the biochemical interactions between TCR and peptide-MHC and the underlying mechanisms.

For this purpose, the PSL affinity dataset was transformed into a scoring matrix: each amino acid exchange at each position was assigned an individual exchange score, calculated as fold-change between the pSL9 affinity and the respective PSL peptide (Table 5.9).

$$Individual\ exchange\ score = bs - 868Z11 - CD3\frac{pSL9\ K_D}{p(nx)K_D},$$

$$with\ n\ representing\ position\ in\ nonameric\ sequence\ and\ x\ representing\ amino\ acid\ substituted$$

Based on the resulting matrix, each potential peptide could then be assigned a PSL score calculated from the individual exchange scores by multiplication of all ratios and base 10 logarithmic transformation

$$PSL\ score = log_{10}\prod_{n=1}^{9} Individual\ exchange\ sore\ (nx),$$

$$with\ n\ representing\ position\ in\ nonameric\ peptide\ sequence\ and\ x\ representing\ amino\ acid$$

Table 5.9 Individual exchange scores calculated for bs-868Z11-CD3 binding affinities to pSL9 PSL.

	Peptide Position								
	1	**2**	**3**	**4**	**5**	**6**	**7**	**8**	**9**
G	0.12	0.20	0.00	0.01	0.01	0.03	0.46	0.34	0.49
P	0.45	0.02	0.00	0.01	0.00	0.25	1.03	0.02	0.08
A	0.65	0.38	0.00	0.03	0.04	0.07	1.00	0.45	0.57
V	0.66	0.45	0.01	0.02	0.12	1.00	0.01	0.55	0.45
L	0.08	1.00	0.03	0.06	0.26	0.42	0.00	0.24	1.00
I	0.28	0.44	0.01	0.01	0.08	0.44	0.00	0.92	0.57
M	0.09	0.58	0.00	0.00	0.09	0.14	0.04	0.50	0.51
F	0.07	0.45	0.11	0.00	0.01	0.01	0.01	0.02	0.32
Y	0.03	0.12	1.00	0.00	0.00	0.01	0.00	0.01	0.37
W	0.01	0.05	0.11	0.00	0.00	0.00	0.00	0.02	0.11
H	0.01	0.14	0.04	0.05	0.01	0.02	0.03	0.35	0.28
K	0.20	0.05	0.00	0.00	0.02	0.00	0.00	0.22	0.08
R	0.86	0.04	0.01	0.00	0.00	0.00	0.00	0.48	0.67
Q	0.03	0.40	0.01	0.01	0.01	0.01	0.07	0.24	0.65
N	0.12	0.16	0.01	1.00	0.03	0.02	0.09	0.35	0.42
E	0.01	0.09	0.00	0.00	0.00	0.00	0.00	0.08	0.00
D	0.08	0.04	0.00	0.00	0.00	0.01	0.00	0.18	0.00
S	1.00	0.47	0.00	0.06	0.06	0.02	0.36	0.81	0.53
T	0.55	0.70	0.00	0.02	1.00	0.11	0.06	1.00	0.67
H	0.01	0.14	0.04	0.05	0.01	0.02	0.03	0.35	0.28

To evaluate whether this strategy would have predictive value, PSL scores were calculated for all 140 peptides from the test pool and plotted against the measured binding affinities (Table 5.10. Fig. 5.29).

Overall, the correlation between PSL score and K_D values was robust when expressed as pearson correlation coefficient. The pearson r was statistically significant and indicated a moderate to strong relationship between both datasets.

Table 5.10 Exemplary PSL score calculation for the 8 strongest binders from the bs-8686Z11-CD3 binding motif derived 140 peptide pool.

Peptide Sequence	Individual Exchange Scores									PSL Score
	1	2	3	4	5	6	7	8	9	
RVYNTVPLV	0.86	0.45	1.00	1.00	1.00	1.00	1.03	0.24	0.45	-1.360679348
RMYNLVSRI	0.86	0.58	1.00	1.00	0.26	1.00	0.36	0.48	0.57	-1.885550029
ASFNVIPSL	0.65	0.47	0.11	1.00	0.12	0.44	1.03	0.81	1.00	-2.818263115
SLYNMVPSI	1.00	1.00	1.00	1.00	0.09	1.00	1.03	0.81	0.57	-1.370913008
TVWNTLSSL	0.55	0.45	0.11	1.00	1.00	0.42	0.36	0.81	1.00	-2.456651731
ALYNVIAMA	0.65	1.00	1.00	1.00	0.12	0.44	1.00	0.50	0.57	-2.002590841
AIYNLLPDI	0.65	0.44	1.00	1.00	0.26	0.42	1.03	0.18	0.57	-2.480988541
STYNLLSTS	1.00	0.70	1.00	1.00	0.26	0.42	0.36	1.00	0.53	-1.826691048

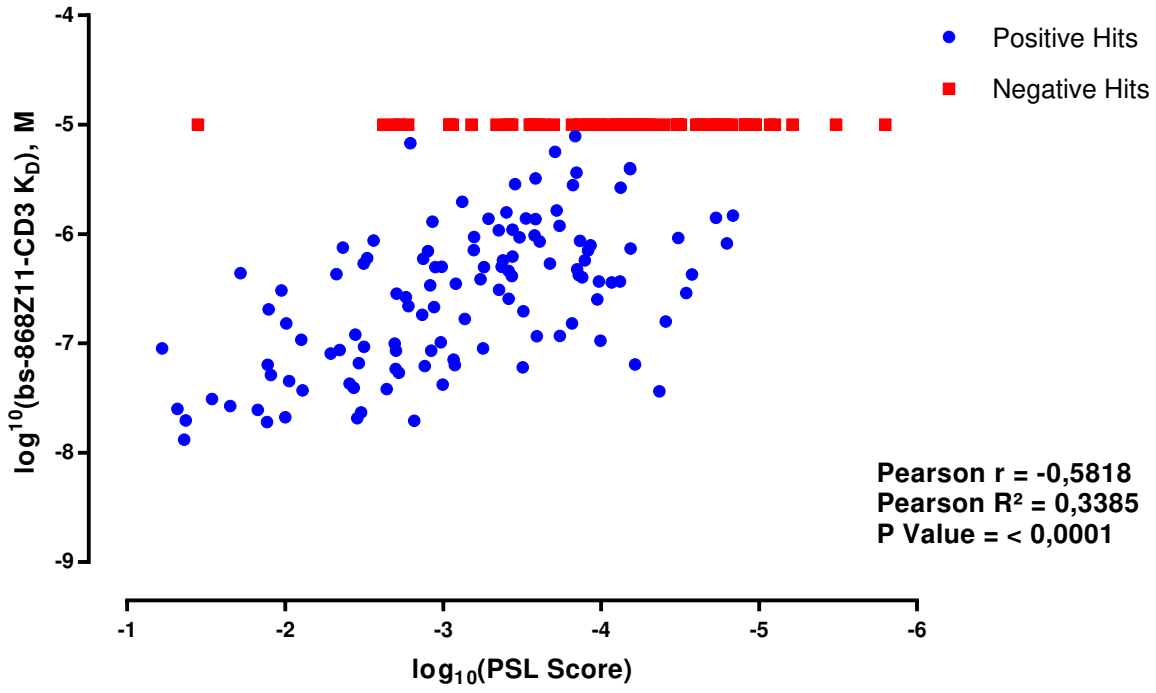

Fig. 5.29 Correlation between calculated PSL score and measured bs-8686Z11-CD3 binding affinity.

5.3.6. Unbiased screening against healthy tissue-based peptide libraries

Due the compatibility of the bs-868Z11-CD3 bsTCR with cost-effective biosensor regeneration and the significance of binding affinity for its function, a screening strategy was devised to detect interactions with high risk peptides detected on healthy tissues (HT peptides) without motif-based filter.

An exemplary 1995 high risk peptide pool was created by including peptides that matched HLA-A*02:01 specific characteristics (length between 9 and 11 amino acids and good predictive score for HLA-A*02:01 binding) and that were detected on 8% or more of 574 samples from different tissues and donors previously by LC-MS analysis with XPRESIDENT. The HT peptides were synthesized as previously described and peptide purity was between 96.97 and 7.5% with a median of 75.74%.

In an initial test run, peptide-MHC complexes were produced by DS-A2 peptide loading for 672 peptides with a final concentration of 25 µg/ml or 555 nM. The peptide-MHC samples were then screen for binding to immobilized bs-868Z11-CD3, on the Octet RED384 in combination with positive control samples, envisioned as a yes or no-hit screening with further activities for binding signals above a certain response threshold. The procedure was repeated on three separate occasions (Fig. 5.30 a).

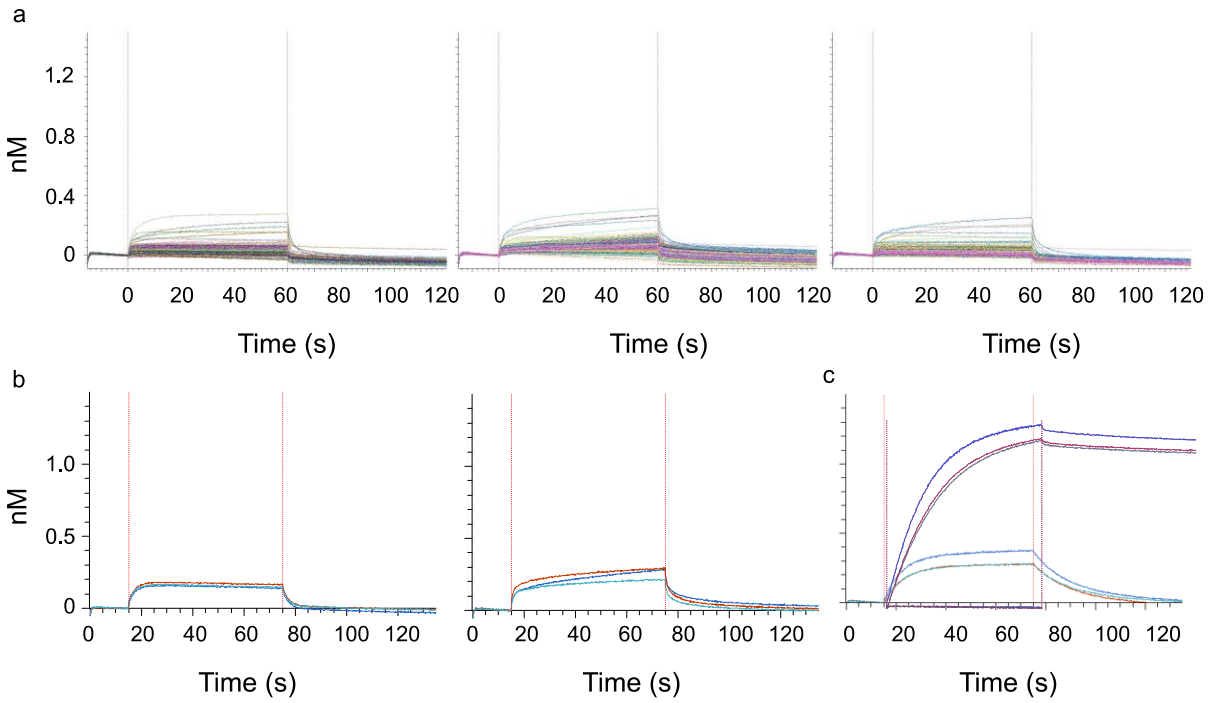

Fig. 5.30 Healthy tissue expressed high risk peptide screening against bs-868Z11-CD3. (a) Screening of 672 peptides in three separate assays using different DS-A2 batches for peptide loading reactions. (b) Even low affinity interactions expected to be below 1 µM were detected with good reproducibility. (c) Positive controls showcasing a strong 18.2 nM K_D interaction, a weak 604 nM interaction K_D and a non-recognized control peptide for reference.

Based on the feasibility experiment, the remaining peptides were tested using the identical setup. Increase binding could be observed for 4 peptides from the extended peptide pool, but sensorgram curves exhibited bi-phasic behaviour which could be indicative with unspecific background interactions (Fig. 5.31 a).

To corroborate the results, all peptides were also tested using the Jurkat-NFAT activation assays with 10 µM peptide loading and a 10 nM bsTCR concentration for maximized sensitivity. No T cell activation was observed with the 4 conspicuous peptides from the binding kinetics screening. Weak responses against three different HT peptides (HT peptides 001 to 003) could be detected: activation levels were between 2- and 20-fold increase over unloaded T2 cell background. A follow up assay using a bsTCR titration series and 100 nM peptide loaded T2 cells did not result in significant activation by the three peptides. In comparison, the bs-868Z11-CD3 pSL9 interaction used as control resulted in an over 300-fold increase with 10 µM loading and a 177-fold increase with 100 nM loading.

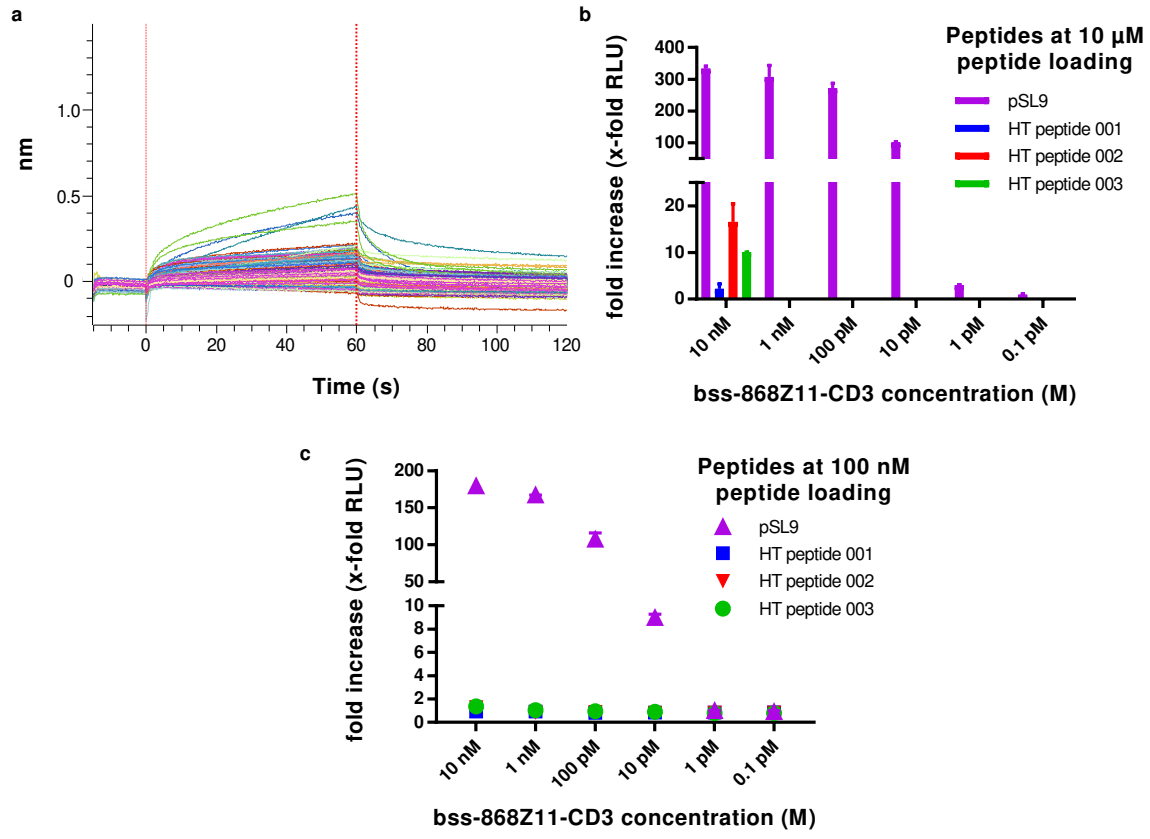

Fig. 5.31 Screening of 1995 HT peptides against bs-868Z11-CD3 on the Octet RED384 and using Jurkat-NFAT and peptide loaded target cells. (a) Grouped sensorgrams for the 1995 separate binding measurements. (c) Jurkat-NFAT activation by bs-868Z11-CD3 against T2 loaded target cells with pSL9 and the three most noticeable peptides at 10µM. (c) Comparison of Jurkat-NFAT activation by bs-868Z11-CD3 for the same HT peptides and pSL9 with 100 nM peptide loading.

5.3.7. Summary

In summary, screening of bs-868Z11-CD3 as exemplary was possible using both cellular as well as kinetic binding screenings with good comparability. Alanine scanning and PSL screening were most effective and a PSL-based search lead to identification of multiple potential off-target interactions. Using the kinetic measurement setup, screening of healthy tissue based high risk peptide libraries as an alternative approach to binding motif driven analysis could be demonstrated.

6. Discussion

6.1. Overview

Active utilization of peptide-MHC molecules as target class for cancer immunotherapy has steadily increased since the first results demonstrating that the immunopeptidome presented on tumor tissue can exhibit differences compared to healthy tissues. Amongst the many different approaches possible, those based on the use of T cell receptors as substantial part of the therapeutic modality have arisen naturally, as it is the designated interaction partner of peptide-MHC complexes. With this rise in use and an accompanying increase in experimental modification of the TCR molecule, e.g. affinity increases through sequence modification, a substantial need for careful and through characterization of these constructs has arisen as well, especially in light of the unpredicted fatal toxicities that have occurred in clinical trials.

The work presented in this dissertation was designed and performed with the intention to characterize existing and new strategies that are specifically aimed at determining the binding motif of TCRs, which can help excluding TCRs with a higher chance for off-target cross-reactivity or allow to actively predict and verify such peptide ligands. It was possible to analyze TCRs in different affinity ranges and formats, covering both adoptive cell therapy and bispecific T cell engager approaches, with different binding motif determining strategies as well as different readout approaches for direct comparison. In an active use of one of these datasets, prediction and detection of a potentially risky off-target interaction could be shown for one of these TCRs. In addition, proof of concept could be demonstrated for an unbiased screening approach not reliant on binding motif generation that could help to further increase the safety of approaches using affinity enhanced TCRs.

6.2. Disulfide-stabilized MHC class I molecules for peptide-MHC complex generation

Quick and flexible generation of pMHC complexes is a key requirement to facilitate the collection of large datasets against many different peptide-MHC complexes. Traditional refolding techniques are able to produce large amounts of individual complexes, but the throughput is unsuited to produce libraries with more than a few dozen different complexes. The disulfide-stabilized and functionally-empty HLA-A*02:01 molecule offers a throughput increasing alternative: it can be refolded and purified without the use of typically required high-affinity peptides and the resulting monomers can form peptide-MHC complexes after addition of peptides in a one-step loading procedure.

Even though the disulfide bridge enhances the stability of the MHC molecule, introduction does not inhibit or significantly alter binding of the currently investigated TCRs to DS-A2 pMHC complexes compared to the wild type. While the UV-mediated peptide ligand exchange offers similar throughput,

its exchange efficiency is dependent on rapid complex stabilization by the new peptide during the UV exposure. Especially lower-affinity peptides can fail to do so, resulting in a decreased functional pMHC concentration. This makes it a less reliable tool to produce pMHCs as soluble analytes for binding kinetics, since precise knowledge of the concentration is necessary to obtain correct curve fitting results. In addition, not needing an UV exposure step could enable different applications that benefit from temporal separation of MHC utilization and peptide loading, e.g. the production of microarrays or the use in microfluidic devices.

While affinity measurements were the only use case investigated in this work, other researchers were able to show that the molecule is also suited to prepare tetramer reagents for flow cytometry experiments (*120*). Interestingly, improved staining with respect to stain index analysis could be observed compared to conventional tetramers with wild type molecules, but the mechanism behind this effect is currently not understood in detail.

Due to the positioning in the F-pocket region this modification might be applicable in many more alleles: analysis using the IPD-IMGT/HLA database confirms that both the tyrosine and alanine residues modified are well conserved in almost all HLA-A alleles for example, and proof of concept for refolding has already been demonstrated by other researches for HLA-A*24:02 and HLA-B*07:02 (Saini et al., in press). Should no major differences be observed in further studies with more TCRs, which would be advisable due to the nature of the modification and the intended use case, this modification could significantly enhance the accessibility and scope of pMHC-based analysis.

6.3. Screening strategies and technologies for cellularly expressed T cell receptors

As outlined in the introduction, comprehensive screening is necessary in most instances of adoptive cellular transfer or other approaches relying on TCR mediated activity. In cellular screening systems, provision of effector cells can be an issue for large screening experiments, especially early in development when no expandable clone, e.g. with a lentiviral transduced TCR, is available. Using CD8+ T cells is an obvious choice, but a positional scanning library screen with 3 peptide loading concentrations in duplicates ultimately requires 500 million CD8+ T cells, factoring in all the losses due to thawing, stimulation and electroporation. This necessitates the processing of many leukapheresis samples to obtain a sufficient amount of CD8+ T cells, not factoring in donor to donor variations that can disqualify some samples due to background issues.

The Jurkat-NFAT effector cell line offers a suitable alternative for this kind of screening approaches. While less sensitive overall when compared to an IFN-gamma readout, the results obtained in combination with the 1G4 TCR were comparable over a broad range of different interaction strengths with respect to relative magnitude, matching the experiences made previously in smaller screening

panels with different TCRs recognizing the same target. While the investigated cell line still contains a native TCR, which means background due to combinations with the transfected TCR could still be an issue, this could be solved if necessary, by using a TCR negative Jurkat variant as starting cell line instead. In addition, the CD8 coreceptor can be co-transfected as demonstrated by Aarnoudse et al. to more closely resemble a regular CD8+ T cell if necessary(*118*).

But even at its current state, the advantages of the system are significant: without any laborious stimulation steps, working benches with one billion Jurkat-NFAT cells can be produced and frozen starting with only 10 million in a week. The assay is also particularly robust, producing results with no significant intra-assay changes and only 2-fold inter-assay differences even months apart and multiple reagent lot changes. The readout is also significantly quicker compared to an ELISA or ELISPOT assay and did not suffer from corner well effects, making assays slightly more efficient in processing.

Using this assay setup and a manual electric 96-channel pipette, the aforementioned PSL screening approach could be accomplished in effectively two days for the 1G4 TCR. The results from this analysis were principally in line with the general expectations for TCR behavior and the published literature regarding 1G4 in particular: both alanine scanning and the full PSL approach revealed an interaction with pESO9V that was mostly based on position 4, 5 and 6 of the peptide. This matches the crystal structure analysis published by Chen et al., that identified a protruding peg-like structure of the methionine and tryptophan. This provides most of the interaction with the 1G4 through non-covalent interactions with amino acids from CDR3 alpha and beta as well as CDR1 alpha domains. Interestingly, exchanges at position 8 were also non-favored, although this amino acid has no directly obvious strong contribution to the interaction. This could indicate that changes at this position have an indirect effect on the interaction, for example by altering the structure of the peptide within the binding groove. Such spatially distant effects have been described for the ILA1 TCR by Cole et al, for example(*91*).

When analyzed in detail, the PSL dataset offered a more nuanced picture: while the trend was in line with decreases or increases in activation with alanine substituted peptides, other substitutions at the same position were sometimes more or less tolerated. Using position 6 an example, the reason for this seems to be obvious for most of the other substitutions: valine, leucine and methionine were particularly well tolerated at this position, as well as phenylalanine and tyrosine.

These amino acids shared more physiochemical properties with the isoleucine in the initial peptide compared to alanine for example and thus were probably able to retain a similar structure and thus interaction with the TCR. Thus, combining alanine scanning with a physiochemical analysis, for example the peptide:MHC binding energy covariance matrix (PMBEC) or BLOSUM matrix could result in similar conclusion while only requiring an alanine scan(*121*). This may be a valid strategy during the

first characterization steps after TCR identification, when dozens of different TCRs are still potential candidates for further development.

But there were also exceptions that did not fit this pattern: although the methionine is described to be integral to the interaction, substitution of a glutamine produced a similar binding affinity in the cellular screening as well as the kinetic screening. This was unexpected, as their side chain properties are very distinct. Mutagenesis in the published structure did indicate though that the side chain may actually fit well in the existing pocket without requiring structural reorganization of the whole peptide, even with different side chain conformations, and it could form favorable interactions with CDR backbone amides. Identifying such cases, especially when no crystal structure is available, could be an advantage when using a PSL-based screening approach.

In comparison, the PS-SCL assay did not provide a deeper understanding or reveal more tolerated exchanges. On the contrary, only very few responses could be observed overall and those mostly correlated with the wild type amino acid at that position. While the assay is well established in the literature, with multiple publications in the last decade, the magnitude of the responses demonstrated can vary significantly according to the presented datasets, ranging from strong and distinct (*71*) to much less detailed (*78*), similarly to the results obtained for 1G4. Therefore, although the approach could allow for better detection of cross-reactive peptides in general, more work is necessary to identify which variables contribute to the large discrepancy observed between different experiments.

While ultimately feasible, performing the alanine scanning or PSL screening using refolded soluble TCRs and kinetic measurements did not result in a strong advantage compared to the cellular system. Although an overall correlation between the measured affinity constants and the reporter cell activation could be observed, the sensitivity was higher for the latter within the range of feasible sTCR protein concentrations used for the Octet screening. Even within the measurable range, weaker cellular activation than expected based on determined affinity could be observed that was not directly attributable to known variables, e.g. relatively diminished presentation of these peptides on the target cells due to weak affinity for the peptide-MHC complex. Generating these as soluble complexes using the disulfide-stabilized HLA-A*02 and high peptide concentrations is more predictable, therefore representing one potential advantage of the kinetic screening approach.

While it is unlikely that the unfavorable substitutions at the anchor positions 2 and 9, which apparently did not impede 1G4 TCR binding in the kinetic screening but were unable to stimulate in the cellular screening, can occur in different peptides actually presented *in vivo* in case of HLA-A*02:01 based on the reported MHC preferences, substitutions in different positions could lead to weak pMHC binders

in combination with the other 8 fixed amino acids but be well tolerated with other TCR compatible substitutions in a different peptide(*19*).

In any case, peptide loading concentration should be selected very carefully and the potential differences even within one concentration should be considered, especially when classification of activation levels like in PSL screenings is intended. As shown here and by others, T cell activation can be diminished at higher peptide loading concentrations for the strongest interactions, leading to a potentially distorted image if an insufficient concentration range is used(*122*, *123*).

6.4. Screening strategies and technologies for bispecific T cell engagers

For screening of bsTCRs, in this case bs-868Z11-CD3, the Jurkat-NFAT system could effectively be employed as well, demonstrating high sensitivity as effector cell and an efficient workflow in combination with bsTCR titration series and no-wash target cell peptide loadings in 96 well plates. Using the 96-channel pipette, 12 plate experiment setups covering 6 bsTCR concentrations for EC50 determination were achievable, making nuanced analysis and comparison of the individual interactions possible.

With this approach, it was possible to demonstrate the strong influence of the binding affinity for a respective peptide-MHC complex on the mediated T cell activation when all other variables, e.g. affinity of the T cell engaging domain, were identical. Particularly the k_{off} value seemed to be predictive which fits with the expected mechanism of a bispecific T cell engager, binding to a target cell and coating it with a very long interaction half-life to achieve potent stimulation of adjacent effector cells.

The binding preferences determined for 868Z11 using the pSL9 PSL library revealed a distinct TCR binding motif, with particular focus on positions 3 to 6. This is in good alignment with the alanine scanning and the structure of the non-maturated 868 TCR published by Cole et al., which revealed particular importance of the interaction with asparagine at position 4 and threonine at 5. Comparison with the alanine scanning approach was similar to the 1G4 example: the former was capable of predicting the trend at the respective position, results for the individually substituted amino acids differed significantly. Many of those patterns were explainable with similar physiochemical properties, for example well tolerated isoleucine or leucine exchanges instead of valine at position 6, but outliers like leucine instead of threonine at position 5 could be observed as well.

Screening of the PS-SCL library resulted in more detectable activation compared to the 1G4 experiments but did not reveal a significantly different binding motif, with all of the activating pools corresponding to strong exchanges identified using the pSL9 PSL. The results were very comparable

with a PS-SCL experiment reported by Szomolay et al. using a cellularly expressed variant of the non-maturated 868 TCR(*124*),

Multiple different approaches have been proposed to convert TCR binding motifs, either identified by PSL flow cytometry experiments, PSL ELISPOT assays or PS-SCL ELISAs, into search motifs to identify ligands matching the positions tolerated(*93*, *124*, *125*). These approaches either use cut off values, excluding all possibilities below the threshold without any weighting based on relative strength of the responses or scoring algorithms that factor in these differences through weighting systems. To investigate which approach was compatible with an affinity-based dataset, an initial cut off value was employed to assemble a testing library containing 140 peptides. Almost all amino acids permitted by the search motif were represented in the testing library based on sequences identified in the human proteome, but not verified as actually HLA-A*02:01 presented. When comparing the distribution of the permitted amino acids at each position and their relation to the measured affinity, combination of individually strong substitutions led to relatively stronger interactions with the assembled peptide, even if the overall sequence identity compared to pSL9 was low. Creation of a scoring algorithm based on relative changes in affinity compared to pSL9 in the PSL and retrospective analysis of the testing library supported that analysis, as summarization of the relative changes had significant predictive value.

Based on these results, it could be speculated that the PSL screening approach is mainly detecting the possibility of individual replacements within the limits of one relatively defined structure of the pMHC-TCR complex. It is therefore questionable whether this approach would also allow prediction of peptides that exhibit no structural similarity and potentially distinct non-covalent interaction pattern. As demonstrated by Riley et al, the structural flexibility of different peptides in the MHC binding groove can enable cross-reactivity even without structural mimicry or changes in the TCR CDR loop structure(*92*). Discovery of such peptides should in theory be possible with motifs produced using the PS-SCL library but was not successful in the presented experiments as the resulting motif was much less detailed compared to the PSL-based motif.

Despite the discussed limitations, examples like the identification of the ALYNVLAKV interaction or the – although retrospective – detection of the cross-reactive Titin peptide highlight the potential value of positional screening approaches in detecting at least some off-target interactions.

In this context, PSL screenings could be particularly useful to either screen and compare TCRs from different donors that recognize the same target or different affinity maturated variants of one particular TCR, with the intention to identify candidates whose binding motif predicts the lowest risk for the existence of structurally similar and potentially reactive peptides in the proteome. It should

not be regarded as an absolute and final assessment of cross-reactivity though and further technological and experimental advantages will be necessary to improve our understanding and predictive capabilities. This could include libraries with higher degrees of complexities, e.g. by combining and screening peptides with multiple substitutions compared to the wild type sequence at the same time, or simply generating much more datasets comprising TCR sequences and recognized peptide-MHCs or peptide-MHC binding motifs, ideally in combination with crystal structures, to allow development of robust *in silico* prediction engines based on TCR sequences or structural information.

The demonstrated screening also highlights the necessity of repositories that go beyond the proteome information included in the UniProt or NCBI databases. While 24 peptides from the testing library for 868Z11 were capable of HLA-A*02:01 presentation and above µM interactions with the TCR, only two were previously detected on tissue samples according to the XPRESIDENT database. Without tools to differentiate between actually relevant and theoretical off-target interactions, cross-reactive peptide ligands can likely be identified for almost every TCR due to their cross-reactive nature. Databases like the immune epitope database IEDB, the SysteMHC atlas or SWATHAtlas data repository, which provide and curate T cell epitope data or tissue- and allele-specific immunoproteomic datasets, represent publicly available tools that could potentially be of use in that regard(*126*, *127*). In addition, sequence similarity screenings solely based on the amino acid sequence of potential targets might represent an auxiliary approach prior to TCR identification, which could help to prioritize targets that have a comparatively distinct sequence, e.g. by using algorithms like Expitope 2.0 which uses sequence similarity and RNA expression data to calculate risk factors(*128*). Given the currently sparse information about successful or non-successful attempts using peptide-MHC targets it is hard to evaluate though whether such tools can contribute significantly to improve clinical success.

A currently common approach to discover the existence of cross-reactive ligands that are most likely presented *in vivo* without exact knowledge of the respective peptide sequences is screening against cultured healthy tissue cell lines. In theory, such screenings would also be able to detect interactions with peptides that have no structural similarity to a known target, but as the Titin cross-reactivity has already demonstrated suspension or adherent cell cultures may not be representative of their spatially organized *in vivo* counter parts. Since it is known that mechanotransduction and structural organization can have an impact on gene and protein expression, it is very possible that this will in turn also influence the resulting immunopeptidome(*129*).

Thus, testing commercially available cell lines of tissues only isolated from a limited pool of individuals might not account for all potentially presented peptides in the population, even within the same allele, and ultimately represents an undefined peptide-MHC library. Selection of high-risk or tissue-specific

peptide libraries from immunopeptidome databases as demonstrated in this proof-of-concept could represent a more standardized alternative. While its peptide-MHC coverage is ultimately linked to the quality and extent of the library, its makeup is much more defined and controllable. In combination with bispecific T cell engagers, screening such a library for peptide-MHC binding affinity using a kinetic screening approach can result in data that has considerably predictive value for its function and enable a high throughput. While the here demonstrated measurement of 2000 peptides took two days and was therefore only marginally faster compared to the accompanying cellular measurements, higher throughput options using similar approaches are also available. For example, the demonstrated approach using the Octet RED384 could easily be performed on a device by the same manufacturer but with 6-fold increased throughput by using 96 instead of 16 biosensors in parallel. With this approach, screening of 5000 peptide-MHCs against one bispecific T cell engager represents a manageable task during routine development.

Instead of using chemical peptide synthesis and peptide-MHC complex generation, cellular display systems like phage or yeast display can also be employed to engineer custom peptide-MHC libraries. Birnbaum and Ghee et al. have designed a single-chain peptide-MHC based yeast display, where each yeast cell has the potential to expresses one particular randomly generated peptide(*130*, *131*). Yeast cells expressing peptide-MHC molecules recognized by specific TCRs are enriched using flow cytometry and fluorescently labelled TCRs and peptides presented by those cells identified using next generation sequencing. While this approach was capable of demonstrating the surprisingly broad variety of peptides one TCR can bind, the size and random nature of these libraries mean not all potentially existing peptides are represented while actually identified peptide ligands do often not exist in the proteome.

Novel technologies using DNA barcode based encoding of peptide-MHC multimers have increased the number of multimers that can be used in parallel, enabling at least 1000 different and defined peptides to be used for staining cellularly-expressed T cell receptors or fluorescently labelled soluble TCRs (*125*, *132*). In contrast to the affinity data generated by the kinetic screening approach, the readout is avidity-based, making interpretation of the data less straight forward. In addition, the competing nature of the individual peptide-MHC complexes for binding to one TCR presented on a cell surface could prove to be challenging with respect to the sensitivity of the readout.

Through the advances in microarray technology, even larger kinetic screenings could be possible. Peptide-based microarrays can already be produced with incredible density of tens or hundreds of thousands different spots despite spatial separation, using digital micromirror device created masks and photolithography(*133*, *134*). Microarrays like this are already used for whole-proteome profiling

of antibody repertoires(*135*). In addition, technologies have been developed that allow binding kinetics measurements on such microarrays instead of using fluorescence scanners(*136–139*). This represents a significant advantage, as fluorescent measurements only reveal steady state binding levels, whereas the kinetic and particularly the off rate seems to the most descriptive property.

Unfortunately, conventional peptide arrays are not suitable to screen TCRs or pMHC-recognizing antibodies since the peptide must be presented in the context of the MHC complex for proper analysis. Production of peptide-MHC microarrays has been attempted previously, but mostly resulted in unsatisfactory results with respect to quality and stability of the produced microarrays(*140–143*). The development of the disulfide-stabilized empty MHC molecule could offer a potential way to improve upon previous results: when coupled with peptide loading in plates, spotting and immobilization on a streptavidin-functionalized microarray and kinetic measurement using the aforementioned kinetic screening platform, it was possible to measure robust binding of the soluble 1G4 TCR to pESO9V loaded peptide-MHCs on 384 spots in parallel (Fig. 4.1)

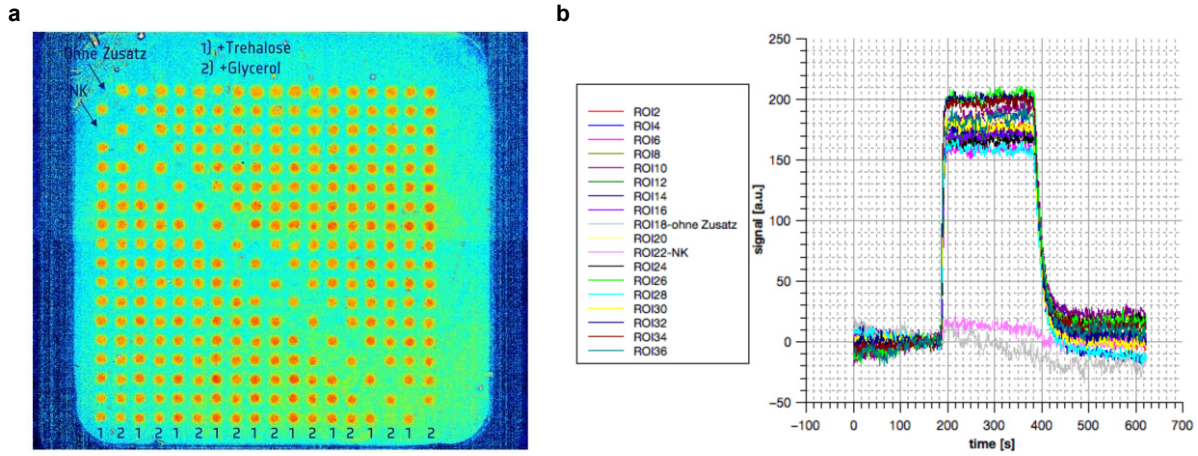

Fig. 6.1 Microarray-based kinetic screening of pESO9V peptide-MHC and 1G4 sTCR interaction. (a) The image created by the bscreen visualizes strong binding to individual spots in red whereas absence of binding to the background is depicted in with a blue and green color scale. (b) Sensorgrams depicting binding to individual pESO9V peptide-MHC or control spots (ROI) after background subtraction.

Reduction of the individual spot size could likely enable 5000 and potentially up to 20000 individual spots within the useable microarray area, a range that could allow immunopeptidome-scale screenings within hours instead of days or weeks. Especially when combined with prior on-array peptide synthesis as alternative to conventional synthesis and spotting, screening specifically designed tissue- or immunopeptidome-representing microarrays could be a realistic and convenient tool in the safety screening arsenal.

7. Acknowledgements

The HLA-A*02:01 Y84C A139C mutant was conceived and first produced by the group of Prof. Dr. Sebastian Springer at the Jacobs University Bremen GmbH. My thanks go to him and to his lab members Dr. Raghavendra Anjanappa and Ankur Saikia for the close collaboration as well as Dr. Sunil Kumar Saini and Dr. Martian Zacharias who also contributed to this development.

In addition, Dr. Maria Garcia-Alai and Dr. Rob Meijers from the EMBL Hamburg, DESY Outstation, performed the crystallization experiments and crystal imaging leading to the crystal structure of the HLA-A*02:01 Y84C A139C ESO9V molecule in complex with the soluble 1G4 TCR. Dr. Gabriele Pszolla from Immatics biotechnologies GmbH Tübingen performed the crystal structure analysis.

Martin Hofmann and his CMC biologics group at Immatics biotechnologies GmbH Tübingen performed the design and production the bs-868Z11-CD3 construct based on the cited literature.

Access to the XPRESIDENT immunopeptidomics database was enabled by Immatics GmbH Tübingen. My thanks go to Dr. Heiko Schuster, Martin Primer, Heike Hoffmann and Anja Arthur who offered great support with mass spectrometry and data analysis and to Dr. Jens Fritsche and Dr. Gisela Schimmack for assistance with access to the database.

Peptide synthesis was mostly performed by the CMC group of Sonja Dorner and Christian Flohr at Immatics biotechnologies GmbH Tübingen.

The first microarray experiments referenced in the discussion section were performed in collaboration with Biametrics GmbH, now Biocopy. My thanks go to Dr. Günther Proll, Dr. Florian Pröll and Dr. Peter Fechner for the exciting collaboration.

All experiments if not stated otherwise were performed at and financed by Immatics biotechnologies GmbH Tübingen.

8. Danksagung

Wie so oft ist es schwierig allen gebührend zu danken, die diesen Weg begleitet haben, ich möchte es dennoch versuchen.

Zuallererst geht ein großer Dank an Prof. Hans-Georg Rammensee, ohne dessen Mentorschaft und Fürsprechen eine Doktorarbeit in dieser sehr spannenden Konstellation nicht möglich gewesen wäre.

Ebenfalls möchte ich Prof. Stefan Stevanović für seine Bereitschaft danken diese Dissertation initial bis noch nach seinem Ruhestand als Gutachter zu begleiten.

Ein ebenfalls sehr großer Dank geht an Dr. Dominik Maurer, der nicht nur die Rahmenbedingungen für diese Arbeit maßgeblich mit ermöglicht hat, sondern mir als erster Ansprechpartner stets mit Rat und Tat zur Seite stand.

Darüber hinaus geht ein großes Dankeschön an die gesamte Immatics Familie: es sind so viele Namen und Kollegen über die zuvor genannten hinaus und aus allen möglichen Abteilungen, die diese Arbeit in unterschiedlichsten Varianten über die Zeit unterstützt und begleitet haben, sei es im Labor, im Büro oder beim gemeinsamen Feierabend. Es ist ebenso ungerecht einzelne wie unmöglich alle Personen aufzuzählen, nicht vergessen werden sollte aber mit Sicherheit Dr. Steffen Walter, ohne den ich mit hoher Wahrscheinlichkeit nie in dieser wunderbaren Umgebung gelandet wäre.

Nicht vergessen werden sollten aber auch die Elche: auch wenn die Labore durch einige Luftmeter getrennt waren habe ich mich spätestens auf der CIMT in jedem Jahr doch ein bisschen wie einer von euch fühlen dürfen.

In guter Erinnerung bleiben mir auch Prof. Sine Reker Hadrup und ihre Arbeitsgruppe an der DTU, darunter insbesondere Dr. Amalie Kai Bentzen: auch wenn letztlich nicht jedes gemeinsame Experiment erfolgreich war würde ich diese Kollaboration jederzeit wieder eingehen, danke dafür.

Selbiges trifft auf die Kooperation mit Prof. Sebastian Springer und seiner Arbeitsgruppe an der Jacobs Universität Bremen zu: ich bin sehr stolz das Disulfid-A2 Projekt gemeinsam mit Raghavendra Anjanappa anvertraut bekommen zu haben und bin sehr gespannt zu sehen, was die Zukunft für diese Technologie noch bereit hält.

Last but not least möchte ich meiner Familie und meiner wunderbaren Frau danken: Mama, Papa, Patrick und Anne, ohne Menschen wie euch im Rücken die einen auch bei mehr oder weniger großen Anfällen der Selbstzweifel stützen wäre so ein Projekt ungleich schwerer wenn nicht gar unmöglich. Danke, dass ihr für mich da wart und es hoffentlich weiter bleiben werdet.

9. Abbreviations

ADCC	antibody-dependent cytotoxicity
ALL	acute lymphoblastic leukaemia
β_2 m	beta $_2$ microglobulin
BiTE	bispecific T cell engager
BSA	bovine serum albumin
bsTCR	bispecific T cell receptor
CAR-T	chimeric Antigen Receptor T cell
CDR	complementarity determining region
DNA	deoxyribonucleic acid
DS-A2	disulfide bridge stabilized HLA-A*02:01 complex
ELISA	enzyme-linked immunosorbent assay
FCS	fetal calf serum
FPLC	fast protein liquid chromatography
GM	dipeptide H-Glycine-Methionine-OH
HLA	human leukocyte antigen
HS	human serum
IFN-g	interferon gamma
IPSC	induced pluripotent stem cell
IPTG	isopropyl-β-D-thiogalactopyranoside
Jurkat-NFAT	GloResponse NFAT-RE-luc2 Jurkat cell line
kDa	kilodalton
K_D	dissociation constant
k_{on}	association rate
k_{off}	dissociation rate
MACS	magnetic activated cell sorting
MAGE	melanoma-associated antigen
MART-1	melanoma associated antigen recognized by T cells
MBP	myelin basic protein
MHC	major histocompatibility complex
NY-ESO-1	New York esophageal squamos cell carcinoma-1
PAGE	Polyacrylamide-Gel electrophoresis
pEBV	EBV BLMF-$1_{280-288}$ GLCTLVAML
pMLA	Melan-A $MART1_{26-35}$ ELAGIGILTV
pESO9V	NY-ESO-$1_{157-165}$ 9V SLLMWITQV
pSL9	HIV-1 p17 GAG_{77-85} SLYNTVATL
PSL	Positional Scanning Library
PS-SCL	Positional Scanning Synthetic Combinatorial Peptide Library
RNA	ribonucleic acid
scTv	single chain linked T cell receptor variable fragments
SEC	size exclusion chromatography
sTCR	soluble T cell receptor
TCM	T cell medium
TCR	T cell receptor
TIL	tumor infiltrating lymphocyte
WT-A2	wild type HLA-A*02:01 complex

10. References

1. J. B. Swann, M. J. Smyth, Immune surveillance of tumors. *J. Clin. Invest.* **117**, 1137–1146 (2007).

2. D. Ribatti, The concept of immune surveillance against tumors: The first theories. *Oncotarget*. **8**, 7175–7180 (2017).

3. G. P. Dunn, A. T. Bruce, H. Ikeda, L. J. Old, R. D. Schreiber, Cancer immunoediting: from immunosurveillance to tumor escape. *Nat. Immunol.* **3**, 991–998 (2002).

4. C. P. M. Duong, C. S. M. Yong, M. H. Kershaw, C. Y. Slaney, P. K. Darcy, Cancer immunotherapy utilizing gene-modified T cells: From the bench to the clinic. *Mol. Immunol.* (2015), doi:10.1016/j.molimm.2014.12.009.

5. C. J. Melief, Cancer immunotherapy by dendritic cells. *Immunity*. **29**, 372–383 (2008).

6. J. Oates, N. J. Hassan, B. K. Jakobsen, ImmTACs for targeted cancer therapy: Why, what, how, and which. *Mol. Immunol.* **67**, 67–74 (2015).

7. U. Sahin *et al.*, Personalized RNA mutanome vaccines mobilize poly-specific therapeutic immunity against cancer. *Nature* (2017), doi:10.1038/nature23003.

8. S. A. Rosenberg, N. P. Restifo, Adoptive cell transfer as personalized immunotherapy for human cancer. *Science (80-.).* **348**, 62–68 (2015).

9. A. S. Bear, C. R. Cruz, A. E. Foster, T cells as vehicles for cancer vaccination. *J. Biomed. Biotechnol.* **2011** (2011), p. 417403.

10. T. Blankenstein, M. Leisegang, W. Uckert, H. Schreiber, Targeting cancer-specific mutations by T cell receptor gene therapy. *Curr. Opin. Immunol.* **33**, 112–119 (2015).

11. S. Walter *et al.*, Multipeptide immune response to cancer vaccine IMA901 after single-dose cyclophosphamide associates with longer patient survival. *Nat. Med.* **18**, 1254–1261 (2012).

12. R. Elahi, E. Khosh, S. Tahmasebi, A. Esmaeilzadeh, Immune Cell Hacking: Challenges and Clinical Approaches to Create Smarter Generations of Chimeric Antigen Receptor T Cells. *Front. Immunol.* **9**, 1717 (2018).

13. R. D. Schreiber, L. J. Old, M. J. Smyth, Cancer immunoediting: Integrating immunity's roles in cancer suppression and promotion. *Science (80-.).* **331**, 1565–1570 (2011).

14. M. D. Vesely, R. D. Schreiber, Cancer immunoediting: antigens, mechanisms, and implications to cancer immunotherapy. *Ann. N. Y. Acad. Sci.* **1284**, 1–5 (2013).

15. S. Maximiano, P. Magalhães, M. P. Guerreiro, M. Morgado, Trastuzumab in the Treatment of Breast Cancer. *BioDrugs*. **30**, 75–86 (2016).

16. R. Nahta, F. J. Esteva, Trastuzumab: Triumphs and tribulations. *Oncogene*. **26**, 3637–3643 (2007).

17. H.-G. Rammensee, K. Falk, O. Rötzschke, MHC molecules as peptide receptors. *Curr. Opin. Immunol.* **5**, 35–44 (1993).

18. C. V. Harding, Pathways of antigen processing. *Curr. Opin. Immunol.* **3**, 3–9 (1991).

19. H. G. Rammensee, K. Falk, O. Rötzschke, Peptides naturally presented by MHC class I molecules. *Annu. Rev. Immunol.* **11**, 213–44 (1993).

20. M. M. Davis, P. J. Bjorkman, T-cell antigen receptor genes and T-cell recognition. *Nature*. **334**, 395–402 (1988).

21. Y. Kawakami *et al.*, Identification of a human melanoma antigen recognized by tumor-infiltrating lymphocytes associated with in vivo tumor rejection. *Proc. Natl. Acad. Sci.* **91**, 6458–6462 (2006).

22. Y. Kawakami *et al.*, Cloning of the gene coding for a shared human melanoma antigen recognized by autologous T cells infiltrating into tumor. *Proc. Natl. Acad. Sci. U. S. A.* **91**, 3515–9 (1994).

23. M. J. Besser *et al.*, Adoptive transfer of tumor-infiltrating lymphocytes in patients with metastatic melanoma: Intent-to-treat analysis and efficacy after failure to prior immunotherapies. *Clin. Cancer Res.* **19**, 4792–4800 (2013).

24. S. A. Rosenberg *et al.*, Use of Tumor-Infiltrating Lymphocytes and Interleukin-2 in the Immunotherapy of Patients with Metastatic Melanoma. *N. Engl. J. Med.* **319**, 1676–1680 (1988).

25. G. T. Gibney, L. M. Weiner, M. B. Atkins, Predictive biomarkers for checkpoint inhibitor-based immunotherapy. *Lancet Oncol.* **17**, e542–e551 (2016).

26. H. G. Rammensee, H. Singh-Jasuja, HLA ligandome tumor antigen discovery for personalized vaccine approach. *Expert Rev. Vaccines*. **12**, 1211–1217 (2013).

27. P. Van Der Bruggen *et al.*, Tumor-specific shared antigenic peptides recognized by human T cells. *Immunol. Rev.* **188**, 51–64 (2002).

28. S. Bobisse, P. G. Foukas, G. Coukos, A. Harari, Neoantigen-based cancer immunotherapy. *Ann. Transl. Med.* **4**, 262–262 (2016).

29. P. G. Coulie, B. J. Van Den Eynde, P. Van Der Bruggen, T. Boon, Tumour antigens recognized by T lymphocytes: At the core of cancer immunotherapy. *Nat. Rev. Cancer*. **14**, 135–146 (2014).

30. T. N. Schumacher, W. Scheper, P. Kvistborg, Cancer Neoantigens. *Annu. Rev. Immunol.* **37**, 173–200 (2019).

31. D. A. Morgan, F. W. Ruscetti, R. Gallo, Selective in vitro growth of T lymphocytes from normal human bone marrows. *Science (80-.).* **193**, 1007–1008 (1976).

32. Y. Zhao *et al.*, Primary human lymphocytes transduced with NY-ESO-1 antigen-specific TCR genes recognize and kill diverse human tumor cell lines. *J. Immunol.* **174**, 4415–23 (2005).

33. E. Kobayashi *et al.*, A new cloning and expression system yields and validates TCRs from blood lymphocytes of patients with cancer within 10 days. *Nat. Med.* **19**, 1542–6 (2013).

34. R. A. Morgan *et al.*, Cancer regression in patients after transfer of genetically engineered lymphocytes. *Science (80-.).* **314**, 126–129 (2006).

35. J. Zhang, L. Wang, The emerging world of TCR-T cell trials against cancer: A systematic review. *Technol. Cancer Res. Treat.* **18**, 153303381983106 (2019).

36. J. D. Stone, D. M. Kranz, Role of T Cell Receptor Affinity in the Efficacy and Specificity of Adoptive T Cell Therapies. *Front. Immunol.* **4**, 1–16 (2013).

37. S. Zhong *et al.*, T-cell receptor affinity and avidity defines antitumor response and autoimmunity in T-cell immunotherapy. *Proc. Natl. Acad. Sci.* **110**, 6973–8 (2013).

38. M. P. Tan *et al.*, T cell receptor binding affinity governs the functional profile of cancer-specific CD8+ T cells. *Clin. Exp. Immunol.* **180**, 255–70 (2015).

39. M. M. Davis *et al.*, Ligand recognition by alpha beta T cell receptors. *Annu. Rev. Immunol.* **16**, 523–544 (1998).

40. J. D. Stone, D. T. Harris, D. M. Kranz, TCR affinity for p/MHC formed by tumor antigens that are self-proteins: impact on efficacy and toxicity. *Curr. Opin. Immunol.* **33**, 16–22 (2015).

41. S. A. Richman, D. M. Kranz, Display, engineering, and applications of antigen-specific T cell receptors. *Biomol. Eng.* **24**, 361–373 (2007).

42. J. D. Stone, A. S. Chervin, D. H. Aggen, D. M. Kranz, *T cell receptor engineering* (2012; http://www.ncbi.nlm.nih.gov/pubmed/22230570), vol. 503.

43. R. Ashfield, B. K. Jakobsen, Making high-affinity T-cell receptors: a new class of targeted therapeutics. *IDrugs*. **9**, 554–9 (2006).

44. P. F. Robbins *et al.*, Single and dual amino acid substitutions in TCR CDRs can enhance antigen-specific T cell functions. *J. Immunol.* **180**, 6116–6131 (2008).

45. J.-L. Chen *et al.*, Structural and kinetic basis for heightened immunogenicity of T cell vaccines. *J. Exp. Med.* **201**, 1243–55 (2005).

46. P. F. Robbins *et al.*, A pilot trial using lymphocytes genetically engineered with an NY-ESO-1-reactive T cell receptor: Long term follow up and correlates with response. *Clin. Cancer Res.* (2014), doi:10.1158/1078-0432.CCR-14-2708.

47. P. F. Robbins *et al.*, Tumor regression in patients with metastatic synovial cell sarcoma and melanoma using genetically engineered lymphocytes reactive with NY-ESO-1. *J. Clin. Oncol.* **29**, 917–924 (2011).

48. A. Gerry *et al.*, Preclinical safety testing of an affinity-optimised MAGE-A10 T cell receptor for adoptive T cell therapy. *J. Immunother. Cancer*. **3**, P14 (2015).

49. J. Zhao, Q. Lin, Y. Song, D. Liu, Universal CARs, universal T cells, and universal CAR T cells. *J. Hematol. Oncol.* **11**, 132 (2018).

50. C. Graham, A. Jozwik, A. Pepper, R. Benjamin, Allogeneic CAR-T Cells: More than Ease of Access? *Cells*. **7**, 155 (2018).

51. M. Martinez, E. K. Moon, CAR T Cells for Solid Tumors: New Strategies for Finding, Infiltrating, and Surviving in the Tumor Microenvironment. *Front. Immunol.* **10**, 128 (2019).

52. M. H. Kershaw, J. A. Westwood, P. K. Darcy, Gene-engineered T cells for cancer therapy. *Nat. Rev. Cancer*. **13**, 525–541 (2013).

53. C. Bonini, Engineering T-Cells Beyond Chimeric Antigen Receptor. *Blood*. **128** (2016) (available at http://www.bloodjournal.org/content/128/22/SCI-13?sso-checked=true).

54. T. M. Schmitt, I. M. Stromnes, A. G. Chapuis, P. D. Greenberg, New strategies in engineering T-cell receptor gene-modified T cells to more effectively target malignancies. *Clin. Cancer Res.* **21**, 5191–5197 (2015).

55. M. T. Bethune *et al.*, Domain-swapped T cell receptors improve the safety of TCR gene therapy. *Elife*. **5** (2016), doi:10.7554/eLife.19095.

56. K. Wennhold, A. Shimabukuro-Vornhagen, M. Von Bergwelt-Baildon, B Cell-Based Cancer Immunotherapy. *Transfus. Med. Hemotherapy*. **46**, 36–46 (2019).

57. A. Simpson, O. Caballero, Monoclonal antibodies for the therapy of cancer. *BMC Proc.* **8**, O6 (2014).

58. A. P. Levene, Therapeutic monoclonal antibodies in oncology. *J. R. Soc. Med.* **98**, 146–152 (2005).

59. J. K. H. Liu, The history of monoclonal antibody development - Progress, remaining challenges and future innovations. *Ann. Med. Surg.* **3**, 113–116 (2014).

60. G. Winter, W. J. Harris, Humanized antibodies. *Immunol. Today*. **14**, 243–246 (1993).

61. R. Nahta, Molecular Mechanisms of Trastuzumab-Based Treatment in HER2-Overexpressing Breast Cancer. *ISRN Oncol.* **2012**, 1–16 (2012).

62. D. Müller, R. E. Kontermann, Bispecific Antibodies. *Handb. Ther. Antibodies Second Ed.* **1**–**4**, 265–310 (2014).

63. S. E. Sedykh, V. V Prinz, V. N. Buneva, G. A. Nevinsky, Bispecific antibodies: design, therapy, perspectives. *Drug Des. Devel. Ther.* **12**, 195–208 (2018).

64. M. J. Coloma, S. L. Morrison, Design and Production of Novel Tetravalent Bispecific Antibodies. *Nat. Biotechnol.* **15**, 159–163 (1997).

65. M. J. Newman, D. J. Benani, A review of blinatumomab, a novel immunotherapy. *J. Oncol. Pharm. Pract.* **22**, 639–645 (2016).

66. J. Lai *et al.*, TCR-like antibodies mediate complement and antibody-dependent cellular cytotoxicity against Epstein-Barr virus-transformed B lymphoblastoid cells expressing different HLA-A∗02 microvariants. *Sci. Rep.* **7**, 9923 (2017).

67. Høydahl, Frick, Sandlie, Løset, Targeting the MHC Ligandome by Use of TCR-Like Antibodies. *Antibodies*. **8**, 32 (2019).

68. Z. Wu, B. H. Santich, H. Liu, C. Liu, N. K. V. Cheung, in *Methods in Molecular Biology* (2018; http://www.ncbi.nlm.nih.gov/pubmed/29116509), vol. 1701, pp. 255–269.

69. G. Bossi, S. Buisson, J. Oates, B. K. Jakobsen, N. J. Hassan, ImmTAC-redirected tumour cell killing induces and potentiates antigen cross-presentation by dendritic cells. *Cancer Immunol. Immunother.* **63**, 437–448 (2014).

70. Y. Li *et al.*, Directed evolution of human T-cell receptors with picomolar affinities by phage display. *Nat. Biotechnol.* **23**, 349–54 (2005).

71. L. Wooldridge *et al.*, A single autoimmune T cell receptor recognizes more than a million different peptides. *J. Biol. Chem.* **287**, 1168–1177 (2012).

72. A. K. Sewell, Why must T cells be cross-reactive? *Nat. Rev. Immunol.* **12**, 669–677 (2012).

73. M. W. Rohaan, J. H. Van Den Berg, P. Kvistborg, J. B. A. G. Haanen, Adoptive transfer of tumor-infiltrating lymphocytes in melanoma: A viable treatment option. *J. Immunother. Cancer*. **6**, 102 (2018).

74. S. Yeh *et al.*, Ocular and Systemic Autoimmunity after Successful Tumor-Infiltrating Lymphocyte Immunotherapy for Recurrent, Metastatic Melanoma. *Ophthalmology*. **116**, 981-989.e1 (2009).

75. G. P. Linette *et al.*, Cardiovascular toxicity and titin cross-reactivity of affinity-enhanced T cells in myeloma and melanoma. *Blood*. **122**, 863–871 (2013).

76. B. J. Cameron *et al.*, Identification of a Titin-derived HLA-A1-presented peptide as a cross-reactive target for engineered MAGE A3-directed T cells. *Sci. Transl. Med.* **5**, 197ra103 (2013).

77. M. C. C. Raman *et al.*, Direct molecular mimicry enables off-target cardiovascular toxicity by an enhanced affinity TCR designed for cancer immunotherapy. *Sci. Rep.* **6**, 18851 (2016).

78. H. M. Bijen *et al.*, Preclinical Strategies to Identify Off-Target Toxicity of High-Affinity TCRs. *Mol. Ther.* (2018), doi:10.1016/J.YMTHE.2018.02.017.

79. A. Kunert, M. Obenaus, C. H. Lamers, T. Blankenstein, R. Debets, *Clin. Cancer Res.*, in press, doi:10.1158/1078-0432.CCR-17-1012.

80. T. C. Manning *et al.*, Alanine scanning mutagenesis of an alphabeta T cell receptor: mapping the energy of antigen recognition. *Immunity*. **8**, 413–425 (1998).

81. K. W. Wucherpfennig, J. L. Strominger, Molecular mimicry in T cell-mediated autoimmunity: Viral peptides activate human T cell clones specific for myelin basic protein. *Cell*. **80**, 695–705 (1995).

82. R. Martin *et al.*, Molecular Mimicry and Antigen-Specific T Cell Responses in Multiple Sclerosis and Chronic CNS Lyme Disease. *J. Autoimmun.* **16**, 187–192 (2001).

83. C. Pinilla *et al.*, Combinatorial Peptide Libraries as an Alternative Approach to the Identification of Ligands for Tumor-reactive Cytolytic T Lymphocytes. *Cancer Res.* **61**, 5153–5160 (2001).

84. V. Rubio-Godoy *et al.*, Combinatorial peptide library-based identification of peptide ligands for tumor-reactive cytolytic T lymphocytes of unknown specificity. *Eur. J. Immunol.* **32**, 2292–2299 (2002).

85. V. Rubio-Godoy *et al.*, Positional Scanning-Synthetic Peptide Library-Based Analysis of Self- and Pathogen-Derived Peptide Cross-Reactivity with Tumor-Reactive Melan-A-Specific CTL. *J. Immunol.* **169**, 5696–5707 (2002).

86. V. Rubio-Godoy *et al.*, Toward Synthetic Combinatorial Peptide Libraries in Positional Scanning Format (PS-SCL)-based Identification of CD8 + Tumor-reactive T-Cell Ligands : A Comparative Analysis of PS-SCL Recognition by a Single Tumor-reactive CD8+ Cytolytic T-Lymphocyte clone. *Cancer Res.* **62**, 2058–2063 (2002).

87. J. J. Nino-Vasquez *et al.*, A powerful combination: The use of positional scanning libraries and biometrical analysis to identify cross-reactive T cell epitopes. *Mol. Immunol.* **40** (2004), pp. 1063–1074.

88. D. B. Wilson *et al.*, Specificity and degeneracy of T cells. *Mol. Immunol.* **40** (2004), pp. 1047–1055.

89. K. W. Wucherpfennig, Structural basis of molecular mimicry. *J. Autoimmun.* **16**, 293–302 (2001).

90. D. K. Cole *et al.*, Hotspot autoimmune T cell receptor binding underlies pathogen and insulin peptide cross-reactivity. *J. Clin. Invest.* **126**, 2191–2204 (2016).

91. D. K. Cole *et al.*, *J. Biol. Chem.*, in press, doi:10.1074/jbc.M116.741603.

92. T. P. Riley *et al.*, T cell receptor cross-reactivity expanded by dramatic peptide–MHC adaptability. *Nat. Chem. Biol.* **14**, 934–942 (2018).

93. J. Harper *et al.*, An approved in vitro approach to preclinical safety and efficacy evaluation of

engineered T cell receptor anti-CD3 bispecific (ImmTAC) molecules. *PLoS One*. **13**, e0205491 (2018).

94. D. N. Garboczi, D. T. Hung, D. C. Wiley, HLA-A2-peptide complexes: refolding and crystallization of molecules expressed in Escherichia coli and complexed with single antigenic peptides. *Proc. Natl. Acad. Sci. U. S. A.* **89**, 3429–3433 (1992).

95. J. D. Altman *et al.*, Phenotypic analysis of antigen-specific T lymphocytes. *Science (80-.).* **274**, 94–96 (1996).

96. S. R. Hadrup *et al.*, High-throughput T-cell epitope discovery through MHC peptide exchange. *Methods Mol. Biol.* **524**, 383–405 (2009).

97. K. C. Garcia *et al.*, Alphabeta T cell receptor interactions with syngeneic and allogeneic ligands: affinity measurements and crystallization. *Proc. Natl. Acad. Sci. U. S. A.* **94**, 13838–43 (1997).

98. S. K. Saini *et al.*, Dipeptides promote folding and peptide binding of MHC class I molecules. *Proc. Natl. Acad. Sci.* **110**, 15383–15388 (2013).

99. S. K. Saini *et al.*, Dipeptides catalyze rapid peptide exchange on MHC class I molecules. *Proc. Natl. Acad. Sci. U. S. A.* **112**, 202–207 (2015).

100. B. Rodenko *et al.*, Generation of peptide-MHC class I complexes through UV-mediated ligand exchange. *Nat. Protoc.* **1**, 1120–1132 (2006).

101. S. R. Hadrup *et al.*, Parallel detection of antigen-specific T-cell responses by multidimensional encoding of MHC multimers. *Nat. Methods*. **6**, 520–526 (2009).

102. J. J. Luimstra *et al.*, A flexible MHC class I multimer loading system for large-scale detection of antigen-specific T cells. *J. Exp. Med.* **215**, 1493–1504 (2018).

103. M. Zacharias, S. Springer, Conformational Flexibility of the MHC Class I α1-α2 Domain in Peptide Bound and Free States: A Molecular Dynamics Simulation Study. *Biophys. J.* **87**, 2203–2214 (2004).

104. Z. Hein *et al.*, Peptide-independent stabilization of MHC class I molecules breaches cellular quality control. *J. Cell Sci.* **127**, 2885–97 (2014).

105. S. K. Saini *et al.*, Not all empty MHC class I molecules are molten globules: Tryptophan fluorescence reveals a two-step mechanism of thermal denaturation. *Mol. Immunol.* **54**, 386–396 (2013).

106. A. Varela-Rohena *et al.*, Control of HIV-1 immune escape by CD8 T cells expressing enhanced T-cell receptor. *Nat. Med.* **14**, 1390–1395 (2008).

107. D. H. Aggen *et al.*, Identification and engineering of human variable regions that allow expression of stable single-chain T cell receptors. *Protein Eng. Des. Sel.* **24**, 361–372 (2011).

108. J. M. Boulter *et al.*, Stable, soluble T-cell receptor molecules for crystallization and therapeutics. *Protein Eng.* **16**, 707–711 (2003).

109. B. Laugel *et al.*, Design of soluble recombinant T cell receptors for antigen targeting and T cell inhibition. *J. Biol. Chem.* **280**, 1882–1892 (2005).

110. Z. Zhu, P. Carter, Identification of heavy chain residues in a humanized anti-CD3 antibody important for efficient antigen binding and T cell activation. *J. Immunol.* **155**, 1903–10 (1995).

111. W. Kabsch, XDS. *Acta Crystallogr. D. Biol. Crystallogr.* **66**, 125–32 (2010).

112. P. Evans, Scaling and assessment of data quality. *Acta Crystallogr. Sect. D Biol. Crystallogr.* **62**, 72–82 (2006).

113. A. Vagin, A. Teplyakov, Molecular replacement with MOLREP. *Acta Crystallogr. Sect. D Biol. Crystallogr.* **66**, 22–25 (2010).

114. O. Kovalevskiy, R. A. Nicholls, F. Long, A. Carlon, G. N. Murshudov, Overview of refinement procedures within REFMAC 5: utilizing data from different sources . *Acta Crystallogr. Sect. D Struct. Biol.* **74**, 215–227 (2018).

115. P. Emsley, B. Lohkamp, W. G. Scott, K. Cowtan, Features and development of Coot . *Acta Crystallogr. Sect. D Biol. Crystallogr.* **66**, 486–501 (2010).

116. V. B. Chen *et al.*, MolProbity : all-atom structure validation for macromolecular crystallography . *Acta Crystallogr. Sect. D Biol. Crystallogr.* **66**, 12–21 (2010).

117. B. E. Willcox *et al.*, Production of soluble alphabeta T-cell receptor heterodimers suitable for biophysical analysis of ligand binding. *Protein Sci.* **8**, 2418–2423 (1999).

118. C. A. Aarnoudse, M. Krüse, R. Konopitzky, N. Brouwenstijn, P. I. Schrier, TCR reconstitution in Jurkat reporter cells facilitates the identification of novel tumor antigens by cDNA expression cloning. *Int. J. Cancer*. **99**, 7–13 (2002).

119. T. Weinschenk *et al.*, Integrated functional genomics approach for the design of patient-individual antitumor vaccines. *Cancer Res.* **62**, 5818–5827 (2002).

120. S. K. Saini *et al.*, Empty peptide-receptive MHC class I molecules for efficient detection of antigen-specific T cells. *Sci. Immunol.* **4**, eaau9039 (2019).

121. Y. Kim, J. Sidney, C. Pinilla, A. Sette, B. Peters, Derivation of an amino acid similarity matrix for peptide:MHC binding and its application as a Bayesian prior. *BMC Bioinformatics*. **10**, 394 (2009).

122. M. Aleksic *et al.*, Dependence of T cell antigen recognition on T cell receptor-peptide MHC confinement time. *Immunity*. **32**, 163–74 (2010).

123. G. Bossi *et al.*, Examining the presentation of tumor-associated antigens on peptide-pulsed T2 cells. *Oncoimmunology*. **2**, e26840 (2013).

124. B. Szomolay *et al.*, Identification of human viral protein-derived ligands recognized by individual major histocompatibility complex class I (MHCI)-restricted T-cell receptors. *Immunol. Cell Biol.* **94**, 1–10 (2016).

125. A. K. Bentzen *et al.*, T cell receptor fingerprinting enables in-depth characterization of the interactions governing recognition of peptide–MHC complexes. *Nat. Biotechnol.* **36**, 1191–1196 (2018).

126. W. Shao *et al.*, The SysteMHC Atlas project. *Nucleic Acids Res.* **46**, D1237–D1247 (2018).

127. E. Caron, R. Aebersold, A. Banaei-Esfahani, C. Chong, M. Bassani-Sternberg, in *Immunity* (Cell Press, 2017; https://www.sciencedirect.com/science/article/pii/S1074761317303175), vol. 47, pp. 203–208.

128. V. Jaravine, A. Mösch, S. Raffegerst, D. J. Schendel, D. Frishman, Expitope 2.0: A tool to assess immunotherapeutic antigens for their potential cross-reactivity against naturally expressed proteins in human tissues. *BMC Cancer*. **17**, 892 (2017).

129. C. Uhler, G. V. Shivashankar, Regulation of genome organization and gene expression by

nuclear mechanotransduction. *Nat. Rev. Mol. Cell Biol.* **18** (2017), pp. 717–727.

130. M. E. Birnbaum *et al.*, Deconstructing the peptide-MHC specificity of t cell recognition. *Cell*. **157**, 1073–1087 (2014).

131. M. H. Gee *et al.*, Antigen Identification for Orphan T Cell Receptors Expressed on Tumor-Infiltrating Lymphocytes. *Cell*. **172**, 549-563.e16 (2018).

132. A. K. Bentzen *et al.*, Large-scale detection of antigen-specific T cells using peptide-MHC-I multimers labeled with DNA barcodes. *Nat. Biotechnol.* **34**, 1037–1045 (2016).

133. V. I. Lyamichev *et al.*, Stepwise Evolution Improves Identification of Diverse Peptides Binding to a Protein Target. *Sci. Rep.* **7**, 12116 (2017).

134. J. P. Pellois *et al.*, Individually addressable parallel peptide synthesis on microchips. *Nat. Biotechnol.* **20**, 922–926 (2002).

135. A. Zandian *et al.*, Whole-Proteome Peptide Microarrays for Profiling Autoantibody Repertoires within Multiple Sclerosis and Narcolepsy. *J. Proteome Res.* **16**, 1300–1314 (2017).

136. P. Fechner *et al.*, Size does matter! Label-free detection of small molecule-protein interaction. *Anal. Bioanal. Chem.* **406**, 4033–51 (2014).

137. G. Proll, G. Markovic, L. Steinle, G. Gauglitz, Reflectometric interference spectroscopy. *Methods Mol. Biol.* **503**, 167–78 (2009).

138. G. Proll *et al.*, Potential of label-free detection in high-content-screening applications. *J. Chromatogr.* **1161**, 2–8 (2007).

139. G. Gauglitz, G. Proll, Strategies for label-free optical detection. *Adv. Biochem. Eng. Biotechnol.* **109**, 395–432 (2008).

140. S. E. Brooks *et al.*, Application of the pMHC Array to Characterise Tumour Antigen Specific T Cell Populations in Leukaemia Patients at Disease Diagnosis. *PLoS One*. **10**, e0140483 (2015).

141. J. D. Stone, W. E. Demkowicz, L. J. Stern, HLA-restricted epitope identification and detection of functional T cell responses by using MHC-peptide and costimulatory microarrays. *Proc. Natl. Acad. Sci.* **102**, 3744–9 (2005).

142. G. A. Kwong *et al.*, Modular nucleic acid assembled p/MHC microarrays for multiplexed sorting of antigen-specific T cells. *J. Am. Chem. Soc.* **131**, 9695–703 (2009).

143. G. Deviren, K. Gupta, M. E. Paulaitis, J. P. Schneck, Detection of antigen-specific T cells on p/MHC microarrays. *J. Mol. Recognit.* **20**, 32–8 (2007).

11. Supplementary Tables and Figures

Table S1: Data collection and refinement statistics 1G4/DS-A2/pESO9V

	1G4/DS-A*02/SLLMWITQV
Data collection	
Space group	$P2_1$
Cell dimensions	
a, *b*, *c* (Å)	75.44, 53.67, 121.74
α, β, γ (°)	90.0 98.0 90.0
Resolution (Å)	2.50 (2.60 – 2.50) *
R_{pim}	0.037 (0.69)
$I / \sigma I$	9.6 (1.1)
CC (1/2)	100.0 (0.68)
Completeness (%)	99.3 (99.1)
Redundancy	4.8 (5.0)
Refinement	
Resolution (Å)	30 – 2.50
No. reflections	33552
R_{work} / R_{free}	0.229 (0.273)
No. atoms	
Protein	3180
Ligand/ion	19
Water	589
B-factors	
Protein	98.1
Ligand/ion	97.8
Water	66.2
R.m.s. deviations	
Bond lengths (Å)	0.002
Bond angles (°)	0.47

Table S2: Kinetic measurements results of bs-868Z11-CD3 binding to immobilized peptide-MHCs loaded with pSL9 PSL peptides using DS-A2 generated pMHCs.

Peptide	Response	KD (M)	KD Error	ka (1/Ms)	ka Error	kdis (1/s)	kdis Error	Rmax	Full X^2	Full R^2
SLYNTVATL	2.7882	1.85E-09	1.11E-10	1.03E+05	2.11E+02	1.90E-04	1.14E-05	3.0177	0.2717	0.9996
GLYNTVATL	2.4931	2.48E-08	1.24E-10	1.08E+05	2.30E+02	2.68E-03	1.21E-05	2.7624	0.2261	0.9995
PLYNTVATL	2.4811	2.22E-09	1.48E-10	1.15E+05	3.39E+02	2.55E-04	1.69E-05	2.6325	0.4831	0.9991
ALYNTVATL	2.7122	1.62E-09	1.07E-10	1.05E+05	2.10E+02	1.69E-04	1.12E-05	2.922	0.2502	0.9996
VLYNTVATL	2.5266	2.00E-09	1.11E-10	1.07E+05	2.30E+02	2.13E-04	1.19E-05	2.7135	0.2575	0.9995
LLYNTVATL	2.4984	3.73E-08	1.31E-10	1.05E+05	2.08E+02	3.93E-03	1.14E-05	2.8324	0.1815	0.9996
ILYNTVATL	2.7638	5.87E-09	1.19E-10	1.08E+05	2.44E+02	6.32E-04	1.27E-05	2.9864	0.3338	0.9995
MLYNTVATL	2.564	2.93E-08	1.24E-10	1.09E+05	2.21E+02	3.19E-03	1.18E-05	2.865	0.214	0.9996
FLYNTVATL	2.5624	3.91E-08	1.33E-10	1.10E+05	2.21E+02	4.31E-03	1.19E-05	2.8984	0.2008	0.9996
YLYNTVATL	2.2331	8.49E-08	2.91E-10	1.21E+05	3.48E+02	1.03E-02	1.91E-05	2.6712	0.2741	0.9992
WLYNTVATL	1.1601	2.45E-07	3.20E-09	1.94E+05	2.42E+03	4.77E-02	1.89E-04	1.7104	0.6718	0.9959
HLYNTVATL	1.5507	2.09E-07	1.55E-09	1.45E+05	1.01E+03	3.03E-02	7.09E-05	2.1912	0.4918	0.9979
KLYNTVATL	2.4769	1.50E-08	1.08E-10	1.01E+05	1.90E+02	1.51E-03	1.05E-05	2.7413	0.1699	0.9997
RLYNTVATL	2.4521	2.56E-09	1.32E-10	1.05E+05	2.60E+02	2.68E-04	1.37E-05	2.6474	0.3167	0.9994
QLYNTVATL	2.2226	1.04E-07	3.61E-10	1.10E+05	3.31E+02	1.15E-02	1.98E-05	2.7589	0.2644	0.9992
NLYNTVATL	2.6035	1.77E-08	9.20E-11	1.07E+05	1.75E+02	1.90E-03	9.37E-06	2.8606	0.1464	0.9997
ELYNTVATL	1.626	2.00E-07	1.65E-09	1.35E+05	1.05E+03	2.69E-02	7.21E-05	2.2615	0.6998	0.997
DLYNTVATL	0.3777	1.31E-08	1.47E-10	4.08E+05	2.93E+03	5.35E-03	4.60E-05	0.3835	0.0787	0.9868
TLYNTVATL	2.8732	8.69E-10	1.04E-10	1.09E+05	2.19E+02	9.46E-05	1.13E-05	3.0721	0.2905	0.9996
SGYNTVATL	0.3857	1.17E-08	8.57E-11	3.90E+05	1.63E+03	4.57E-03	2.75E-05	0.3914	0.0429	0.9943
SPYNTVATL	0.3403	6.81E-09	1.01E-10	4.27E+05	2.71E+03	2.91E-03	3.89E-05	0.3379	0.0559	0.9863
SAYNTVATL	2.5641	2.15E-09	1.30E-10	1.25E+05	3.52E+02	2.69E-04	1.63E-05	2.6914	0.5	0.9991
SVYNTVATL	2.7781	1.52E-09	1.10E-10	1.10E+05	2.36E+02	1.68E-04	1.21E-05	2.9685	0.3114	0.9996
SIYNTVATL	2.7858	1.32E-09	1.07E-10	1.11E+05	2.32E+02	1.47E-04	1.18E-05	2.9713	0.3027	0.9996
SMYNTVATL	2.7192	2.80E-09	1.10E-10	1.08E+05	2.29E+02	3.03E-04	1.18E-05	2.9163	0.2869	0.9996
SFYNTVATL	1.1463	3.69E-09	2.08E-10	2.44E+05	2.00E+03	8.97E-04	5.00E-05	1.1481	0.9432	0.989
SYYNTVATL	0.087	2.06E-08	4.86E-10	6.85E+05	1.44E+04	1.41E-02	1.53E-04	0.0874	0.0298	0.9273
SHYNTVATL	0.2046	3.68E-08	4.33E-10	5.21E+05	5.61E+03	1.91E-02	9.09E-05	0.2149	0.0373	0.987
SKYNTVATL	0.6227	2.98E-08	2.97E-10	3.45E+05	2.82E+03	1.03E-02	5.83E-05	0.6422	0.2465	0.9865
SRYNTVATL	0.7603	2.05E-08	2.42E-10	3.51E+05	3.03E+03	7.19E-03	5.80E-05	0.7609	0.4309	0.9816
SQYNTVATL	2.8241	2.90E-09	1.20E-10	1.15E+05	2.76E+02	3.34E-04	1.37E-05	3.0063	0.4169	0.9994
SNYNTVATL	0.1017	1.08E-08	1.50E-10	7.57E+05	8.46E+03	8.19E-03	6.76E-05	0.1041	0.012	0.9662
SEYNTVATL	0.188	7.35E-09	1.02E-10	5.70E+05	4.57E+03	4.19E-03	4.76E-05	0.1879	0.0241	0.9788
SDYNTVATL	0.195	7.78E-09	9.54E-11	5.48E+05	3.87E+03	4.26E-03	4.28E-05	0.1946	0.0215	0.9811
SSYNTVATL	1.8107	1.40E-09	1.93E-10	1.75E+05	9.82E+02	2.45E-04	3.38E-05	1.8392	1.1378	0.9951
STYNTVATL	2.6652	2.36E-09	1.46E-10	1.10E+05	3.13E+02	2.60E-04	1.60E-05	2.8528	0.5037	0.9992
SLANTVATL	0.2208	4.78E-08	2.81E-09	6.89E+05	3.85E+04	3.29E-02	5.97E-04	0.2073	0.3992	0.9196
SLVNTVATL	1.1995	3.23E-07	5.89E-09	1.62E+05	2.84E+03	5.24E-02	2.70E-04	1.9504	1.1635	0.9935
SLLNTVATL	2.2618	1.04E-07	5.15E-10	1.15E+05	4.98E+02	1.20E-02	2.91E-05	2.7888	0.5783	0.9983
SLINTVATL	1.4697	2.16E-07	1.97E-09	1.67E+05	1.45E+03	3.62E-02	1.01E-04	2.0921	0.6421	0.9972
SLMNTVATL	0.6285	2.37E-07	9.86E-09	3.35E+05	1.32E+04	7.95E-02	1.05E-03	0.8971	1.3812	0.9741
SLFNTVATL	2.5565	2.29E-08	1.17E-10	9.98E+04	1.92E+02	2.29E-03	1.08E-05	2.8739	0.1833	0.9997
SLWNTVATL	2.4685	1.80E-08	9.76E-11	1.16E+05	2.13E+02	2.09E-03	1.07E-05	2.6779	0.1763	0.9996
SLHNTVATL	2.4422	6.57E-08	2.50E-10	1.20E+05	3.55E+02	7.89E-03	1.89E-05	2.8367	0.375	0.999
SLRNTVATL	1.3361	2.38E-07	2.44E-09	1.50E+05	1.47E+03	3.56E-02	1.10E-04	1.9479	0.633	0.9965
SLQNTVATL	0.8561	2.92E-07	1.06E-08	2.42E+05	8.36E+03	7.06E-02	7.73E-04	1.3174	1.993	0.9795
SLNNTVATL	1.2176	4.03E-07	5.20E-09	1.35E+05	1.68E+03	5.41E-02	1.83E-04	2.185	0.5078	0.9973
SLTNTVATL	0.3586	7.89E-08	4.94E-09	6.95E+05	4.14E+04	5.48E-02	1.06E-03	0.3807	1.1454	0.925
SLYGTVATL	1.3138	2.91E-07	3.09E-09	1.87E+05	1.90E+03	5.44E-02	1.67E-04	2.0682	0.5047	0.9978
SLYPTVATL	0.7965	2.56E-07	8.35E-09	2.85E+05	8.82E+03	7.28E-02	7.35E-04	1.1762	1.466	0.983
SLYATVATL	2.4743	8.87E-08	4.21E-10	1.29E+05	5.27E+02	1.15E-02	2.79E-05	2.954	0.684	0.9983
SLYVTVATL	2.1165	1.22E-07	7.54E-10	1.36E+05	7.65E+02	1.66E-02	4.27E-05	2.6392	0.8359	0.9974
SLYLTVATL	2.7113	4.52E-08	1.59E-10	1.20E+05	2.80E+02	5.43E-03	1.43E-05	3.0549	0.3135	0.9994
SLYITVATL	1.5068	2.25E-07	2.61E-09	1.62E+05	1.78E+03	3.64E-02	1.28E-04	2.1647	1.0619	0.9955
SLYMTVATL	0.3241	6.61E-08	4.24E-09	6.31E+05	3.85E+04	4.17E-02	8.29E-04	0.3201	1.015	0.9116
SLYHTVATL	2.5742	7.26E-08	3.29E-10	1.18E+05	4.30E+02	8.60E-03	2.33E-05	3.0176	0.6041	0.9986

SLYQTVATL	1.8127	1.91E-07	1.55E-09	1.53E+05	1.17E+03	2.92E-02	7.64E-05	2.4974	0.8577	0.9973
SLYSTVATL	2.6449	4.93E-08	1.77E-10	1.22E+05	3.06E+02	6.03E-03	1.55E-05	2.9933	0.3399	0.9993
SLYTTVATL	2.212	1.36E-07	9.36E-10	1.29E+05	8.14E+02	1.75E-02	4.84E-05	2.8199	1.0754	0.997
SLYNGVATL	0.3334	7.43E-08	4.32E-09	5.42E+05	2.99E+04	4.03E-02	7.46E-04	0.344	1.0064	0.9195
SLYNAVATL	2.166	7.81E-08	3.96E-10	1.23E+05	5.19E+02	9.61E-03	2.71E-05	2.5468	0.588	0.9979
SLYNVVATL	2.535	1.88E-08	1.37E-10	9.39E+04	2.11E+02	1.77E-03	1.23E-05	2.8667	0.2342	0.9996
SLYNLVATL	2.6243	5.56E-09	1.18E-10	1.01E+05	2.18E+02	5.60E-04	1.18E-05	2.8654	0.2633	0.9996
SLYNIVATL	2.4436	2.58E-08	1.30E-10	9.57E+04	1.97E+02	2.47E-03	1.14E-05	2.787	0.1832	0.9996
SLYNMVATL	2.692	2.76E-08	1.13E-10	1.25E+05	2.53E+02	3.44E-03	1.22E-05	2.9369	0.257	0.9995
SLYNFVATL	0.865	4.19E-07	8.17E-09	2.00E+05	3.74E+03	8.37E-02	4.50E-04	1.5715	0.4462	0.9959
SLYNYVATL	0.341	6.63E-08	4.30E-09	7.42E+05	4.58E+04	4.92E-02	9.64E-04	0.3489	1.105	0.9177
SLYNHVATL	0.565	3.90E-07	1.49E-08	2.62E+05	9.59E+03	1.02E-01	1.14E-03	0.9779	0.6437	0.9858
SLYNKVATL	1.7997	1.77E-07	1.42E-09	1.41E+05	1.06E+03	2.49E-02	6.80E-05	2.4253	0.8718	0.9969
SLYNRVATL	0.4609	9.25E-08	5.49E-09	5.32E+05	3.00E+04	4.93E-02	9.32E-04	0.4974	1.9326	0.921
SLYNQVATL	1.1426	3.41E-07	5.62E-09	1.64E+05	2.60E+03	5.60E-02	2.55E-04	1.9025	0.8157	0.9951
SLYNNVATL	2.1399	9.63E-08	5.28E-10	1.30E+05	6.23E+02	1.25E-02	3.32E-05	2.5746	0.6902	0.9977
SLYNDVATL	0.2749	2.76E-07	1.85E-08	3.39E+05	2.15E+04	9.34E-02	1.97E-03	0.3954	0.5238	0.9447
SLYNSVATL	2.5425	4.68E-08	1.59E-10	1.21E+05	2.79E+02	5.68E-03	1.43E-05	2.8736	0.2667	0.9994
SLYNTGATL	2.2576	9.64E-08	4.40E-10	1.31E+05	5.22E+02	1.26E-02	2.81E-05	2.7232	0.5263	0.9985
SLYNTPATL	2.8213	9.43E-09	1.14E-10	1.14E+05	2.51E+02	1.07E-03	1.27E-05	3.041	0.344	0.9995
SLYNTAATL	2.6323	3.77E-08	1.39E-10	1.13E+05	2.43E+02	4.27E-03	1.28E-05	2.9621	0.2506	0.9995
SLYNTLATL	2.8202	2.52E-09	1.23E-10	1.11E+05	2.70E+02	2.80E-04	1.36E-05	3.0188	0.4182	0.9994
SLYNTIATL	2.7765	1.73E-09	1.12E-10	1.11E+05	2.46E+02	1.92E-04	1.25E-05	2.9641	0.338	0.9995
SLYNTMATL	2.3766	2.21E-08	1.00E-10	1.09E+05	1.91E+02	2.42E-03	1.01E-05	2.6256	0.1395	0.9997
SLYNTFATL	1.2504	2.96E-07	1.95E-09	1.12E+05	7.06E+02	3.30E-02	6.20E-05	2.001	0.1986	0.9987
SLYNTYATL	1.0713	3.46E-07	2.35E-09	4.69E+04	3.07E+02	1.62E-02	3.03E-05	2.0877	0.0895	0.9991
SLYNTWATL	0.3602	6.80E-07	1.13E-08	2.45E+04	4.00E+02	1.66E-02	4.53E-05	1.1018	0.0209	0.9984
SLYNTHATL	1.5008	1.12E-07	5.43E-10	9.24E+04	3.84E+02	1.04E-02	2.57E-05	1.9416	0.2054	0.9988
SLYNTQATL	1.5683	2.04E-07	1.05E-09	1.21E+05	5.89E+02	2.46E-02	4.20E-05	2.2265	0.2522	0.9988
SLYNTNATL	1.8495	1.17E-07	5.23E-10	1.38E+05	5.58E+02	1.61E-02	3.07E-05	2.2969	0.3399	0.9986
SLYNTEATL	0.7708	6.00E-07	6.36E-09	8.61E+04	8.91E+02	5.17E-02	1.19E-04	1.7085	0.0936	0.9987
SLYNTDATL	1.138	3.68E-07	2.87E-09	1.20E+05	9.02E+02	4.43E-02	9.14E-05	1.979	0.1853	0.9988
SLYNTSATL	1.9255	1.24E-07	7.40E-10	1.44E+05	7.87E+02	1.79E-02	4.28E-05	2.4055	0.6549	0.9976
SLYNTTATL	2.5627	3.11E-08	1.20E-10	1.06E+05	2.02E+02	3.31E-03	1.11E-05	2.8848	0.1823	0.9996
SLYNTVGTL	2.4841	5.15E-09	1.18E-10	9.22E+04	1.86E+02	4.75E-04	1.09E-05	2.7638	0.1857	0.9997
SLYNTVPTL	2.7631	1.18E-09	1.00E-10	1.15E+05	2.35E+02	1.36E-04	1.16E-05	2.9247	0.288	0.9996
SLYNTVVTL	1.0907	3.25E-07	4.61E-09	1.48E+05	2.01E+03	4.80E-02	1.91E-04	1.7804	0.5974	0.9958
SLYNTVITL	0.2963	1.33E-07	7.11E-09	3.96E+05	1.99E+04	5.27E-02	9.19E-04	0.3491	0.6454	0.9415
SLYNTVMTL	2.0458	6.76E-08	1.75E-10	8.70E+04	1.63E+02	5.88E-03	1.05E-05	2.5192	0.0858	0.9997
SLYNTVFTL	1.0001	3.40E-07	4.92E-09	1.59E+05	2.21E+03	5.41E-02	2.18E-04	1.6706	0.4867	0.9962
SLYNTVHTL	2.1079	7.32E-08	2.17E-10	1.04E+05	2.41E+02	7.64E-03	1.42E-05	2.525	0.1538	0.9995
SLYNTVKTL	0.6285	8.66E-07	1.11E-08	5.18E+04	6.55E+02	4.49E-02	9.59E-05	1.7695	0.0557	0.9988
SLYNTVRTL	0.8971	2.82E-07	1.57E-09	1.13E+05	5.99E+02	3.17E-02	5.03E-05	1.408	0.0763	0.999
SLYNTVQTL	2.1764	3.48E-08	1.17E-10	8.97E+04	1.50E+02	3.12E-03	9.09E-06	2.5381	0.0875	0.9998
SLYNTVNTL	2.001	2.75E-08	1.32E-10	9.15E+04	1.86E+02	2.52E-03	1.10E-05	2.3045	0.1143	0.9997
SLYNTVETL	0.4588	3.08E-07	5.38E-09	1.24E+04	2.07E+02	3.83E-03	1.97E-05	1.8221	0.0147	0.9995
SLYNTVSTL	2.4974	5.36E-09	1.30E-10	1.03E+05	2.48E+02	5.53E-04	1.33E-05	2.7177	0.2975	0.9995
SLYNTVTTL	2.3811	4.72E-08	1.35E-10	1.07E+05	1.98E+02	5.06E-03	1.11E-05	2.7383	0.141	0.9997
SLYNTVAGL	2.7164	6.78E-09	1.25E-10	1.15E+05	2.87E+02	7.83E-04	1.43E-05	2.908	0.4104	0.9993
SLYNTVAPL	1.8636	1.55E-07	1.02E-09	1.51E+05	9.31E+02	2.34E-02	5.49E-05	2.4295	0.6805	0.9976
SLYNTVAAL	2.7444	4.03E-09	1.32E-10	1.17E+05	3.14E+02	4.70E-04	1.54E-05	2.9205	0.4998	0.9992
SLYNTVAVL	2.6894	1.56E-09	1.56E-10	1.13E+05	3.53E+02	1.77E-04	1.76E-05	2.8642	0.635	0.999
SLYNTVALL	2.5677	8.30E-09	1.52E-10	1.07E+05	3.07E+02	8.87E-04	1.61E-05	2.7894	0.4595	0.9992
SLYNTVAIL	2.6019	1.72E-09	9.43E-11	1.09E+05	2.01E+02	1.87E-04	1.03E-05	2.7851	0.203	0.9997
SLYNTVAML	2.5175	2.97E-09	8.97E-11	1.09E+05	1.91E+02	3.24E-04	9.75E-06	2.6984	0.172	0.9997
SLYNTVAFL	1.8902	1.34E-07	4.14E-10	1.01E+05	2.78E+02	1.35E-02	1.85E-05	2.4777	0.1398	0.9995
SLYNTVAYL	1.4777	2.25E-07	1.17E-09	1.12E+05	5.52E+02	2.53E-02	4.27E-05	2.1611	0.2065	0.999
SLYNTVAWL	1.76	1.32E-07	4.33E-10	1.09E+05	3.21E+02	1.43E-02	2.08E-05	2.2754	0.142	0.9994
SLYNTVAHL	2.5004	3.13E-09	1.09E-10	1.01E+05	2.01E+02	3.16E-04	1.09E-05	2.725	0.2037	0.9996
SLYNTVAKL	2.6028	1.01E-08	1.28E-10	1.09E+05	2.61E+02	1.09E-03	1.36E-05	2.8289	0.3325	0.9994
SLYNTVARL	2.528	2.55E-09	1.42E-10	1.15E+05	3.30E+02	2.93E-04	1.63E-05	2.6914	0.4834	0.9991

SLYNTVAQL	2.6052	6.86E-09	1.26E-10	1.14E+05	2.85E+02	7.84E-04	1.42E-05	2.7914	0.375	0.9993
SLYNTVANL	2.6542	2.59E-09	1.31E-10	1.13E+05	2.93E+02	2.93E-04	1.47E-05	2.8324	0.4253	0.9993
SLYNTVAEL	2.4726	3.12E-08	1.53E-10	1.07E+05	2.62E+02	3.35E-03	1.42E-05	2.782	0.2823	0.9994
SLYNTVADL	2.5468	9.59E-09	1.40E-10	1.07E+05	2.79E+02	1.03E-03	1.47E-05	2.7699	0.3672	0.9993
SLYNTVASL	2.6949	2.42E-09	1.01E-10	1.11E+05	2.18E+02	2.68E-04	1.11E-05	2.8812	0.2492	0.9996
SLYNTVATG	2.4479	2.70E-09	1.29E-10	1.23E+05	3.40E+02	3.33E-04	1.59E-05	2.5718	0.4338	0.9991
SLYNTVATP	1.2446	1.11E-08	2.84E-10	1.49E+05	9.98E+02	1.66E-03	4.10E-05	1.2719	0.6518	0.9939
SLYNTVATA	2.5549	2.84E-09	9.22E-11	1.11E+05	2.05E+02	3.16E-04	1.02E-05	2.7273	0.1992	0.9996
SLYNTVATV	2.6469	1.72E-09	1.02E-10	1.12E+05	2.24E+02	1.93E-04	1.15E-05	2.8174	0.2473	0.9996
SLYNTVATI	2.5109	2.20E-09	1.00E-10	1.15E+05	2.37E+02	2.53E-04	1.15E-05	2.6671	0.2521	0.9995
SLYNTVATM	2.6596	1.99E-09	1.37E-10	1.08E+05	2.88E+02	2.15E-04	1.48E-05	2.8592	0.4422	0.9993
SLYNTVATF	2.4034	3.63E-09	1.39E-10	9.10E+04	2.15E+02	3.31E-04	1.26E-05	2.6817	0.2381	0.9996
SLYNTVATY	1.8439	2.02E-09	2.43E-10	1.30E+05	6.98E+02	2.62E-04	3.15E-05	1.931	0.967	0.9965
SLYNTVATW	1.121	5.45E-09	3.08E-10	9.73E+04	5.24E+02	5.30E-04	2.99E-05	1.2404	0.2841	0.9976
SLYNTVATH	0.8293	6.01E-09	2.77E-10	1.36E+05	8.44E+02	8.19E-04	3.74E-05	0.8694	0.2572	0.9954
SLYNTVATK	0.9441	1.02E-08	3.68E-10	8.10E+04	4.62E+02	8.28E-04	2.94E-05	1.0982	0.1841	0.998
SLYNTVATR	2.3088	2.34E-09	1.68E-10	1.25E+05	4.55E+02	2.92E-04	2.10E-05	2.4256	0.6867	0.9984
SLYNTVATQ	1.7777	2.34E-09	2.11E-10	1.53E+05	8.21E+02	3.57E-04	3.23E-05	1.8239	0.9486	0.996
SLYNTVATN	2.4216	2.32E-09	1.75E-10	1.24E+05	4.53E+02	2.88E-04	2.16E-05	2.5416	0.7298	0.9986
SLYNTVATE	0.559	8.82E-09	7.31E-10	4.63E+04	4.33E+02	4.08E-04	3.36E-05	0.8132	0.0818	0.9979
SLYNTVATD	0.5186	1.54E-08	9.47E-10	4.60E+04	5.44E+02	7.08E-04	4.27E-05	0.7604	0.1096	0.9967
SLYNTVATS	2.6265	2.64E-09	1.12E-10	1.17E+05	2.70E+02	3.10E-04	1.31E-05	2.7823	0.3401	0.9994
SLYNTVATT	2.7571	1.07E-09	1.31E-10	1.19E+05	3.25E+02	1.27E-04	1.56E-05	2.9139	0.5381	0.9992

Table S3: Kinetic measurements results of bs-868Z11-CD3 binding to immobilized peptide-MHCs loaded with pSL9 PSL peptides using UV-A2 generated pMHCs.

Peptide	Response	KD (M)	KD Error	ka (1/Ms)	ka Error	kdis (1/s)	kdis Error	Rmax	Full X^2	Full R^2
SLYNTVATL	2.3498	1.58E-09	1.04E-10	1.17E+05	2.48E+02	1.84E-04	1.21E-05	2.4859	0.2292	0.9995
GLYNTVATL	2.1637	2.61E-08	1.25E-10	1.20E+05	2.68E+02	3.11E-03	1.32E-05	2.3706	0.2003	0.9994
PLYNTVATL	2.2431	1.55E-09	1.39E-10	1.19E+05	3.47E+02	1.85E-04	1.65E-05	2.3666	0.4015	0.999
ALYNTVATL	2.352	1.03E-09	1.14E-10	1.14E+05	2.62E+02	1.18E-04	1.29E-05	2.4955	0.2677	0.9994
VLYNTVATL	2.3631	1.82E-09	1.21E-10	1.14E+05	2.78E+02	2.07E-04	1.37E-05	2.5095	0.303	0.9994
LLYNTVATL	2.1887	3.93E-08	1.56E-10	1.17E+05	2.83E+02	4.61E-03	1.44E-05	2.452	0.2227	0.9993
ILYNTVATL	2.432	6.52E-09	1.25E-10	1.18E+05	3.01E+02	7.71E-04	1.46E-05	2.5879	0.3498	0.9993
MLYNTVATL	2.1707	3.17E-08	1.31E-10	1.25E+05	2.84E+02	3.94E-03	1.37E-05	2.3858	0.2075	0.9993
FLYNTVATL	2.1503	4.65E-08	1.66E-10	1.24E+05	3.02E+02	5.78E-03	1.51E-05	2.4248	0.2162	0.9993
YLYNTVATL	1.9086	9.70E-08	4.15E-10	1.33E+05	4.98E+02	1.29E-02	2.64E-05	2.2984	0.3348	0.9986
WLYNTVATL	0.9465	2.63E-07	5.06E-09	2.09E+05	3.83E+03	5.48E-02	3.17E-04	1.4233	0.8755	0.9924
HLYNTVATL	1.2617	2.31E-07	2.14E-09	1.63E+05	1.43E+03	3.76E-02	1.05E-04	1.8302	0.4603	0.9973
KLYNTVATL	2.1064	1.41E-08	1.17E-10	1.10E+05	2.41E+02	1.55E-03	1.24E-05	2.3001	0.1818	0.9995
RLYNTVATL	2.1268	1.91E-09	1.24E-10	1.14E+05	2.85E+02	2.17E-04	1.40E-05	2.2624	0.2611	0.9993
QLYNTVATL	1.8895	9.44E-08	3.69E-10	1.27E+05	4.31E+02	1.20E-02	2.33E-05	2.2792	0.2694	0.9989
NLYNTVATL	2.3207	1.85E-08	1.12E-10	1.10E+05	2.25E+02	2.03E-03	1.16E-05	2.5459	0.187	0.9996
ELYNTVATL	1.475	2.09E-07	1.90E-09	1.44E+05	1.24E+03	3.01E-02	8.58E-05	2.0724	0.6724	0.9967
DLYNTVATL	0.5651	7.07E-09	1.59E-10	3.37E+05	2.74E+03	2.38E-03	4.99E-05	0.5625	0.2421	0.9826
TLYNTVATL	2.4197	9.61E-10	1.15E-10	1.21E+05	2.92E+02	1.16E-04	1.38E-05	2.5458	0.3263	0.9993
SGYNTVATL	0.4175	5.23E-09	1.41E-10	3.89E+05	3.33E+03	2.03E-03	5.20E-05	0.4139	0.1539	0.9772
SPYNTVATL	0.3244	7.08E-09	1.47E-10	3.99E+05	3.48E+03	2.83E-03	5.32E-05	0.3245	0.0909	0.9784
SAYNTVATL	2.3267	2.42E-09	1.57E-10	1.34E+05	4.83E+02	3.25E-04	2.10E-05	2.4222	0.7012	0.9984
SVYNTVATL	2.4066	1.34E-09	1.20E-10	1.23E+05	3.14E+02	1.64E-04	1.48E-05	2.5297	0.3637	0.9993
SIYNTVATL	2.4329	1.17E-09	1.27E-10	1.23E+05	3.35E+02	1.44E-04	1.57E-05	2.5558	0.42	0.9992
SMYNTVATL	2.332	2.05E-09	9.81E-11	1.19E+05	2.44E+02	2.43E-04	1.17E-05	2.4595	0.214	0.9995
SFYNTVATL	1.2807	1.31E-09	1.89E-10	2.11E+05	1.40E+03	2.77E-04	3.99E-05	1.2836	0.8203	0.9922
SYYNTVATL	0.069	3.02E-09	1.21E-10	5.75E+05	6.55E+03	1.74E-03	6.68E-05	0.0666	0.0083	0.9403
SHYNTVATL	0.1266	2.53E-08	4.06E-10	5.86E+05	8.36E+03	1.48E-02	1.09E-04	0.1261	0.0305	0.9645
SKYNTVATL	0.521	3.66E-08	3.72E-10	3.42E+05	2.99E+03	1.25E-02	6.52E-05	0.5447	0.1834	0.9871
SRYNTVATL	0.6895	2.05E-08	3.28E-10	3.38E+05	3.91E+03	6.92E-03	7.70E-05	0.6812	0.6002	0.9697
SQYNTVATL	2.4074	3.09E-09	1.34E-10	1.26E+05	3.66E+02	3.89E-04	1.68E-05	2.5282	0.4748	0.999

SNYNTVATL	0.0956	2.58E-09	1.19E-10	5.47E+05	5.84E+03	1.41E-03	6.31E-05	0.0919	0.0144	0.9422
SEYNTVATL	0.1746	5.11E-09	1.25E-10	4.66E+05	4.20E+03	2.38E-03	5.43E-05	0.1715	0.0298	0.9695
SDYNTVATL	0.1854	4.69E-09	1.12E-10	4.82E+05	4.06E+03	2.26E-03	5.06E-05	0.1815	0.0299	0.971
SSYNTVATL	1.8505	1.40E-09	1.97E-10	1.66E+05	9.12E+02	2.33E-04	3.27E-05	1.8854	1.1348	0.9953
STYNTVATL	2.2392	1.69E-09	1.16E-10	1.21E+05	2.97E+02	2.05E-04	1.41E-05	2.3564	0.2879	0.9993
SLANTVATL	0.1633	6.22E-08	3.21E-09	5.75E+05	2.81E+04	3.58E-02	5.86E-04	0.1594	0.1808	0.9354
SLVNTVATL	0.9429	2.86E-07	7.71E-09	2.04E+05	5.26E+03	5.85E-02	4.65E-04	1.4492	1.5481	0.9863
SLLNTVATL	1.9069	1.13E-07	6.20E-10	1.29E+05	6.34E+02	1.46E-02	3.53E-05	2.3527	0.5323	0.9978
SLINTVATL	1.1735	2.34E-07	2.91E-09	1.90E+05	2.25E+03	4.44E-02	1.65E-04	1.7059	0.6776	0.9958
SLMNTVATL	0.4555	1.06E-07	5.82E-09	5.35E+05	2.80E+04	5.64E-02	9.94E-04	0.5122	1.5904	0.9347
SLFNTVATL	2.2235	2.45E-08	1.40E-10	1.11E+05	2.71E+02	2.72E-03	1.41E-05	2.4594	0.2421	0.9993
SLWNTVATL	2.0052	1.86E-08	1.39E-10	1.28E+05	3.58E+02	2.38E-03	1.65E-05	2.1476	0.2872	0.999
SLHNTVATL	1.9497	7.70E-08	2.86E-10	1.41E+05	4.44E+02	1.09E-02	2.16E-05	2.2681	0.2712	0.9989
SLRNTVATL	0.997	2.48E-07	3.40E-09	1.66E+05	2.18E+03	4.12E-02	1.66E-04	1.4649	0.5885	0.9946
SLQNTVATL	0.6019	1.32E-07	6.81E-09	3.95E+05	1.93E+04	5.22E-02	8.73E-04	0.7101	2.6208	0.9394
SLNNTVATL	0.9285	3.82E-07	7.85E-09	1.61E+05	3.18E+03	6.14E-02	3.42E-04	1.6161	0.7291	0.9935
SLTNTVATL	0.2769	4.49E-08	2.83E-09	8.07E+05	4.86E+04	3.62E-02	6.77E-04	0.2669	0.7279	0.9093
SLYGTVATL	1.0757	3.09E-07	4.51E-09	2.04E+05	2.85E+03	6.28E-02	2.65E-04	1.7235	0.5702	0.9964
SLYPTVATL	0.6857	1.86E-07	7.54E-09	3.47E+05	1.34E+04	6.45E-02	8.37E-04	0.9061	1.9345	0.9678
SLYATVATL	2.0516	9.35E-08	4.89E-10	1.47E+05	6.82E+02	1.38E-02	3.37E-05	2.4383	0.6098	0.9978
SLYVTVATL	1.737	1.39E-07	8.89E-10	1.54E+05	9.12E+02	2.14E-02	5.06E-05	2.2108	0.5845	0.9976
SLYLTVATL	2.2701	4.86E-08	1.66E-10	1.37E+05	3.38E+02	6.65E-03	1.58E-05	2.536	0.2576	0.9992
SLYITVATL	1.1981	2.49E-07	3.87E-09	1.77E+05	2.63E+03	4.42E-02	2.02E-04	1.7705	1.0649	0.9936
SLYMTVATL	0.259	5.28E-08	3.18E-09	6.02E+05	3.43E+04	3.18E-02	6.10E-04	0.2456	0.6123	0.9121
SLYHTVATL	2.084	7.78E-08	3.68E-10	1.38E+05	5.51E+02	1.07E-02	2.71E-05	2.4241	0.5013	0.9981
SLYQTVATL	1.438	2.19E-07	2.03E-09	1.66E+05	1.47E+03	3.64E-02	1.02E-04	2.0516	0.6345	0.9971
SLYSTVATL	2.2682	5.10E-08	1.86E-10	1.38E+05	3.71E+02	7.02E-03	1.73E-05	2.5441	0.3026	0.9991
SLYTTVATL	1.7914	1.39E-07	1.00E-09	1.41E+05	9.43E+02	1.95E-02	5.37E-05	2.2812	0.7964	0.9967
SLYNGVATL	0.2637	5.61E-08	3.17E-09	5.66E+05	3.03E+04	3.17E-02	5.81E-04	0.2581	0.6166	0.9145
SLYNAVATL	2.1277	8.21E-08	3.38E-10	1.24E+05	4.27E+02	1.02E-02	2.28E-05	2.5204	0.3674	0.9987
SLYNVVATL	2.2466	1.83E-08	1.23E-10	1.05E+05	2.30E+02	1.92E-03	1.23E-05	2.4797	0.1935	0.9995
SLYNLVATL	2.4224	4.26E-09	1.24E-10	1.10E+05	2.66E+02	4.69E-04	1.36E-05	2.5972	0.2991	0.9994
SLYNIVATL	2.1376	2.41E-08	1.31E-10	1.08E+05	2.45E+02	2.61E-03	1.29E-05	2.3749	0.1886	0.9995
SLYNMVATL	2.3145	2.84E-08	1.20E-10	1.37E+05	3.10E+02	3.89E-03	1.38E-05	2.5037	0.2477	0.9993
SLYNFVATL	0.7081	4.07E-07	1.23E-08	2.23E+05	6.48E+03	9.07E-02	7.70E-04	1.2556	0.6848	0.9904
SLYNYVATL	0.2957	5.56E-08	3.62E-09	7.44E+05	4.62E+04	4.14E-02	8.10E-04	0.2904	0.8676	0.9085
SLYNHVATL	0.4841	3.20E-07	1.45E-08	3.03E+05	1.31E+04	9.69E-02	1.34E-03	0.7641	0.7448	0.9767
SLYNKVATL	1.4724	1.98E-07	1.82E-09	1.49E+05	1.30E+03	2.95E-02	8.66E-05	2.0378	0.7216	0.9964
SLYNRVATL	0.3838	5.57E-08	3.38E-09	6.22E+05	3.59E+04	3.47E-02	6.64E-04	0.3756	1.4663	0.9026
SLYNQVATL	0.9979	3.31E-07	6.32E-09	1.74E+05	3.18E+03	5.75E-02	3.07E-04	1.6358	0.8324	0.9935
SLYNNVATL	1.9807	9.75E-08	4.95E-10	1.34E+05	5.98E+02	1.30E-02	3.15E-05	2.3837	0.5135	0.998
SLYNDVATL	0.2669	1.88E-07	1.24E-08	4.00E+05	2.50E+04	7.53E-02	1.62E-03	0.3345	0.5893	0.9329
SLYNSVATL	2.0974	5.18E-08	1.92E-10	1.32E+05	3.60E+02	6.82E-03	1.72E-05	2.3691	0.2655	0.999
SLYNTGATL	1.85	1.10E-07	5.57E-10	1.48E+05	6.78E+02	1.64E-02	3.50E-05	2.2595	0.451	0.9981
SLYNTPATL	2.3511	8.97E-09	1.21E-10	1.32E+05	3.53E+02	1.18E-03	1.56E-05	2.4781	0.3846	0.9991
SLYNTAATL	2.182	4.02E-08	1.64E-10	1.31E+05	3.46E+02	5.25E-03	1.64E-05	2.4214	0.2796	0.9991
SLYNTLATL	2.3647	2.47E-09	1.29E-10	1.31E+05	3.80E+02	3.24E-04	1.69E-05	2.4706	0.4691	0.999
SLYNTIATL	2.2903	1.16E-09	1.29E-10	1.29E+05	3.71E+02	1.49E-04	1.66E-05	2.392	0.4339	0.999
SLYNTMATL	2.0403	2.12E-08	1.18E-10	1.21E+05	2.67E+02	2.56E-03	1.30E-05	2.2172	0.1773	0.9994
SLYNTFATL	1.2907	2.19E-07	1.23E-09	1.10E+05	5.84E+02	2.40E-02	4.34E-05	1.8809	0.1929	0.9986
SLYNTYATL	1.1177	2.11E-07	1.04E-09	4.81E+04	2.19E+02	1.01E-02	1.92E-05	1.9235	0.0602	0.9995
SLYNTWATL	0.2913	6.42E-07	1.09E-08	2.82E+04	4.72E+02	1.81E-02	5.30E-05	0.8212	0.0175	0.9977
SLYNTHATL	1.2418	1.22E-07	5.52E-10	1.05E+05	4.19E+02	1.28E-02	2.66E-05	1.5921	0.1351	0.9987
SLYNTQATL	1.3229	2.05E-07	1.20E-09	1.29E+05	7.19E+02	2.65E-02	5.04E-05	1.8667	0.2317	0.9985
SLYNTNATL	1.4837	1.10E-07	4.63E-10	1.48E+05	5.67E+02	1.63E-02	2.91E-05	1.8127	0.2033	0.9987
SLYNTEATL	0.8742	4.71E-07	3.35E-09	7.91E+04	5.48E+02	3.72E-02	6.16E-05	1.7333	0.0723	0.9991
SLYNTDATL	1.0071	3.79E-07	3.04E-09	1.21E+05	9.41E+02	4.60E-02	9.76E-05	1.7734	0.1494	0.9988
SLYNTSATL	1.7758	1.16E-07	6.07E-10	1.49E+05	7.10E+02	1.73E-02	3.75E-05	2.1876	0.4335	0.9981
SLYNTTATL	2.1585	3.05E-08	1.36E-10	1.20E+05	2.80E+02	3.66E-03	1.39E-05	2.3857	0.2137	0.9993
SLYNTVGTL	2.0164	3.72E-09	1.09E-10	9.90E+04	1.97E+02	3.68E-04	1.07E-05	2.2039	0.1297	0.9996
SLYNTVPTL	2.3796	1.34E-09	9.53E-11	1.29E+05	2.74E+02	1.72E-04	1.23E-05	2.4813	0.2519	0.9995

SLYNTVVTL	1.0998	3.06E-07	3.19E-09	1.34E+05	1.34E+03	4.10E-02	1.20E-04	1.7651	0.363	0.9973
SLYNTVITL	0.3554	2.57E-07	1.19E-08	2.36E+05	1.04E+04	6.08E-02	8.73E-04	0.5114	0.6156	0.9601
SLYNTVMTL	1.8534	6.09E-08	1.81E-10	9.03E+04	1.88E+02	5.50E-03	1.17E-05	2.2453	0.0909	0.9997
SLYNTVFTL	0.9917	3.16E-07	4.21E-09	1.55E+05	1.98E+03	4.88E-02	1.83E-04	1.6041	0.4442	0.9963
SLYNTVHTL	1.8121	7.82E-08	2.22E-10	1.07E+05	2.44E+02	8.39E-03	1.43E-05	2.1822	0.1093	0.9995
SLYNTVKTL	0.4756	6.69E-07	1.17E-08	8.37E+04	1.44E+03	5.60E-02	2.06E-04	1.115	0.0835	0.9971
SLYNTVRTL	0.6032	2.93E-07	3.30E-09	1.34E+05	1.45E+03	3.94E-02	1.24E-04	0.9474	0.1328	0.9966
SLYNTVQTL	1.6244	3.97E-08	1.31E-10	1.00E+05	1.94E+02	3.98E-03	1.07E-05	1.8689	0.0731	0.9996
SLYNTVNTL	1.6503	2.90E-08	1.01E-10	1.08E+05	1.82E+02	3.12E-03	9.50E-06	1.8439	0.0628	0.9997
SLYNTVETL	0.359	6.77E-07	2.68E-08	7.85E+03	3.07E+02	5.31E-03	3.05E-05	2.245	0.0201	0.9988
SLYNTVSTL	2.237	4.49E-09	1.36E-10	1.13E+05	3.09E+02	5.09E-04	1.53E-05	2.3896	0.3346	0.9992
SLYNTVTTL	2.1154	4.44E-08	1.45E-10	1.10E+05	2.29E+02	4.90E-03	1.24E-05	2.411	0.1455	0.9995
SLYNTVAGL	2.4273	8.73E-09	1.13E-10	1.21E+05	2.80E+02	1.05E-03	1.34E-05	2.585	0.2928	0.9994
SLYNTVAPL	1.2654	2.50E-07	2.68E-09	1.70E+05	1.74E+03	4.24E-02	1.35E-04	1.8788	0.5735	0.9969
SLYNTVAAL	2.4801	5.77E-09	1.13E-10	1.19E+05	2.77E+02	6.86E-04	1.34E-05	2.6344	0.3075	0.9994
SLYNTVAVL	2.4336	2.05E-09	1.25E-10	1.20E+05	3.11E+02	2.45E-04	1.49E-05	2.569	0.3753	0.9992
SLYNTVALL	2.3067	1.55E-08	1.34E-10	1.11E+05	2.70E+02	1.72E-03	1.42E-05	2.5155	0.2626	0.9994
SLYNTVAIL	2.2862	1.53E-09	1.20E-10	1.20E+05	3.04E+02	1.83E-04	1.44E-05	2.4087	0.3182	0.9993
SLYNTVAML	1.9843	4.08E-09	8.69E-11	1.29E+05	2.53E+02	5.26E-04	1.12E-05	2.0748	0.1512	0.9995
SLYNTVAFL	1.6229	1.21E-07	3.56E-10	1.07E+05	2.80E+02	1.29E-02	1.75E-05	2.0753	0.1012	0.9994
SLYNTVAYL	1.0517	2.80E-07	2.68E-09	1.29E+05	1.18E+03	3.61E-02	9.93E-05	1.6357	0.3048	0.9974
SLYNTVAWL	1.6125	1.03E-07	3.78E-10	1.11E+05	3.54E+02	1.15E-02	2.11E-05	1.9971	0.1588	0.9991
SLYNTVAHL	2.1749	4.96E-09	1.18E-10	1.11E+05	2.58E+02	5.52E-04	1.31E-05	2.3274	0.2241	0.9994
SLYNTVAKL	2.2586	1.36E-08	1.58E-10	1.12E+05	3.37E+02	1.52E-03	1.71E-05	2.4547	0.3963	0.999
SLYNTVARL	2.2011	4.81E-09	1.48E-10	1.20E+05	3.70E+02	5.75E-04	1.76E-05	2.3315	0.4325	0.9989
SLYNTVAQL	2.2612	1.07E-08	1.04E-10	1.19E+05	2.49E+02	1.27E-03	1.21E-05	2.4193	0.2025	0.9995
SLYNTVANL	2.3162	4.69E-09	1.11E-10	1.18E+05	2.68E+02	5.52E-04	1.30E-05	2.461	0.2558	0.9994
SLYNTVAEL	2.0762	5.69E-08	1.54E-10	1.14E+05	2.22E+02	6.46E-03	1.21E-05	2.4048	0.1196	0.9996
SLYNTVADL	2.2113	2.40E-08	1.29E-10	1.14E+05	2.56E+02	2.73E-03	1.33E-05	2.4345	0.2027	0.9995
SLYNTVASL	2.2704	2.18E-09	1.05E-10	1.25E+05	2.89E+02	2.73E-04	1.31E-05	2.3778	0.2662	0.9994
SLYNTVATG	2.1338	1.85E-09	1.29E-10	1.35E+05	4.07E+02	2.50E-04	1.74E-05	2.2181	0.4275	0.9988
SLYNTVATP	1.588	2.35E-09	1.62E-10	1.93E+05	9.97E+02	4.54E-04	3.10E-05	1.6011	0.7588	0.9954
SLYNTVATA	2.3805	1.94E-09	1.11E-10	1.27E+05	3.11E+02	2.47E-04	1.41E-05	2.4887	0.3296	0.9993
SLYNTVATV	2.2816	2.38E-09	1.36E-10	1.24E+05	3.61E+02	2.94E-04	1.68E-05	2.3957	0.426	0.999
SLYNTVATI	2.3955	1.84E-09	1.28E-10	1.27E+05	3.57E+02	2.34E-04	1.62E-05	2.5058	0.4437	0.999
SLYNTVATM	2.3853	2.38E-09	1.23E-10	1.15E+05	2.87E+02	2.74E-04	1.41E-05	2.533	0.325	0.9993
SLYNTVATF	2.1123	5.15E-09	1.35E-10	9.28E+04	2.17E+02	4.78E-04	1.25E-05	2.3466	0.1816	0.9996
SLYNTVATY	1.2105	2.50E-09	2.26E-10	1.41E+05	7.53E+02	3.53E-04	3.19E-05	1.2507	0.4176	0.9964
SLYNTVATW	1.0378	4.45E-09	2.80E-10	1.09E+05	5.75E+02	4.83E-04	3.03E-05	1.118	0.2574	0.9973
SLYNTVATH	0.7692	1.31E-09	2.28E-10	1.61E+05	9.72E+02	2.10E-04	3.66E-05	0.7838	0.2257	0.995
SLYNTVATK	0.7593	3.24E-09	2.46E-10	1.46E+05	8.62E+02	4.74E-04	3.58E-05	0.7825	0.2008	0.9956
SLYNTVATR	0.8744	1.65E-09	2.71E-10	1.53E+05	1.04E+03	2.53E-04	4.15E-05	0.8954	0.355	0.9944
SLYNTVATQ	1.6697	1.45E-09	1.92E-10	1.53E+05	7.56E+02	2.22E-04	2.93E-05	1.7134	0.7285	0.9965
SLYNTVATN	2.1387	1.48E-09	1.71E-10	1.42E+05	5.88E+02	2.11E-04	2.42E-05	2.2059	0.8112	0.9977
SLYNTVATE	0.4773	4.22E-09	5.10E-10	7.55E+04	5.73E+02	3.19E-04	3.84E-05	0.5619	0.0765	0.9971
SLYNTVATD	0.5079	3.60E-09	5.45E-10	7.25E+04	5.94E+02	2.61E-04	3.95E-05	0.6074	0.0989	0.9964
SLYNTVATS	2.3776	1.97E-09	1.47E-10	1.26E+05	4.06E+02	2.48E-04	1.85E-05	2.4953	0.5746	0.9988
SLYNTVATT	2.4385	1.79E-09	1.43E-10	1.21E+05	3.68E+02	2.16E-04	1.73E-05	2.5714	0.527	0.9989

Table S4: Kinetic measurement results for bs-868Z11-CD3, immobilized using Anti-Fab2, and soluble DS-A2 peptide-MHC molecules loaded individually with pSL9 based PSL peptides.

Peptide	KD (M)	KD Error	k_{on} ($M^{-1}s^{-1}$)	k_{on} Error	k_{off} (s^{-1})	k_{off} Error	Full X^2	Full R^2
SLYNTVATL	3.81E-09	1.49E-10	1.03E+05	1.45E+02	3.91E-04	1.53E-05	0.262	0.9993
GLYNTVATL	3.05E-08	3.55E-10	1.04E+05	3.42E+02	3.19E-03	3.56E-05	1.0915	0.9966
PLYNTVATL	8.54E-09	3.46E-10	9.65E+04	3.03E+02	8.24E-04	3.33E-05	1.2363	0.9969
ALYNTVATL	5.82E-09	3.18E-10	1.04E+05	3.14E+02	6.04E-04	3.29E-05	1.2791	0.9969
VLYNTVATL	5.74E-09	2.24E-10	1.05E+05	2.27E+02	6.04E-04	2.35E-05	0.6719	0.9984
LLYNTVATL	4.99E-08	2.99E-10	1.04E+05	2.67E+02	5.17E-03	2.80E-05	0.5623	0.9981
ILYNTVATL	1.35E-08	2.35E-10	1.06E+05	2.40E+02	1.43E-03	2.47E-05	0.6748	0.9982
MLYNTVATL	4.19E-08	2.95E-10	1.09E+05	2.93E+02	4.56E-03	2.96E-05	0.6922	0.9978
FLYNTVATL	5.22E-08	3.07E-10	1.15E+05	3.20E+02	6.02E-03	3.13E-05	0.6452	0.9976
YLYNTVATL	1.24E-07	5.65E-10	1.15E+05	4.01E+02	1.43E-02	4.21E-05	0.4931	0.9972
WLYNTVATL	4.62E-07	4.57E-09	1.66E+05	1.48E+03	7.66E-02	3.27E-04	0.1216	0.9955
HLYNTVATL	3.43E-07	2.50E-09	1.34E+05	8.87E+02	4.60E-02	1.43E-04	0.1908	0.9961
KLYNTVATL	1.91E-08	2.14E-10	9.03E+04	1.67E+02	1.73E-03	1.91E-05	0.3239	0.999
RLYNTVATL	4.42E-09	5.15E-10	8.86E+04	3.93E+02	3.92E-04	4.56E-05	2.0699	0.9944
QLYNTVATL	1.38E-07	5.55E-10	9.85E+04	3.05E+02	1.36E-02	3.50E-05	0.3534	0.9981
NLYNTVATL	3.13E-08	3.42E-10	9.84E+04	2.98E+02	3.08E-03	3.23E-05	0.9466	0.9973
ELYNTVATL	4.85E-07	4.84E-09	9.29E+04	8.66E+02	4.50E-02	1.63E-04	0.4525	0.9948
DLYNTVATL	4.49E-08	3.46E-10	9.55E+04	2.77E+02	4.28E-03	3.06E-05	0.7816	0.9977
TLYNTVATL	6.94E-09	2.07E-10	1.02E+05	1.98E+02	7.07E-04	2.10E-05	0.544	0.9988
SGYNTVATL	1.86E-08	4.56E-10	8.40E+04	3.18E+02	1.56E-03	3.79E-05	1.3876	0.9964
SPYNTVATL	1.65E-07	2.27E-09	6.80E+04	7.29E+02	1.12E-02	9.66E-05	2.2025	0.9852
SAYNTVATL	1.00E-08	1.28E-10	1.02E+05	1.23E+02	1.02E-03	1.30E-05	0.2052	0.9995
SVYNTVATL	8.47E-09	1.64E-10	1.01E+05	1.55E+02	8.57E-04	1.65E-05	0.3327	0.9992
SIYNTVATL	8.68E-09	9.77E-11	1.02E+05	9.42E+01	8.89E-04	9.97E-06	0.1192	0.9997
SMYNTVATL	6.55E-09	2.07E-10	1.01E+05	1.95E+02	6.61E-04	2.08E-05	0.4808	0.9987
SFYNTVATL	8.52E-09	3.97E-10	9.54E+04	3.41E+02	8.13E-04	3.77E-05	1.5251	0.996
SYYNTVATL	3.26E-08	3.90E-10	5.83E+04	1.62E+02	1.90E-03	2.21E-05	0.23	0.9989
SWYNTVATL	8.16E-08	1.74E-09	4.46E+04	4.66E+02	3.64E-03	6.77E-05	0.9827	0.991
SHYNTVATL	2.73E-08	8.86E-10	6.92E+04	4.66E+02	1.89E-03	5.99E-05	2.1947	0.9915
SKYNTVATL	7.43E-08	1.57E-09	5.08E+04	5.00E+02	3.77E-03	7.06E-05	2.0162	0.9899
SRYNTVATL	1.02E-07	2.33E-09	4.84E+04	6.42E+02	4.95E-03	9.17E-05	0.6946	0.9837
SQYNTVATL	9.41E-09	2.19E-10	1.09E+05	2.35E+02	1.03E-03	2.37E-05	0.6976	0.9984
SNYNTVATL	2.45E-08	6.68E-10	6.85E+04	3.45E+02	1.68E-03	4.50E-05	1.7367	0.9953
SEYNTVATL	4.09E-08	1.77E-09	5.16E+04	6.23E+02	2.11E-03	8.78E-05	4.5691	0.9843
SDYNTVATL	1.01E-07	1.68E-09	6.51E+04	6.61E+02	6.56E-03	8.69E-05	3.2507	0.9854
SSYNTVATL	8.17E-09	1.97E-10	9.64E+04	1.72E+02	7.88E-04	1.89E-05	0.4063	0.999
STYNTVATL	5.41E-09	1.49E-10	9.87E+04	1.35E+02	5.34E-04	1.47E-05	0.2427	0.9994
SLGNTVATL	No fit							
SLPNTVATL	No fit							
SLANTVATL	No fit							
SLVNTVATL	5.11E-07	5.80E-09	1.95E+05	2.01E+03	9.96E-02	4.80E-04	0.0769	0.9966
SLLNTVATL	1.32E-07	8.45E-10	1.21E+05	6.09E+02	1.60E-02	6.33E-05	1.038	0.9944
SLINTVATL	4.77E-07	5.50E-09	1.40E+05	1.48E+03	6.69E-02	3.15E-04	0.325	0.9939

SLMNTVATL	1.07E-06	5.52E-08	2.35E+05	1.12E+04	2.50E-01	5.13E-03	0.1244	0.979
SLFNTVATL	3.47E-08	1.92E-10	9.54E+04	1.59E+02	3.31E-03	1.75E-05	0.2445	0.9992
SLWNTVATL	3.36E-08	1.91E-10	9.34E+04	1.53E+02	3.14E-03	1.71E-05	0.2479	0.9992
SLHNTVATL	9.09E-08	3.31E-10	1.16E+05	2.84E+02	1.06E-02	2.85E-05	0.3676	0.9984
SLKNTVATL	No fit							
SLRNTVATL	5.55E-07	5.54E-09	9.64E+04	9.00E+02	5.35E-02	1.88E-04	0.1675	0.9957
SLQNTVATL	6.29E-07	9.45E-09	2.62E+05	3.51E+03	1.65E-01	1.11E-03	0.0384	0.9961
SLNNTVATL	4.74E-07	5.90E-09	1.81E+05	2.05E+03	8.59E-02	4.48E-04	0.1049	0.9953
SLENTVATL	No fit							
SLDNTVATL	No fit							
SLSNTVATL	No fit							
SLTNTVATL	3.01E-06	3.45E-06	1.88E+05	2.15E+05	5.66E-01	6.50E-02	0.1123	0.9199
SLYGTVATL	5.33E-07	1.20E-08	2.07E+05	4.15E+03	1.11E-01	1.12E-03	0.5678	0.9842
SLYPTVATL	5.54E-07	1.44E-08	3.62E+05	8.18E+03	2.00E-01	2.58E-03	0.0884	0.9892
SLYATVATL	1.15E-07	6.46E-10	1.40E+05	6.09E+02	1.60E-02	5.72E-05	0.9354	0.9952
SLYVTVATL	1.80E-07	9.65E-10	1.31E+05	5.98E+02	2.35E-02	6.64E-05	0.4669	0.9962
SLYLTVATL	6.70E-08	3.12E-10	1.11E+05	2.85E+02	7.44E-03	2.89E-05	0.5152	0.9981
SLYITVATL	5.25E-07	5.68E-09	1.18E+05	1.18E+03	6.19E-02	2.55E-04	0.2208	0.9949
SLYMTVATL	1.88E-06	2.10E-06	3.58E+05	3.96E+05	6.72E-01	1.11E-01	0.09	0.876
SLYFTVATL	No fit							
SLYYTVATL	No fit							
SLYWTVATL	No fit							
SLYHTVATL	8.11E-08	6.16E-10	1.38E+05	7.03E+02	1.12E-02	6.26E-05	1.8422	0.9923
SLYKTVATL	No fit							
SLYRTVATL	No fit							
SLYQTVATL	2.84E-07	3.23E-09	1.71E+05	1.73E+03	4.86E-02	2.53E-04	0.6721	0.9898
SLYETVATL	No fit							
SLYDTVATL	No fit							
SLYSTVATL	5.95E-08	2.69E-10	1.27E+05	3.13E+02	7.57E-03	2.87E-05	0.5404	0.9981
SLYTTVATL	1.61E-07	7.59E-10	1.35E+05	5.34E+02	2.18E-02	5.63E-05	0.3965	0.9968
SLYNGVATL	6.03E-07	1.50E-07	5.42E+05	1.29E+05	3.27E-01	2.34E-02	0.0452	0.9399
SLYNPVATL	No fit							
SLYNAVATL	9.66E-08	5.82E-10	1.27E+05	5.41E+02	1.22E-02	5.20E-05	0.9944	0.995
SLYNVVATL	3.07E-08	4.63E-10	9.09E+04	3.58E+02	2.79E-03	4.06E-05	1.3333	0.9958
SLYNLVATL	1.46E-08	3.05E-10	9.80E+04	2.73E+02	1.43E-03	2.97E-05	0.917	0.9976
SLYNIVATL	4.85E-08	3.37E-10	8.41E+04	2.21E+02	4.08E-03	2.62E-05	0.4314	0.9984
SLYNMVATL	4.26E-08	3.52E-10	1.20E+05	4.09E+02	5.12E-03	3.86E-05	1.2415	0.9962
SLYNFVATL	7.26E-07	3.75E-08	2.97E+05	1.36E+04	2.16E-01	5.09E-03	0.3346	0.9697
SLYNYVATL	4.60E-06	9.88E-06	1.37E+05	2.94E+05	6.31E-01	9.34E-02	0.1113	0.8904
SLYNWVATL	No fit							
SLYNHVATL	6.23E-07	4.07E-08	4.00E+05	2.26E+04	2.49E-01	8.17E-03	0.2106	0.9526
SLYNKVATL	2.24E-07	1.05E-09	1.35E+05	5.55E+02	3.02E-02	6.82E-05	0.2572	0.9973
SLYNRVATL	7.78E-07	7.24E-08	3.54E+05	3.19E+04	2.76E-01	6.54E-03	0.02	0.9899
SLYNQVATL	4.72E-07	7.25E-09	2.10E+05	2.90E+03	9.91E-02	6.64E-04	0.131	0.9936
SLYNNVATL	1.19E-07	5.68E-10	1.32E+05	4.88E+02	1.58E-02	4.76E-05	0.5956	0.9966
SLYNEVATL	No fit							

SLYNDVATL	3.91E-05	5.33E-04	1.23E+04	1.67E+05	4.79E-01	5.67E-02	0.1685	0.904
SLYNSVATL	6.91E-08	3.75E-10	1.21E+05	3.86E+02	8.39E-03	3.68E-05	0.7181	0.997
SLYNTGATL	1.34E-07	6.48E-10	1.37E+05	5.33E+02	1.84E-02	5.26E-05	0.5267	0.9965
SLYNTPATL	1.54E-08	1.56E-10	1.19E+05	1.93E+02	1.83E-03	1.82E-05	0.3561	0.999
SLYNTAATL	5.48E-08	3.74E-10	1.10E+05	3.59E+02	6.05E-03	3.62E-05	0.8843	0.9967
SLYNTLATL	9.08E-09	1.01E-10	1.12E+05	1.15E+02	1.02E-03	1.13E-05	0.15	0.9996
SLYNTIATL	8.74E-09	1.86E-10	9.97E+04	1.72E+02	8.71E-04	1.85E-05	0.3788	0.999
SLYNTMATL	2.72E-08	3.66E-10	9.75E+04	3.17E+02	2.65E-03	3.46E-05	0.9551	0.9966
SLYNTFATL	5.79E-07	6.47E-09	7.96E+04	8.39E+02	4.61E-02	1.69E-04	0.1416	0.9946
SLYNTYATL	4.43E-07	8.76E-09	4.61E+04	8.61E+02	2.04E-02	1.33E-04	0.1286	0.9831
SLYNTWATL	1.74E-05	1.28E-05	1.91E+03	1.41E+03	3.33E-02	2.40E-04	0.0063	0.9878
SLYNTHATL	1.75E-07	1.46E-09	7.39E+04	4.94E+02	1.30E-02	6.42E-05	0.3653	0.9929
SLYNTKATL	No fit							
SLYNTRATL	No fit							
SLYNTQATL	2.71E-07	1.50E-09	1.19E+05	5.86E+02	3.22E-02	7.94E-05	0.1392	0.9969
SLYNTNATL	1.79E-07	7.80E-10	1.20E+05	4.42E+02	2.15E-02	5.03E-05	0.2983	0.9974
SLYNTEATL	1.43E-06	5.11E-08	5.54E+04	1.93E+03	7.94E-02	5.83E-04	0.0772	0.99
SLYNTDATL	6.04E-07	7.08E-09	1.12E+05	1.22E+03	6.77E-02	2.89E-04	0.1139	0.995
SLYNTSATL	1.66E-07	6.43E-10	1.43E+05	4.69E+02	2.38E-02	4.93E-05	0.2673	0.9979
SLYNTTATL	3.37E-08	4.58E-10	1.07E+05	4.51E+02	3.59E-03	4.64E-05	1.7673	0.9938
SLYNTVGTL	8.29E-09	4.59E-10	8.24E+04	3.12E+02	6.83E-04	3.77E-05	1.2283	0.996
SLYNTVPTL	3.71E-09	4.42E-10	1.22E+05	5.76E+02	4.51E-04	5.36E-05	4.052	0.9904
SLYNTVVTL	5.99E-07	1.07E-08	1.44E+05	2.37E+03	8.64E-02	6.15E-04	0.1883	0.9892
SLYNTVLTL	No fit							
SLYNTVITL	No fit							
SLYNTVMTL	1.02E-07	4.28E-10	6.90E+04	1.80E+02	7.04E-03	2.31E-05	0.1333	0.9988
SLYNTVFTL	5.14E-07	1.01E-08	1.72E+05	3.07E+03	8.85E-02	7.06E-04	0.1274	0.9897
SLYNTVYTL	No fit							
SLYNTVWTL	No fit							
SLYNTVHTL	1.14E-07	2.51E-10	8.42E+04	1.27E+02	9.63E-03	1.53E-05	0.0763	0.9995
SLYNTVKTL	1.20E-06	5.58E-08	5.35E+04	2.43E+03	6.42E-02	6.41E-04	0.0792	0.9775
SLYNTVRTL	1.28E-06	2.41E-08	2.49E+04	4.61E+02	3.20E-02	9.10E-05	0.0547	0.9967
SLYNTVQTL	5.38E-08	7.00E-10	6.84E+04	3.40E+02	3.68E-03	4.43E-05	0.9296	0.9952
SLYNTVNTL	4.11E-08	8.02E-10	7.22E+04	4.32E+02	2.97E-03	5.51E-05	1.5878	0.9921
SLYNTVETL	1.61E-06	2.46E-07	5.74E+03	8.80E+02	9.22E-03	1.00E-04	0.007	0.989
SLYNTVDTL	No fit							
SLYNTVSTL	1.04E-08	4.47E-10	9.80E+04	4.00E+02	1.02E-03	4.36E-05	1.9634	0.9944
SLYNTVTTL	6.90E-08	2.99E-10	9.23E+04	2.09E+02	6.37E-03	2.36E-05	0.2893	0.9987
SLYNTVAGL	1.14E-08	1.42E-10	1.14E+05	1.65E+02	1.30E-03	1.61E-05	0.302	0.9992
SLYNTVAPL	2.34E-07	1.20E-09	1.35E+05	6.11E+02	3.16E-02	7.71E-05	0.3155	0.9969
SLYNTVAAL	8.50E-09	1.51E-10	1.14E+05	1.75E+02	9.69E-04	1.72E-05	0.3504	0.9991
SLYNTVAVL	6.98E-09	1.19E-10	1.05E+05	1.20E+02	7.31E-04	1.25E-05	0.1881	0.9995
SLYNTVALL	1.58E-08	1.20E-10	9.58E+04	1.03E+02	1.51E-03	1.14E-05	0.1259	0.9996
SLYNTVAIL	4.16E-09	7.48E-10	9.74E+04	6.62E+02	4.05E-04	7.28E-05	5.8607	0.9834
SLYNTVAML	7.69E-09	5.22E-10	9.75E+04	4.63E+02	7.50E-04	5.08E-05	2.7181	0.9922
SLYNTVAFL	1.93E-07	1.68E-09	9.29E+04	6.77E+02	1.80E-02	8.45E-05	0.9456	0.9906

SLYNTVAYL	4.00E-07	3.75E-09	9.61E+04	8.32E+02	3.85E-02	1.39E-04	0.2451	0.994
SLYNTVAWL	2.09E-07	1.94E-09	9.65E+04	7.69E+02	2.01E-02	9.70E-05	1.0358	0.9893
SLYNTVAHL	1.09E-08	5.55E-10	9.19E+04	4.47E+02	1.00E-03	5.07E-05	2.6388	0.9925
SLYNTVAKL	1.73E-08	2.87E-10	1.02E+05	2.76E+02	1.77E-03	2.90E-05	0.9054	0.9975
SLYNTVARL	7.93E-09	3.98E-10	1.06E+05	4.06E+02	8.37E-04	4.19E-05	2.1201	0.9946
SLYNTVAQL	1.59E-08	6.14E-10	1.01E+05	5.74E+02	1.61E-03	6.13E-05	4.0059	0.9888
SLYNTVANL	1.08E-08	6.43E-10	1.01E+05	6.03E+02	1.09E-03	6.46E-05	4.5943	0.9874
SLYNTVAEL	4.73E-08	2.37E-10	9.22E+04	1.79E+02	4.36E-03	2.02E-05	0.291	0.999
SLYNTVADL	2.12E-08	3.17E-10	8.90E+04	2.40E+02	1.88E-03	2.77E-05	0.6889	0.9979
SLYNTVASL	4.68E-09	2.55E-10	1.09E+05	2.71E+02	5.08E-04	2.76E-05	0.918	0.9977
SLYNTVATG	7.71E-09	4.30E-10	1.01E+05	4.05E+02	7.79E-04	4.34E-05	2.1199	0.9943
SLYNTVATP	5.03E-08	1.57E-09	3.41E+04	3.34E+02	1.72E-03	5.08E-05	0.6961	0.9945
SLYNTVATA	6.74E-09	4.88E-10	1.13E+05	5.56E+02	7.61E-04	5.49E-05	3.6905	0.9904
SLYNTVATV	8.41E-09	6.00E-10	1.04E+05	5.95E+02	8.76E-04	6.23E-05	4.752	0.988
SLYNTVATI	6.70E-09	2.87E-10	1.13E+05	3.25E+02	7.53E-04	3.22E-05	1.2712	0.9968
SLYNTVATM	7.45E-09	2.48E-10	9.88E+04	2.26E+02	7.36E-04	2.44E-05	0.6922	0.9982
SLYNTVATF	1.19E-08	2.46E-10	7.18E+04	1.37E+02	8.51E-04	1.76E-05	0.2228	0.9992
SLYNTVATY	1.02E-08	3.37E-10	7.11E+04	1.85E+02	7.24E-04	2.39E-05	0.4625	0.9985
SLYNTVATW	3.32E-08	5.59E-10	3.70E+04	1.34E+02	1.23E-03	2.02E-05	0.0824	0.9991
SLYNTVATH	1.37E-08	3.64E-10	4.75E+04	1.19E+02	6.51E-04	1.72E-05	0.089	0.9993
SLYNTVATK	4.57E-08	1.20E-09	2.70E+04	2.00E+02	1.23E-03	3.11E-05	0.0929	0.9982
SLYNTVATR	5.71E-09	2.30E-10	9.59E+04	1.99E+02	5.48E-04	2.20E-05	0.5532	0.9986
SLYNTVATQ	5.88E-09	3.12E-10	8.96E+04	2.41E+02	5.27E-04	2.79E-05	0.7397	0.9978
SLYNTVATN	9.10E-09	3.77E-10	9.76E+04	3.36E+02	8.88E-04	3.67E-05	1.5971	0.9961
SLYNTVATE	6.96E-06	9.43E-06	3.79E+02	5.13E+02	2.64E-03	8.02E-05	0.1997	0.9908
SLYNTVATD	7.18E-06	8.48E-06	3.95E+02	4.67E+02	2.83E-03	7.30E-05	0.1137	0.9924
SLYNTVATS	7.19E-09	2.13E-10	1.16E+05	2.54E+02	8.33E-04	2.46E-05	0.7637	0.9981
SLYNTVATT	5.66E-09	1.27E-10	1.12E+05	1.42E+02	6.32E-04	1.41E-05	0.2627	0.9994

Table S5: Kinetic measurement results for bs-868Z11-CD3, immobilized using Anti-Fab2, and soluble DS-A2 peptide-MHC molecules loaded individually with 140 predicted off-target peptides.

Peptide	Associated Gene	KD (M)	KD Error	k_{on} ($M^{-1}s^{-1}$)	k_{on} Error	k_{off} (s^{-1})	k_{off} Error	Full X^2	Full R^2
RVYNTVPLV	HIPK3	1.32E-08	1.76E-10	9.50E+04	1.69E+02	1.26E-03	1.66E-05	0.2908	0.9993
RMYNLVSRI	CUL1	1.91E-08	2.52E-10	9.25E+04	2.28E+02	1.76E-03	2.29E-05	0.5429	0.9986
SLYNMVPSI	OVOS	1.97E-08	1.71E-10	1.31E+05	2.89E+02	2.57E-03	2.16E-05	0.586	0.9987
TVYNMVPSI	OVOS	2.07E-08	1.54E-10	1.28E+05	2.50E+02	2.66E-03	1.91E-05	0.4228	0.999
ALYNVIAMA	SECISBP2L	2.11E-08	1.51E-10	9.28E+04	2.25E+02	1.96E-03	1.32E-05	0.114	0.9997
AIYNLLPDI	NCAPD2	2.33E-08	1.82E-10	1.01E+05	1.90E+02	2.36E-03	1.79E-05	0.3299	0.9992
STYNLVSTS	KIAA2018	2.47E-08	2.16E-10	7.07E+04	1.28E+02	1.75E-03	1.49E-05	0.1772	0.9995
SVYNMVPSI	OVOS2	2.68E-08	1.96E-10	1.32E+05	3.26E+02	3.53E-03	2.43E-05	0.6471	0.9984
RTYNVLAIL	ATP8B1	3.11E-08	1.55E-10	7.54E+04	9.93E+01	2.34E-03	1.12E-05	0.0937	0.9997
SVYNLVSIA	KPTN	3.65E-08	2.01E-10	7.97E+04	2.13E+02	2.91E-03	1.40E-05	0.0926	0.9997
RAYNLIGTV	LOC100128501	3.72E-08	1.71E-10	8.94E+04	1.40E+02	3.33E-03	1.43E-05	0.1721	0.9995
ALFNLIPVG	FGF12	3.83E-08	3.22E-10	6.64E+04	1.71E+02	2.54E-03	2.04E-05	0.266	0.999
RIYNVIGTL	FOLH1,FOLH1B	4.53E-08	3.00E-10	5.75E+04	1.28E+02	2.61E-03	1.62E-05	0.1095	0.9994

RIYNVVGTI	NAALAD2	5.15E-08	4.13E-10	5.94E+04	1.81E+02	3.06E-03	2.27E-05	0.2723	0.9989
TLFNLVPNS	CLASP2	5.40E-08	3.31E-10	9.76E+04	2.90E+02	5.28E-03	2.82E-05	0.4822	0.9981
SLFNVISIL	KCNK12, KCNK13	5.83E-08	3.11E-10	6.94E+04	1.64E+02	4.05E-03	1.94E-05	0.2068	0.9992
STFNLVAIS	CCKAR	6.06E-08	2.91E-10	4.96E+04	9.98E+01	3.01E-03	1.31E-05	0.0436	0.9996
TLFNLIPVG	FGF12,FGF13,FGF14	6.32E-08	3.97E-10	6.72E+04	1.98E+02	4.25E-03	2.36E-05	0.3044	0.9988
TIFNLIPNS	CLASP1	6.41E-08	2.67E-10	8.97E+04	1.99E+02	5.75E-03	2.03E-05	0.2655	0.999
ALYNVLAKV	IFFO1,IFFO2	6.59E-08	2.96E-10	1.02E+05	2.63E+02	6.75E-03	2.49E-05	0.3602	0.9986
AVFNLLPHT	SMYD4	7.11E-08	2.72E-10	8.53E+04	1.82E+02	6.07E-03	1.93E-05	0.2344	0.9991
RMYNLLGHM	ZNF710	8.71E-08	7.55E-10	5.30E+04	2.55E+02	4.62E-03	3.33E-05	0.2278	0.9977
STWNTPPNM	KIAA0922	8.98E-08	3.45E-10	9.05E+04	2.28E+02	8.13E-03	2.36E-05	0.2591	0.9989
NIYNLIAII	BICD2	9.32E-08	3.91E-10	1.06E+05	3.10E+02	9.84E-03	2.95E-05	0.3894	0.9983
RIYNLPPEL	WRAP53	9.95E-08	3.78E-10	9.47E+04	2.51E+02	9.42E-03	2.56E-05	0.3026	0.9988
TTFNLPSAA	WDR17	1.02E-07	6.71E-10	7.87E+04	3.47E+02	8.04E-03	3.91E-05	0.579	0.997
MFFNVIAIV	UGGT2	1.06E-07	1.29E-09	5.21E+04	3.95E+02	5.52E-03	5.23E-05	0.0772	0.9934
SLWNTVSGI	HHLA1	1.08E-07	5.04E-10	8.88E+04	2.94E+02	9.60E-03	3.14E-05	0.3873	0.9982
MLWNLLALR	COX7A2	1.17E-07	1.03E-08	1.26E+06	1.05E+05	1.47E-01	4.25E-03	0.0448	0.9675
VFWNLLPTV	C12orf74	1.20E-07	7.20E-10	1.24E+05	5.97E+02	1.49E-02	5.29E-05	0.9116	0.9955
STFNTTSNG	QSER1	1.52E-07	6.60E-09	1.76E+05	7.05E+03	2.67E-02	4.39E-04	0.0311	0.9225
GFFNLLSHV	PCP2	1.59E-07	9.88E-09	6.24E+05	3.64E+04	9.94E-02	2.08E-03	0.0321	0.9717
LLYNVPAVA	APP	1.67E-07	1.27E-08	7.41E+05	5.29E+04	1.24E-01	3.21E-03	0.0164	0.9712
ALFNTISQG	VTA1	1.83E-07	8.26E-10	7.15E+04	2.68E+02	1.31E-02	3.28E-05	0.2214	0.9984
TTFNTLAGS	MUC16	1.97E-07	8.70E-10	9.03E+04	3.44E+02	1.78E-02	3.98E-05	0.1556	0.9981
SLWNLLGNA	LMAN2L	2.14E-07	3.02E-08	1.02E+06	1.35E+05	2.19E-01	1.07E-02	0.0324	0.952
SLYNLLNLT	SLC4A5	2.19E-07	8.40E-10	6.75E+04	2.24E+02	1.48E-02	2.85E-05	0.094	0.9988
GVWNLLSIV	ZSWIM8	2.52E-07	4.59E-08	1.09E+06	1.86E+05	2.74E-01	1.73E-02	0.0545	0.9403
ALFNVVNSI	SLC38A11	2.55E-07	2.10E-09	6.83E+04	4.99E+02	1.74E-02	6.59E-05	0.2897	0.9956
VIYNLLGLA	SH3TC2	2.64E-07	1.88E-09	1.07E+05	7.25E+02	2.83E-02	5.92E-05	0.2115	0.9983
SIFNIVAIA	GPR50	2.84E-07	1.60E-09	4.44E+04	2.37E+02	1.26E-02	2.25E-05	0.0369	0.9995
TVYNTVSEG	SLC39A6	3.04E-07	2.50E-09	4.71E+04	3.50E+02	1.43E-02	4.99E-05	0.2538	0.997
DLWNTLSSL	EFCAB13, ITGB3	3.39E-07	2.60E-08	4.15E+05	3.02E+04	1.41E-01	3.55E-03	0.0238	0.9752
IFFNLLAVL	POMT1	3.50E-07	4.75E-08	8.47E+05	1.08E+05	2.97E-01	1.35E-02	0.023	0.9688
DLFNLLPDV	PSMD7	3.60E-07	1.08E-08	7.69E+04	2.15E+03	2.77E-02	3.14E-04	0.0881	0.9367
LSWNVVPNA	SPCS3	3.67E-07	2.91E-08	4.13E+05	3.09E+04	1.52E-01	3.89E-03	0.0234	0.9734
MLWNLLALH	COX7A2P2	3.67E-07	2.04E-08	1.07E+06	4.75E+04	3.94E-01	1.33E-02	0.1159	0.9595
TIFNTVNTS	TIMMDC1	3.87E-07	2.77E-09	4.20E+04	2.80E+02	1.63E-02	4.19E-05	0.0304	0.9978
KTFNLIPAV	MRPL4	4.13E-07	2.59E-09	1.12E+05	6.52E+02	4.62E-02	1.07E-04	0.1185	0.9979
NLFNVTPLI	ZNF66P	4.28E-07	1.38E-07	1.05E+06	3.19E+05	4.49E-01	4.68E-02	0.0447	0.9139
SYWNIISTV	OR2D3	4.39E-07	4.84E-09	4.56E+04	4.74E+02	2.00E-02	7.23E-05	0.1373	0.9952
GVFNLIAVL	AC002365.5, LOC100288814	4.59E-07	4.94E-09	7.59E+04	7.70E+02	3.48E-02	1.26E-04	0.3268	0.9946
RLFNITSSA	IFITM10	4.74E-07	4.12E-08	2.51E+05	2.08E+04	1.19E-01	3.08E-03	0.0167	0.9706
NLWNLVAVI	WDR17	4.97E-07	1.16E-08	2.07E+05	4.34E+03	1.03E-01	1.04E-03	0.256	0.9836
RIFNLIGMM	HCN1,HCN3	4.98E-07	1.26E-08	2.29E+04	5.51E+02	1.14E-02	8.55E-05	0.0712	0.9889
RLFNVVSRG	TRPV2	5.02E-07	6.55E-09	6.50E+04	8.05E+02	3.26E-02	1.34E-04	0.1875	0.9931

LVFNVIPTL	ABCB6	5.35E-07	3.99E-09	1.33E+05	9.21E+02	7.13E-02	2.00E-04	0.0445	0.9982
TTWNILSSA	COX1	5.36E-07	4.08E-08	2.26E+05	1.65E+04	1.21E-01	2.63E-03	0.0214	0.9794
KLFNVLSTL	NUP210P2	5.76E-07	3.35E-08	2.97E+05	1.65E+04	1.71E-01	2.83E-03	0.0131	0.9912
RVYNLTAKS	VWA3B	5.95E-07	4.57E-09	4.53E+04	3.35E+02	2.69E-02	5.65E-05	0.0219	0.9981
LTFNTISLS	ENTHD1	7.09E-07	2.12E-07	4.78E+05	1.37E+05	3.39E-01	2.72E-02	0.0387	0.929
AQFNLLSST	TP73	7.13E-07	9.97E-09	8.59E+04	1.15E+03	6.12E-02	2.58E-04	0.1658	0.9947
VVYNVLSEL	SP100,SP140L	7.35E-07	6.29E-08	1.84E+05	1.52E+04	1.35E-01	2.89E-03	0.0255	0.9785
KVYNTPSTS	AEBP2	7.51E-07	1.39E-08	1.71E+05	2.91E+03	1.28E-01	9.13E-04	0.0718	0.9945
GIFNIIPST	CAPN7	7.90E-07	8.67E-09	1.32E+05	1.36E+03	1.04E-01	4.00E-04	0.0364	0.9979
NIYNTLSGL	UBR4	8.73E-07	1.71E-08	1.59E+05	2.89E+03	1.38E-01	9.89E-04	0.0564	0.9947
RLFNLTSTF	FLJ44715,FUT11	9.32E-07	2.82E-08	1.72E+05	4.83E+03	1.60E-01	1.79E-03	0.0525	0.9894
TVWNTLSSL	DNAH9	9.39E-07	1.22E-08	4.52E+04	5.73E+02	4.25E-02	1.20E-04	0.0344	0.9971
RLFNMLSAV	CFAP221,PCDP1	9.71E-07	3.06E-08	1.73E+05	5.09E+03	1.68E-01	1.94E-03	0.0714	0.9892
SIWNVTAIA	HTR5A	1.10E-06	5.12E-07	3.21E+05	1.45E+05	3.54E-01	3.47E-02	0.0576	0.9051
ALFNLMSGI	EGR4	1.19E-06	3.21E-08	9.57E+04	2.48E+03	1.14E-01	8.53E-04	0.0645	0.9931
IVYNLLSAM	SLC39A10	1.30E-06	1.62E-07	1.61E+05	1.98E+04	2.10E-01	4.82E-03	0.0245	0.987
ISFNMLPSI	GPR98	1.37E-06	4.65E-08	1.24E+05	4.04E+03	1.70E-01	1.70E-03	0.0581	0.991
NTYNILPGS	C9orf173	1.38E-06	1.17E-07	1.14E+05	9.57E+03	1.57E-01	2.30E-03	0.025	0.9925
RLWNMVNVT	IL12RB2	1.39E-06	2.57E-07	1.52E+05	2.77E+04	2.11E-01	6.87E-03	0.049	0.9763
SAFNITSLI	WAC	1.41E-06	3.21E-07	1.65E+05	3.70E+04	2.32E-01	9.29E-03	0.0314	0.9682
NIFNLPNIV	OMD	1.48E-06	6.62E-07	4.19E+05	1.85E+05	6.20E-01	4.90E-02	0.0905	0.9596
GVYNLPGAS	GPX2	1.58E-06	3.07E-07	1.17E+05	2.23E+04	1.84E-01	5.65E-03	0.0488	0.9756
GTYNVISLV	TRPC4,TRPC5	1.64E-06	4.18E-07	1.23E+05	3.10E+04	2.02E-01	8.00E-03	0.0666	0.965
SIFNTLSDI	SGSM3	1.97E-06	5.86E-08	4.07E+04	1.20E+03	8.01E-02	3.78E-04	0.0856	0.9957
TIFNILSGI	ABCA3	2.66E-06	2.37E-07	4.68E+04	4.13E+03	1.24E-01	1.66E-03	0.1728	0.9807
LLFNLISSS	MON1A	2.79E-06	2.57E-06	1.51E+05	1.38E+05	4.20E-01	4.10E-02	0.0599	0.9183
RTFNLTAGS	PDXDC1	2.85E-06	5.89E-07	4.63E+04	9.54E+03	1.32E-01	2.56E-03	0.0356	0.9845
TVFNILPGG	PAFAH2	3.23E-06	1.06E-06	3.69E+04	1.21E+04	1.19E-01	3.22E-03	0.025	0.968
GLFNIPPAS	CYP2S1	3.91E-06	4.13E-06	8.52E+04	8.97E+04	3.33E-01	2.74E-02	0.0395	0.9216
RMFNIISDS	RASA1	3.99E-06	4.08E-07	1.51E+04	1.54E+03	6.02E-02	4.39E-04	0.0509	0.9862
TTFNIVGTT	GABRA3	6.79E-06	3.10E-06	8.68E+03	3.96E+03	5.89E-02	8.72E-04	0.0351	0.9743
ALFNLMSGV	EGR4	7.87E-06	1.14E-05	3.17E+04	4.60E+04	2.50E-01	1.45E-02	0.1115	0.9454
SVFNITAIA	MTNR1B	1.96E-05	2.39E-04	2.58E+04	3.15E+05	5.06E-01	1.06E-01	0.2805	0.7869
KIYNTPSAS	NCAM1	2.56E-05	2.88E-05	8.86E+03	9.95E+03	2.27E-01	5.62E-03	0.2474	0.9662
LLYNLLGSS	ABCC9	1.41E-04	6.82E-03	3.21E+03	1.55E+05	4.54E-01	5.27E-02	0.1153	0.9007
SLYNMMGEA	TMTC2	No fit							
SLWNLMGNA	LMAN2L	No fit							
GLYNIVGNA	SUMF1	No fit							
LTWNLTPKA	DLEC1	No fit							
LIFNVTGLA	ZDHHC23	No fit							
SIFNITGIA	MTNR1A	No fit							
LTFNLVSDA	CASP8AP2	No fit							
MQWNILAQA	CCRN4L	No fit							
LSWNLVPEA	COL7A1	No fit							
DLWNTLSEA	TRHDE	No fit							
GLFNIPPAF	CYP2S1	No fit							

LIWNILASF	TTC29	No fit
LLFNMLPGG	EXT2	No fit
LVYNIMSSG	FAM120B	No fit
IIYNVPGTG	RNF133	No fit
VIYNVTSDG	TTN	No fit
GTFNLPSDG	BAG6	No fit
KLWNTLNLI	ENPP5	No fit
LMWNIISII	VTCN1	No fit
GLFNTTSNI	SEMA3E	No fit
LIFNTLSLI	PDCD6IP	No fit
SVFNLMNAI	SLC38A6	No fit
LTFNILGQI	DOCK11	No fit
GLFNMVSSL	RRN3	No fit
KIFNIINSL	FER1L5	No fit
AVWNVLGNL	BAG5	No fit
KVFNIVSDL	FSIP2	No fit
DLWNVVSHL	DDX60L	No fit
LQFNTVSKL	JAM2	No fit
MSFNTVSEL	ZNF33A,ZNF33B	No fit
ASWNIVNLL	TRPA1	No fit
ISFNIISAL	MS4A18	No fit
AFFNILNEL	FNBP1L	No fit
LVFNLLPIM	ABCB7	No fit
KIFNTVPDM	ARHGAP26	No fit
MLFNLIGLS	OR10J1	No fit
LLFNLPPGS	VGLL1	No fit
MTFNLIGES	CR1,CR1L	No fit
KVYNIPGIS	KLHL10	No fit
GIYNIPGDS	TNS1	No fit
GLYNLMNIT	INSR	No fit
LTWNMINTT	LRIT3	No fit
IVFNVLSDT	HCN3	No fit
IVFNVVSDT	HCN2,HCN4	No fit
LIFNITASV	SVEP1	No fit
IVFNLTNNV	MNAT1	No fit
KSFNVLSSV	ZNF557	No fit
LAFNILGMV	SLC46A1	No fit
VSWNITGTV	SEH1L	No fit